Control of Multifunctionalities of Nano and Microstructures

Zur Erlangung des akademischen Grades eines

DOKTORS DER INGENIEURWISSENSCHAFTEN (Dr.-Ing.)

von der KIT-Fakultät für Elektrotechnik und Informationstechnik des Karlsruher Instituts für Technologie (KIT)

angenommene

Dissertation

von

M.Sc. KM Samaun Reza
7th August 1994, Dhaka

Tag der mündlichen Prüfung:	20. Dezember 2024
Erster Gutachter:	Prof. Dr. Ulrich Lemmer
Zweiter Gutachter:	apl. Prof. Dr. Hendrik Hölscher

Kurzfassung

Im Laufe der Evolution haben sich Schlangen und Insekten wie Bienen so optimiert, dass sie in unterschiedlichen Umgebungen überleben können. Die Schuppen von Schlangen, insbesondere auf der Bauchseite, weisen häufig Nanostrukturen auf, die die Fortbewegung und Wärmeregulierung verbessern, während die Rückenschuppen multifunktionale Eigenschaften wie verbesserte Benetzung und Tarnung aufweisen. In ähnlicher Weise weist die weibliche Blaue Holzbiene strukturelle Anpassungen auf, mit blau gefärbten Haaren aus einer Kombination von Pigmentierung und Lichtmanipulation durch Nanoporen. Diese Studie vergleicht diese Nano- und Mikrostrukturen bei Schlangen und der Blauen Holzbiene und untersucht ihre Rolle bei der Fortbewegung, Wärmeregulierung und optischen Eigenschaften.

Schlangen entwickeln häufig Nanostrukturen auf ihren Bauchschuppen, um ihre Fortbewegung zu optimieren. Meistens werden stachelförmige Nanomerkmale beobachtet, aber auch Nanolöcher und Nanogitter finden sich auf ihren Schuppen. In dieser Arbeit wird eine vergleichende Studie zu den Nanomustern auf den Bauchschuppen in Verbindung mit der Fortbewegung der Schlangen durchgeführt. Im Gegensatz zu den ventralen Schuppen finden sich auf den dorsalen Schuppen vielfältige Oberflächentopologien. Die Dimensionen dieser Strukturen reichen vom Nanometer- bis zum Mikrometermaßstab. Frühere Studien haben bereits die Multifunktionalität dieser Merkmale vorausgesagt. In dieser Arbeit werden die verbesserten Benetzungseigenschaften der dorsalen Schuppen aufgrund dieser Nano- und Mikrostrukturen weiter erörtert. Einzelheiten werden in Kapitel 3 dargestellt.

Zusätzlich zur Fortbewegung sind die Bauchschuppen von Schlangen manchmal so verändert, dass sie Wärme effizient regulieren. Frühere Studien gehen davon aus, dass Schlangen, die in heißem und feuchtem Klima leben, reflektierende weiße Bauchschuppen entwickeln, um Überhitzung zu vermeiden. In dieser Arbeit wird eine vergleichende Studie über die reflektierenden weißen und transparenten Schuppen durchgeführt. Die Ergebnisse zeigen Nanoporen im Inneren der reflektierenden weißen Schuppen, während die transparenten Schuppen eine amorphe Struktur aufweisen. Diese Nanoporen reflektieren UV-, sichtbares und Nahinfrarot-Licht, um solche Oberflächen zu erhalten. Einzelheiten werden in Kapitel 4 beschrieben.

Einige Schlangen wie die Chinesische Kobra (*Naja atra*) entwickeln anisotrop reflektierende Bauchschuppen. Die Reflexion dieser Schuppen nimmt zu, wenn sie vom Kopf in Richtung Schwanz gekippt werden. Interessanterweise verringert sich die Reflexion, wenn sie von der Schwanz- zur Kopfrichtung gekippt werden. Ein Querschnitt dieser Schuppen zeigt geneigte Mikrokavitäten unter ihrer Außenfläche. Diese gekippten Mikrohohlräume interagieren mit dem sichtbaren Licht, um solche anisotrop reflektierenden Schuppen zu entwickeln. Einzelheiten werden in Kapitel 5 beschrieben.

Die meisten Vipern entwickeln ein Zickzackmuster aus hoch- und niedrigpigmentierten Rückenschuppen. Dieses Erscheinungsbild gewährleistet sowohl Tarnung als auch thermische

Eigenschaften. Die Schuppen innerhalb des Zickzackmusters sind im Vergleich zu den benachbarten Schuppen reich an Melanin. In dieser Arbeit wird eine vergleichende Studie über die hoch- und niedrigpigmentierten Schuppen vorgestellt, um herauszufinden, ob ihre Oberflächentextur für eine effiziente Thermoregulation optimiert ist. Interessanterweise wird ein Unterschied in der Oberflächenstruktur zwischen den hoch- und niedrigpigmentierten Schuppen festgestellt. Die optische Analyse zeigt jedoch, dass diese Strukturen die Wärmeregulierung im Schlangenkörper nicht fördern. Einzelheiten werden in Kapitel 6 beschrieben.

Schlangen, fossile Eidechsen und die meisten Geckos haben eine durchsichtige Hülle, die Brille, auf ihren Augen. Schlangen leben in direktem Kontakt mit dem Boden und unvermeidlichen Schmutzpartikeln. Da sie keine Extremitäten haben, um ihre Brille zu reinigen, wurden in dieser Arbeit die nass-selbstreinigenden Eigenschaften dieser Schuppen untersucht. Im Allgemeinen wurden Nano- und Mikrostrukturen auf der Oberfläche der Schuppen beobachtet. Sie sind jedoch nicht für die Erzielung selbstreinigender Eigenschaften optimiert. Die Ergebnisse zeigen außerdem, dass die Brillen für das sichtbare Licht transparent sind, aber die auf der Schuppenoberfläche gefundenen Strukturen sind nicht optimiert, um das Sehvermögen der Schlangen zu verbessern. Einzelheiten werden in Kapitel 7 beschrieben.

Die weibliche Holzbiene (*Xylocopa caerulea*) entwickelt blau gefärbte Haare auf dem Kopf, dem Thorax und Teilen des Hinterleibs. Frühere Studien legen nahe, dass diese Farbe durch das Pigment erzeugt wird. Die eingehende Analyse in dieser Arbeit zeigt jedoch, dass die Farbe durch eine Kombination aus Pigment und Lichtmanipulation erzeugt wird. Auf der Haaroberfläche sind keine Oberflächenstrukturen zu erkennen, aber ein poröser Haarkern ist vorhanden. Diese Nanoporen interagieren mit dem Licht, so dass eine reflektierende Oberfläche entsteht, und die blauen Pigmente, von denen angenommen wird, dass sie sich um die Haargrenze herum befinden, erzeugen die blaue Farbe. Die optische Analyse bestätigt außerdem, dass die blaue Farbe durch das Pigment erzeugt wird, das durch die Nanoporen im Inneren der Haare stark verstärkt wird. Einzelheiten werden in Kapitel 8 beschrieben.

Das Hauptziel dieser Arbeit bestand darin, die zugrunde liegende Physik dieser Nano- und Mikrostrukturen zu verstehen, die die mechanischen, optischen und thermoregulatorischen Eigenschaften von Schlangen und Bienen verbessern. Diese Strukturen können weiter erforscht werden, um optoelektronische Geräte der nächsten Generation mit verbesserten optischen, mechanischen und thermoregulatorischen Eigenschaften zu entwickeln.

Abstract

Through evolution snakes and bees have optimized themselves to survive across diverse environments. Snake scales, particularly on the ventral side, often feature nano-structures that enhance locomotion and heat regulation, while dorsal scales display multifunctional properties such as improved wetting and camouflage. Similarly, the blue female carpenter bee exhibits structural adaptations, with blue-colored hairs from a combination of pigments and light manipulation through nanopores. This study compares these nano- and micro-structures in snakes and bees, exploring their roles in enhancing locomotion, thermoregulation, and optical properties.

Snakes often develop nano-structures on their ventral scales to optimize their locomotion. Spike-shaped nano-features are mostly observed; nanopits and nano-ridges are also found on their scales. In this work, a comparative study is made on the nano-patterns on their ventral scales in correlation with the snake locomotion. Opposite to the ventral scales, diverse surface topology is found on the dorsal scales. Dimensions of these structures range from the nano-meter to the micro-meter scale. Previous studies have already predicted the multifunctionality of these features. This work further discusses the enhanced wetting properties of the dorsal scales due to these nano- and micro-structures. Details are presented in Chapter 3.

In addition to locomotion, the ventral scales of snakes are sometimes modified for efficient heat retention. Previous studies assume that snakes living in hot and humid climates develop reflecting white ventral scales to avoid overheating. In this work, a comparative study is made on the reflecting white and transparent scales. Results show nanopores inside the reflecting white scales; whereas an amorphous structure within the transparent ones. These nano-pores reflect UV, visible, and near-infrared light to achieve such surfaces. Details are presented in Chapter 4

Some snakes such as the Chinese Cobra (*Naja atra*) develop anisotropically reflecting ventral scales. These scales' reflection increases when tilted from head to tail direction. Interestingly, the reflection reduces when they are tilted from the tail to the head direction. A cross-section of these scales reveals tilted microcavities underneath their external surface. These tilted micro-cavities interact with the visible light to develop such anisotropically reflecting scales. Details are presented in Chapter 5

Most vipers develop a zigzag pattern of high and low-pigmented dorsal scales. Such appearance ensures both camouflage and their thermal melanism properties. Scales within the zigzag are rich in melanin content in comparison with the neighboring scales. In this thesis, a comparative study is presented on the high and low-pigmented scales to understand if their surface texturing is optimized for efficient thermoregulation. Interestingly a difference in surface structure is observed between the high and low pigmented scales. However, the optical analysis shows that these structures do not promote enhanced thermoregulation in the snake body. Details are presented in Chapter 6

Snakes, fossorial lizards, and most geckos develop a transparent integument called spectacle on their eyes. Snakes live in direct contact with the ground with unavoidable dirt particles. As they do not have any extremities to clean their spectacles, in this thesis wet self-cleaning properties of these scales are explored. In general, nano- and micro-structures are observed on their scale surface. However, they are not optimized to achieve self-cleaning properties. The results further show that spectacles are transparent for the visible light but the structures found on the scale surface are not optimized to enhance the vision of snakes. Details are presented in Chapter 7

The female carpenter bee (*Xylocopa caerulea*) develops blue-colored hairs on the head, thorax, and parts of the abdomen. Previous studies suggest that this color is produced by the pigment. However, the in-depth analysis made in this thesis reveals that the color is produced as a combination of pigment and light manipulation. No surface textures are observed on the hair surface; however, a porous hair core is found. These nanopores interact with the light to develop a reflecting surface and the pigments are assumed to be located around the hair boundary to produce the blue color. The optical analysis further confirms that the blue color is produced by the pigment which is strongly enhanced by nanopores found inside the hairs. Details are presented in Chapter 8.

The main objective of this thesis remained to understand the underlying physics of these nano- and micro-features which enhance the mechanical, optical, and thermoregulatory properties in the snakes and bees. These structures can be further explored to develop next-generation devices with enhanced optical, mechanical, and thermoregulatory properties.

Table of Contents

List of Figures

List of Tables

Abbreviations

AFM	atomic force microscope
CA	contact angle
LFM	lateral force microscopy
PDMS	polydimethylsiloxane
PMMA	poly (methyl methacrylate)
PTFE, Teflon	polytetrafluoroethylene
SEM	scanning electron microscope
C_{tor}	torsional force constant
C_z	spring constant
E	elastic modulus
F_{fric}	frictional force
F_{load}	normal load
G	torsional modulus
l	length of the tip
L	length of the cantilever
m	correcting parameter of AFM force calibration
S_{ver}	deflection sensitivity
t	thickness of the cantilever
U_{ver}	setpoint
U_{dis}	threshold voltage for zero normal load
ΔU_{lat}	difference of lateral voltage
v	sliding velocity
w	width of the cantilever
W_{AA}	work of cohesion of material A

W_{AB}	work of adhesion of interface between A and B
W_{BB}	work of cohesion of material B
β	constant of calculating contact angle
Υ_A	surface energy of material A
Υ_{AB}	surface energy of the interface between A and B
Υ_B	surface energy of material B
Υ_l	surface energy of liquid
Υ_s	surface energy of solid

1 Introduction

Over millions of years of evolution, different organisms have modified themselves to ensure existence in their respective habitats [1-4]. For centuries, their optimizing strategies have inspired humans to address challenges in everyday life [5-9]. Numerous artificial products have been developed mimicking the nano-and micro-textures that these creatures evolved. Examples include strong adhesive tapes inspired by gecko feet [8, 10], self-cleaning surfaces inspired by lotus leaves [11], drag-reducing aircraft wings or swimming suits inspired by shark skin [8, 12-13], anti-slippery vehicle tires inspired by tree frog toe pads [8, 14-16]. In addition to these achievements, some organisms developed optical strategies for their survival. Complex photonic structures in these organisms produced different colors for communication [17-18], mating [19], camouflage [20-21], and even thermoregulation [22]. These structural colors are produced by ordered or quasi-ordered arrangement of complex nanostructures [23-25].

Being inspired by these previous studies, this thesis presents an in-depth analysis of the snake scales and hairs of the female carpenter bee. A study is made on the functionality of snake scales compared to the respective nano- and micro-structures frequently observed on the scale's surface or embedded within. Mechanical, optical, and thermoregulatory adaptations of these scales are discussed. The results show that these nano- and micro-structures enhance specific properties in snakes. In addition to snake scales, the mechanism of color enhancement in the hairs of female carpenter bees is explained. The results show that nanostructures strongly enhance the reflection of these pigmentary blue hairs. In general, this thesis highlights the functionality of nano- and micro-structures found in different creatures which ensure their survival in their respective habitats.

In nature, snakes are the most common reptiles. More than 25 clads of tetrapods have evolved producing a total of around 4300 species of snakes, which represents 19% of the terrestrial vertebrate diversity [26-28]. They are widely distributed in different geographic regions and habitats. Snakes have originated from the group the limbless lizards which don't have any extremities for locomotion. Therefore, they locomote in direct contact with the substratum through their ventral scales (scales found on the abdomen) [29-33]. As a result, these scales unavoidably endure friction and wear during locomotion which presumably possess interesting tribological properties. Over the years, extensive research has been conducted on snake scales to understand the underlying physics of their locomotion and scale properties. The investigation started nearly 150 years ago when Leydig found micro-ornamentations on the uppermost layer of

the epidermis in contact with the environment, the so-called “Oberhäutchen” [34]. After that, many studies have been conducted, mainly by electron microscopy, to reveal the topography of these ornamentations on ventral scales as well as dorsal scales (scales found on the back) [35-43]. On the ventral scales, a spike-shaped structure is frequently observed from head to tail direction of the snake [44-51]. It is widely accepted that the main function of these structures is to optimize frictional contact with the substrate (ground, trees, etc.). More specifically, these nano- and microstructures might reduce friction [47, 52-54], create frictional anisotropy [44-51, 55-56], or optimize the respective locomotion performance [57].

Multifunctionalities of the ventral and dorsal scales of snakes

Snakes usually follow four distinct locomotion traits: lateral undulation, sidewinding, concertina, and rectilinear. In Chapter 3 of this thesis, a comparative study is presented on the nanostructures found on the snake ventral scales in correlation with their respective locomotion gears. Results show that the surface topographies of these scales are optimized to ease snake locomotion. Besides, the wetting and optical response of these structures were also recorded. Results confirm that the scales are mostly transparent in the visible regime and are hydrophobic in contact with water. Interestingly, hydrophilic scales are even observed; mostly caused by the texturing of their scale surface.

In difference to ventral scales diverse nano- and micro-structures are found on the dorsal scales. These structures have been referred to as verrucate [35], canaliculate ridges [36], cristate apical [41], crosshatched [37, 40], papillate [42], and reticulate or porous structures [43]. With the ongoing exploration of these micro dermatoglyphic patterns on snake scales, the function or capability of these structures has attracted serious attention. Investigations in the early days attempted to use these microdermatoglyphics to indicate the ecological or phylogenetic relationship between different species [42, 62]. In 2020 Tsai *et al*. revealed that the evolution of scale microstructures is dominated by both phylogenetic and ecological constraints [63]. Together with results obtained on different reptiles (e.g. lizards), other authors hypothesized that these micro-ornamentations could cause light scattering to prevent solar radiation from penetrating the organism [35, 64], enhance dark coloration [65], help in water harvesting [66], contribute to anti-contamination (self-cleaning) properties [62, 67-68], or sound production [69-70]. Therefore, it seems like, the dorsal scales of snakes feature diverse micro-ornamentations due to individual demands for their respective habitat and ecology. To further learn about the multifunctionality; in addition to the ventral scales, a detailed analysis is presented on their micro-ornamentations, wetting, and optical responses of the dorsal scales in Chapter 3. The dimension of these structures

ranges from nano-meter to micro-meter scale. In general, a higher contact angle is observed on the dorsal scales. However, the contact angles are not high enough to conclude that these structures promote self-cleaning properties. But these contact angles can help snakes to enhance their wetting properties. Much reduced transmittance is observed for the dorsal scales in comparison with the ventral scales. This reduction might be caused due to the absorption of melanin and light scattering by the nano- and micro-structures.

Nanopores create a broadband reflection in snake scales

In addition to locomotion, ventral scales of some species are also optimized for thermoregulatory properties. In 2014, Moreno-Azocar *et al*. stated that snakes living closer to the equator mostly develop brighter venters [58]. Later, Goldenberg *et al*. further stated that snakes living in hot and humid climates would develop less melanic ventral scales which might help them to avoid overheating [59]. However, these studies do not explain the mechanism through which snakes develop such reflecting white ventral scales. To address this research question, in this work, the topological and optical properties of reflecting white scales are studied in comparison with the transparent or translucent ventral scales. Results presented in Chapter 4, evidence that nanopores found inside the reflecting white scales scatter light to develop such thermoregulatory reflecting white surfaces. An amorphous structure with no nanopores found inside the transparent or translucent scales further confirms the statement.

Micro-cavities developing anisotropically reflecting scales in snakes

Interestingly, some snakes living in Western Asia develop anisotropically reflecting ventral scales. Chinese Cobras originating from Western China are often found to develop white scales; whereas black venters are found on the species endemic to the Eastern region [60-61]. Ventral scales of this species appear whitish when tilted from head to tail direction. However, they appear dark (mostly caused by melanin) when tilted along the tail-to-head direction. In this thesis, extensive research was conducted to understand the mechanism through which these snakes develop such anisotropically reflecting scales. Results in Chapter 5, confirm that these scales develop alternate layers of tilted microcavities underneath the external surface of the ventral scales. These tilted microcavities are in alternate layers with the scale material (keratin). The combination of the scale materials with these tilted microcavities interacts with the visible light to develop such anisotropically reflecting surfaces.

Differences in surface topography with the variation in optical appearance

Most ectotherms tend to develop a dark-colored appearance. Alongside camouflage, this dark coloration has a thermoregulatory impact on these cold-blooded reptiles. The thermal melanism hypothesis predicts an ecological advantage for dark-colored animals in cold environments [71]. Recent studies on lizards have confirmed such predictions [72-74]. However, these dark-colored snakes are often vulnerable to predators as it increases their detectability [75-78]. It appears to be that melanism is a tradeoff between camouflage and thermoregulation. Interestingly, most Vipers exhibit a zigzag pattern on their dorsal scales [83]. The scales within the zigzag pattern are highly pigmented in comparison with the other neighboring scales [83]. Such patterns might favor snakes to camouflage and also maintain their melanistic properties [84]. In 2020, Martínez-Freiría *et al*. conducted an extensive analysis of the high-pigmented dorsal scales within the zigzag pattern of 39 Eurasian Vipers [77]. The study concluded that the concentration of pigments of these scales within the zigzag pattern is optimized for thermoregulation. Interestingly, diverse nano- and micro-structures are observed on these scales. Thus a comparative study is made on the topological and optical properties of high and low-pigmented scales of some snake species in Chapter 6 to understand if these structures have an effect in modifying their thermal properties. Results indicate that both topological and optical properties differ with the variation in pigment concentration of these scales. However, in difference to a previous study [65], the surface textures on the dorsal scales are not optimized to enhance transmittance properties; rather the reflectance increases when light incidences on these nano- and micro-structures.

Micro-ornamentation and spectral transmittance of the spectacle scales

In difference to eyelidded animals, the eyes of snakes, fossorial lizards, and most geckos are covered by a transparent integument often called brille or spectacle [85]. This fixed membrane is developed from the fusion of eyelids during their embryonic stage [86]. These spectacles provide mechanical protection to the cornea, minimize water evaporation, and even protect against solar radiation [87-89]. In 1999, Campbell *et al.* revealed the shallow micropits on the spectacles of Carpet Python (*Morelia spilota*) and concluded that such structures could help filter the transmission of a certain infrared range [90]. These previous studies were conducted to understand the topological and optical properties of some snake species [85, 91-92]. However, another question remained; how do snakes clean their spectacles as they do not have any extremities for wiping? Therefore, the wettability of the spectacles was investigated in comparison with the

surface textures to learn about possible wet self-cleaning properties. In addition to that, the optical properties of the spectacles were also investigated. The observations and analysis presented in Chapter 7 indicate that the spectacles develop nanopits, narrow channels, and narrow boundaries on the surface. However, these structures do not promote specific functionality or enhance optical properties. The benefits to snakes for the development of these nanopits, narrow channels, and boundaries are yet to be understood.

Nanopores enhance the reflection of the blue hair of the female carpenter bee

Carpenter bees (*Xylocopa caerulea)* have brightly colored bodies and/or wings [93]. The body of male *X. caerulea* features a blackish cuticle; whereas, the female *X. caerulea* has bright blue hairs on its head, thorax, and part of the abdomen. In 1926, Mason predicted that this blue color is produced by pigments [95]. Recently, Stavenga further concluded that the color is produced by a bile pigment Bilin, as spectra of the hairs showed high absorption around 605 nm [94]. However, no rigorous proof was presented to verify that the vibrant blue color is generated by the pigments only. Therefore, the morphological and optical properties of the blue hairs of *X. caerulea* are studied in detail. Results presented in Chapter 8 confirm that a nanoporous core exists inside the blue hairs. These nanopores act as a white scatterer for back reflection. In agreement with these previous studies, results indicate that the blue color is partly produced by a pigment; however, the reflection is strongly enhanced due to the interaction of light with the nanopores found inside the hair.

Snake scales have been studied for years to understand their multi-functionality [34-54, 62, 64-70, 85-90]. Inspired by the previous studies, Weibin Wu started an investigation on snake scales in 2016. As the snakes molt in around 3-4 months enough samples were not available to summarize his findings. Besides, only two spectacle scales are available from one completely shaded skin. With the availability of scales belonging to snake species from different geographical locations and habitats, I went on with an elaborate study in 2020 for further investigations. In this study, several physical theories are discussed to explain the functionality of scales. These theories are validated through in-depth analysis of numerous snake species. Therefore, in Chapters 3 and 7, some results are recalled from the thesis of Weibin Wu to summarize the findings. At the end of these chapters, the results adapted from Weibin Wu's thesis are explicitly mentioned.

2 Theory, Materials, and Methods

Over the billions of years of evolution, nature has optimized itself to survive in its respective habitat. This thesis discusses some of snakes' and bees' mechanical, optical, and thermoregulatory optimizations. The results show that nano- and micro-structures found in their scales or hairs are modified to achieve such properties. The basic theoretical background is necessary for a better understanding of the underlying physics of these nano- and micro-structures. Parts of this chapter introduce the theories that are further explored to explain the mechanism through which they perform such multi-functions. To verify the assumptions series of investigations were conducted. Therefore, in the later part of this chapter characterization techniques and relevant tools are explained.

2.1 Snake-inspired mechanics

2.1.1 Snake locomotion

The locomotion of limbless animals is different in comparison to the limbed species as it relies entirely on the vertebral column, ribs, and trunk for propulsion. Most commonly snakes follow four specific types of locomotion traits: Lateral Undulation, Sidewinding, Concertina, and Rectilinear. Figure 2.1 shows a schematic of the four fundamental locomotion gears [96]. Previous studies show that snakes develop different nano-structures on their ventral scales to ease their locomotion [44-57]. In this thesis, a comparative study is being made on these nano-structures in correlation with the locomotion trait. Thus locomotion traits are discussed here in brief. The theoretical basis will relate to the findings presented in Chapter 3.

Lateral Undulation is the most common locomotion trait. When snakes move on a surface using this gear, the body deforms locally exerting external forces against the surface. The lateral force vectors generated due to this external thrust cancel each other and the resultant force vector propels the body forward. Snakes achieve fine control over the direction of force exertion by the postural adjustment of the body. In such locomotion, lateral frictional force is dominant where large dorsal muscles are activated unilaterally at each bend of the body.

Sidewinding gear is mostly used by snakes on smooth or slippery surfaces while crawling. In such locomotion, initially, each part of the body is sequentially placed in static friction with the substrate. Then segments of the body are lifted off the surfaces; thus it rolls along the ground from neck to tail forming a characteristics track. When it settles down in a new position, the front part initiates a new track while the rear part completes the old track. In this

trait, the snake relies on static friction to travel diagonally relative to the track it forms on the ground. Muscle activity is similar to lateral undulation; however, they are also activated bilaterally in the regions where being lifted.

Concertina gear is used when snakes crawl through tunnels, narrow passages, or while climbing. It involves alternate pulling of the body into bends and then straightening the body to move forward. Initially, the front part of the body moves and when it rests on the substrate, the rear part is pulled up into bends again. Static frictional force is important in concertina locomotion as snakes activate blocks of muscles unilaterally in the regions of bending.

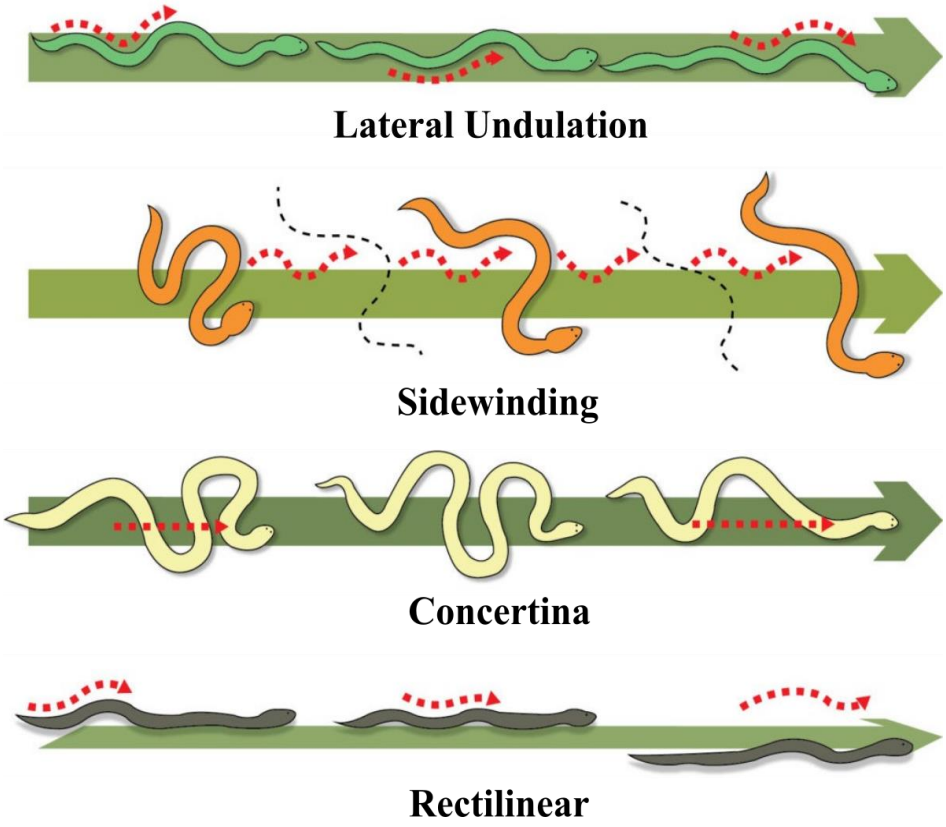

Figure 2.1 Different traits of snake locomotion. The figure is reproduced from [96].

Rectilinear often called the caterpillar locomotion, involves snake movement in a straight line. In this trait, initially, ventral scales are alternatively lifted slightly from the ground and pulled forward; later they are pulled downward and backward. As scales stick to the ground, the body is pulled forward over them. When the body moves far enough to stretch the scales, the cycle repeats. Unlike lateral undulation, sidewinding, or concertina locomotion bilateral active

muscles are activated in this gear where snakes mostly rely on their static frictional force to the substrate.

It is very difficult to classify snakes based on their respective locomotion traits, as a snake can follow all four locomotion traits when needed. The sidewinding gear is quite different from the other traits; thus, Reiser *et al*. divided several vipers into groups of sidewinding and non-sidewinding species [57]. They showed that non-sidewinding vipers often grow nanostructures on their ventral scales to develop anisotropic frictional force which helps them in locomotion. On the other hand, sidewinding vipers develop nanopits on their ventral scales resulting in frictionally isotropic surfaces which assists in sidewinding locomotion. Previously, Berthe *et al*. assumed that the ridge-like structures found on the ventral scales of tree-climbing snake species assist them in climbing by generating frictional anisotropy [52]. Inspired from the previous studies ventral scales of numerous snake species from different geographic locations, habitats, and families are analyzed in this thesis. A comparative study is made on the dimensions of the structures and their corresponding frictional force property. Results are presented in Chapter 3.

2.1.2 Ventral scales of snakes showing anisotropic frictional force

In 2021, Reiser *et al*. showed that the nano-structures found on the ventral scales of snakes assist them in lateral undulation-type locomotion by generating anisotropic frictional force [57]. Previously, in 2020 Wu *et al*. showed that these anisotropic frictional forces vary among the species with the difference in height of these nano-patterns [56]. In this thesis, the anisotropic frictional force of the ventral scales of some snake species is studied in comparison with the physical property (mass, length) of the snake body. For a better understanding of such nano-scale frictional forces, some theories are discussed.

2.1.2.1 Adhesion

Adhesion is defined as the tendency of particles or surfaces to adhere together [97]. Adhesion work of material A is related to the surface energy by [98]

$$\boldsymbol{W_{AA} = 2\gamma_A} \qquad \textbf{2.1}$$

where W_{AA} is called the work of cohesion and γ_A is the surface energy

When material A is in contact with material B, surface energy γ_{AB} is associated with the interface of these two materials. Work of adhesion in this circumstance is defined as the variation of surface energy during the contacting process or the reversible work needed to separate them. Work of adhesion, when two materials (A, B) are in contact, is related by Dupre equation which is [98]

$$W_{AB} = \gamma_A + \gamma_B - \gamma_{AB} = \frac{1}{2}W_{AA} + \frac{1}{2}W_{BB} - \gamma_B \quad \textbf{2.2}$$

Thus a conventional method to determine adhesion is to measure the surface energy. Adhesion forces or work of adhesion can be also measured on a nanoscale using AFM. This is conducted by analyzing the force-distance curves. In this work, the frictional force of the ventral scales of snakes is analyzed. The adhesion force of the cantilever in contact with the snake scales is measured to calculate the anisotropic friction force of the snake scales. The methodology is explained in detail in section 2.4.2.

2.1.2.2 Friction

Friction is defined as the force resisting the relative motion of solid surfaces, fluid layers, and material elements sliding against each other. In terms of lubrication, friction is classified into dry and lubricated friction. Terrestrial snakes mostly rely on dry friction to ease their locomotion. In 1699 Guillaume Amontons first published the laws of friction which are later commonly accepted as Amontons' laws of friction [99]:

1. Friction force is proportional to normal load

2. Friction force is independent of the apparent area of contact

3. Dynamic friction is independent of the relative sliding speed

The three laws of friction can be summarized as [100]

$$F_{fric} = \mu . F_{load} \quad \textbf{2.3}$$

here, μ is the friction coefficient which is a material property of the surface. However, it is also influenced by other factors such as the humidity of the environment or roughness of the sliding surface. The friction coefficient is independent of the contact area and the sliding velocity. F_{fric} and F_{load} represent the frictional force and normal load, respectively.

2.1.3 Water harvesting properties of snake scales

Some rattlesnakes living in deserts have been found drinking water collected on their body scales during rain [101]. Phadnis *et al*. assumed that surface textures of the dorsal scales of these species enhance such a water harvesting phenomenon [101]. Their study showed that nano-structures on

their scale surface reduce the surface energy of the scales to increase the water contact angle. A higher contact angle results in the formation of a small puddle on the snake's body and snakes are found to drink water from these puddles. Inspired by this work, the wetting properties of scales of numerous snake species from different habitats and geographic locations were analyzed in this study. The results in Chapter 3 show high water contact angles for the dorsal scales which is caused due to their surface textures. However, lower contact angles were observed on the ventral scales. In addition, the wetting properties of the spectacle (found on the eyes) scales were also measured to determine if they promote self-cleaning properties as they locomote on the ground with unavoidable dust and dirt. The results (presented in Chapter 7) confirm that the spectacles do not show self-cleaning properties as they have very low contact angles. To correlate wetting properties with the nano- and micro-structures found on ventral, dorsal, and spectacle scales of snakes, the wetting theory is discussed here. Results on the wetting behavior of scales are presented in Chapters 3 and 7.

When a liquid droplet comes in contact with a solid surface, their interaction results in the spreading of the liquid. This interaction is described by the Wetting theory. Molecules in a liquid droplet are bound to each other by intermolecular forces. The molecules around the center are balanced; however, the ones located around the edges are mostly positioned toward the center. This results in the net pulling of the outer molecules to the droplet center. The input energy required to move a molecule from the center to the edge within a droplet is called interfacial surface tension (γ). It is defined as the work necessary for the displacement per unit surface.

In 1805, Young defined the relation between the contact angle (θ) of a droplet with the surface tension, γ_{IJ} of liquid vapor (LV), liquid-solid (LS), and solid-vapor (SV) interfaces using three-phase model where droplet was considered small enough for gravity to be negligible in reference to Figure 2.2 [102].

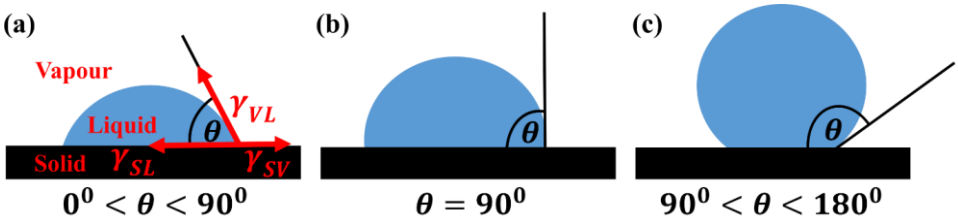

Figure 2.2: (a) Solid-liquid-vapor triple line is defined by Young's equation. Surfaces with contact angle $0^0 < \theta < 90^0$ *are hydrophilic (b, c) whereas* $90^0 \leq \theta \leq 180^0$ *are hydrophobic*

$$\cos\theta = \frac{\gamma_{SV} - \gamma_{SL}}{\gamma_{LV}} \qquad 2.4$$

Based on the contact angle, states of solid surfaces are separated into different types.

$$\mathbf{0^0 < \theta < 90^0}\text{ , }\mathbf{hydrophilic}$$

$$\mathbf{90^0 \leq \theta \leq 180^0}\text{ , }\mathbf{hydrophobic}$$

Glass and most non-fluorinated polymers are hydrophilic. Hydrophobicity can be obtained by reducing the surface energy of the solid surface. This could be achieved by fluorinating or chemically modifying the surfaces. However, a contact angle above 120^0 cannot be achieved on smooth surfaces [103-104]. Thus surfaces are roughened or modified to develop superhydrophobic surfaces ($\theta > 150^0$) [105-108]. Eq. 2.1 is applicable for homogenous or smooth surfaces. Therefore, to analyze the wetting properties of structured surfaces, Wenzel and Cassie-Baxter wetting states need to be defined [109-112].

Wenzel State describes the phenomenon when the droplet wets the structured surface completely penetrating the topography (Fig 2.3a). The contact angle on the structured surface can be derived from the contact angle for the unstructured surface.

$$\boldsymbol{cos\,\theta_{wenzel} = r.cos\theta_0\,;r \geq 1} \qquad \textbf{2.5}$$

here, r is defined as the ratio of the actual surface area to the projected surface area of the surface. As $r > 1$, roughness and surface topography always enhance the wettability of bulk material. Thus, a lower contact angle will be recorded on a structured hydrophilic surface in comparison with a non-structured surface; whereas, a higher contact angle will be recorded for a structured surface in comparison with the non-structured hydrophobic surfaces [105-106, 112-113].

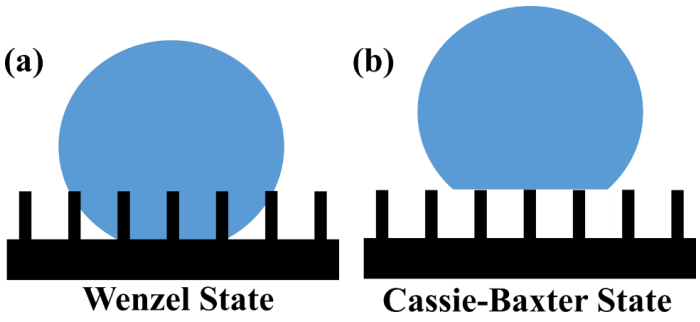

Figure 2.3: Schematic of different wetting states associated with increasing (or decreasing) the surface contact angle by structuring the surface. (a) Wenzel state: droplet penetrates the surface topography and wets the structured surface completely. (b) Cassie-Baxter state: droplets partially rest on the surface topography and do not penetrate the features.

Cassie-Baxter State describes the phenomenon when the droplet partially rests on the topography and does not penetrate the features (Fig 2.3b) [103, 107, 114]. Thus air pockets are

created which increase the contact angle by reducing the liquid-solid contact area. Resultant contact angle on the structured surface-

$$\boldsymbol{\cos\theta_{CB} = \phi_S r_S \cos\theta_{OS} + \phi_{air} r_{air} \cos\theta_{Oair}} \qquad \textbf{2.6}$$

here, ϕ_S and ϕ_{air} are area fractions of wetted solid and air respectively and r_S and r_{air} are respective roughness factors of the wetted solid and air. In the specific case of a droplet resting on the structures Eq. 2.6 can be simplified using $\theta_{Oair} = 180^0$, $r_{air} = 1$, and $\phi_{air} = 1 - \phi_S$

$$\boldsymbol{\cos\theta_{CB} = -1 + \phi_S(r_S \cos\theta_{OS} + 1)} \qquad \textbf{2.7}$$

Contact angle in a Cassie-Baxter wetting state depends on the solid-liquid contact area which is often higher than the structured surfaces in a Wenzel state.

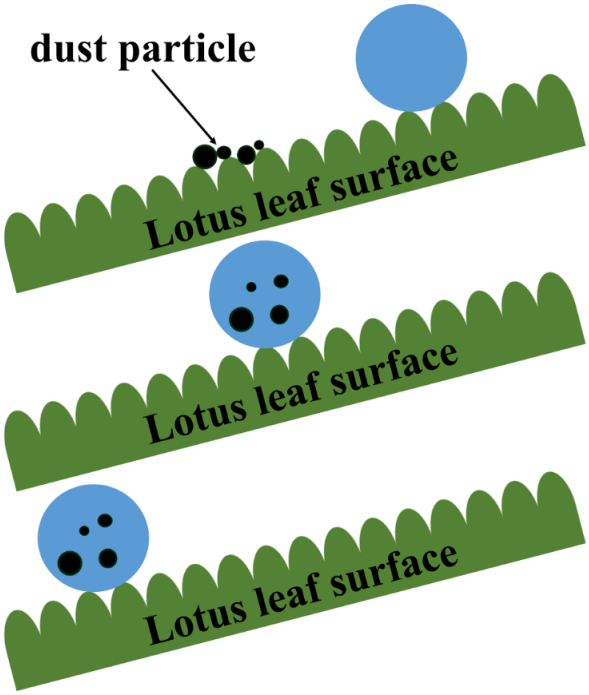

Figure 2.4: Schematic of self-cleaning properties of Lotus leaves. The microstructures on the leaf surface develop a high contact angle which results in a low roll-off angle. Water droplet rolls off the surface collecting the possible debris and particles. The figure is adapted from [115].

The wettability of surfaces can be controlled by developing different nano- and microstructures on the surface. Such textures reduce the surface energy by decreasing the resultant adhesion by reducing the contact area. This reduced surface energy results in a high water contact angle (CA) which results in a lower roll-off angle. Thus the water droplet tends to roll off at lower

angles along with the possible debris often accumulated on the surface. Barthlott *et al.* in 1997 pointed out the self-cleaning properties of lotus leaves (*Nelumbo nucifera*) [11]. Their analysis showed that the natural micro-structures on the leaf surface result in high contact angles which promote self-cleaning of surfaces as the droplet rolls off along with the possible debris collected on the leaves. The schematic explaining the theory is presented in Figure 2.4. The theory was later popularized as the Lotus effect. As snakes develop a variety of structures on their scales, in this thesis, the wettability of these scales was measured to determine if the scales promote wet self-cleaning properties.

2.2 Snake-inspired photonics

2.2.1 Mechanism of coloration

Snakes are often distinguished by the variety of their colors and diverse patterns. Specific colors are mostly produced by pigments. Chromatophores found in snakeskin produce black, red, and yellow color. Chromatophores are cells responsible for producing pigmentary colors. In vertebrates, these cells are developed embryologically from neural crest tissue and they migrate to the skin in their embryonic stage. Snakes mostly develop four different types of Chromatophores. Melanophores, erythrophores, and xanthophores develop black, red, and yellow colors respectively in snakeskin. Iridophore develops a white color by reflecting incident light. However, many other colors such as blue, green, brown, and purple are often found on the snakeskin. These colors are mostly produced by the variation in composition of the basic colors, due to the interaction of basic colors with the hemoglobin in the blood supply of the dermis or due to the reflection by iridophores. Interestingly, white-colored snake scales can be also produced due to the scattering of light. Results presented in Chapter 4 confirm that some snakes generate nanopores within their ventral scales. These nanopores scatter the visible light to develop reflecting white scales. In Chapter 8 the results further show that similar nanopores are also found within the blue hairs of female carpenter bees. These nanopores interact with the visible light to enhance the coloration of the pigmentary blue and develop a whitish central region. The whiteness is produced in the snake scales and bee hairs due to the scattering of light when incident upon interfaces with different refractive indices. Thus, basic interactions of light at interfaces are explained first describing the certain conditions to be fulfilled for light to reflect over a broadband spectrum. Different mechanism of light scattering is further discussed. The theoretical background will benefit in understanding all the chapters in general.

2.2.2 Light interaction at interfaces

Nature produces structural colors by optimizing the interaction of light at the interfaces of two dielectric media with refractive indices n_1 and n_2. Reflection and transmission of light at interfaces can be generalized if dielectric materials with constant layer thickness are alternated periodically. Light can interfere constructively producing wavelength-selective reflection and transmission provided that the layer thickness is comparable to the incident light wavelength. [116-117].

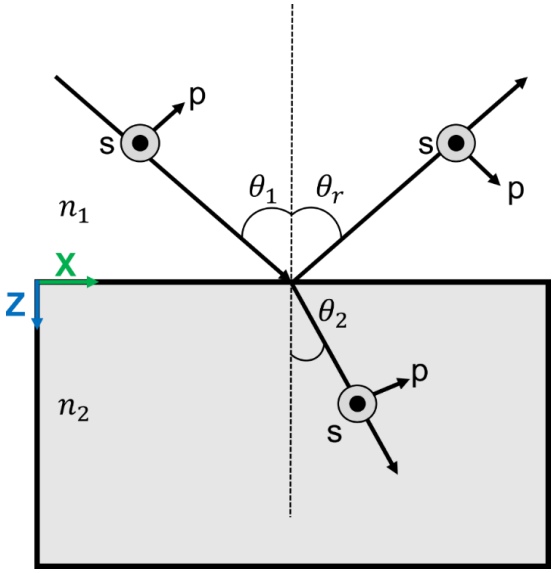

Figure 2.5 Schematics of light incidence, reflection, and transmission at an interface of two isotropic media with refractive indices n_1 and n_2, respectively, and their respective angles θ_1, and θ_2 with respect to the normal. P-polarized light has the wave vector in the plane, whereas s-polarized light has the wave vector normal to it.

A schematic of light incidence, reflection, and transmission at an interface of two isotropic media with refractive indices n_1 and n_2 is shown in Figure 2.5. Reflected light bounces off the interface and propagates to the first medium following the condition $\theta_r = -\theta_1$, where θ_1 and θ_r are the angles of incidence and reflection of the propagating light wave with respect to normal of the interfaces respectively. The refracted light propagates into the second medium at angle θ_2 obeying Snell's law.

$$\boldsymbol{n_1 \sin \theta_1 = n_2 \sin \theta_2} \qquad \textbf{2.8}$$

Electric field intensity of reflection and transmission depends on the polarization of incident light. An electric field vector polarized in the plane of incidence is defined as p-polarized (transverse magnetic, TM) light. The electric field vector polarized in the plane of optical interference (normal to the plane of incidence) is referred to as s-polarized (transverse electric, TE) light. The amplitudes of the reflected and transmitted light are given by Fresnel's amplitude reflection and transmission coefficients via

$$r_s = \frac{n_1 cos\theta_1 - n_2 cos\theta_2}{n_1 cos\theta_1 + n_2 cos\theta_2} \quad \textbf{2.9}$$

$$t_s = \frac{2n_1 cos\theta_1}{n_1 cos\theta_1 + n_2 cos\theta_2} \quad \textbf{2.10}$$

$$r_p = \frac{n_1 cos\theta_2 - n_2 cos\theta_1}{n_1 cos\theta_2 + n_2 cos\theta_1} \quad \textbf{2.11}$$

$$t_s = \frac{2n_1 cos\theta_1}{n_1 cos\theta_2 + n_2 cos\theta_1} \quad \textbf{2.12}$$

The reflectance *R* and transmittance *T* for the different light polarizations and as well as unpolarized light conditions can be given by

$$R_{s.p} = |r_{s.p}|^2 \quad \textbf{2.13}$$

$$R = \frac{R_s + R_p}{2} \quad \textbf{2.14}$$

$$\boldsymbol{T_{s.p} = \frac{n_2 cos\theta_2}{n_1 cos\theta_1} \left|t_{s.p}\right|^2} \quad \textbf{2.15}$$

$$\boldsymbol{T = \frac{T_s + T_p}{2}} \quad \textbf{2.16}$$

The equations already validate that *R* strongly depends on the incidence angle for thin films. This phenomenon results in a metallic and iridescent appearance for multilayers. For thin film interference, reflection at every interface is to be iterated. Light constructively interferes when optical path length differences are equal to the integer multiple of the wavelength, that is $m\lambda$, where, m is a positive integer and λ the considered optical wavelength. Light destructively interferes when the optical path length difference is a half-integer, that is $(\, m - \frac{1}{2}\lambda)$.
Therefore, the following interference conditions can be deducted by Snell's law.

Constructive interference:

$$\boldsymbol{m\lambda = 2\,.\,(n_1 d_1 cos\theta_1 + n_2 d_2 cos\theta_2)} \quad \textbf{2.17}$$

Destructive interference:

$$\boldsymbol{(\, m - \frac{1}{2}\lambda) = 2\,.\,(n_1 d_1 cos\theta_1 + n_2 d_2 cos\theta_2)} \quad \textbf{2.18}$$

where n_1, n_2 are the refractive indices and d_1, d_2 are the thicknesses of the layers.

For a multilayer system with *N* alternating layers of two different materials with refractive indices $n_2, n_{3,}$ and thicknesses d_1, d_2 and for the condition $n_2 > n_{3,}$ peak, reflectance can be deduced by specifying the conditions for constructive interference of light beams that are reflected from different optical interfaces. In reference to Figure 2.1b, light incidents on the multilayer stack at an angle θ_1. Considering Snell's law, constructive interference of light reflected off two parallel-oriented consecutive interfaces leads to the relation-

$$m\lambda = 2\,.\,\left(d_1.\sqrt{n_2^2 - n_1^2 sin^2\theta_1} + d_2.\sqrt{n_3^2 - n_1^2 sin^2\theta_1}\right) \quad 2.19$$

To achieve broadband reflection equal intensity of reflected light is required over the entire spectrum of consideration. This can be obtained by combining multi-layers with alternate refractive indexes and varying thickness [4]. When each layer contributes to the constructive interference of a specific wavelength (Fig 2.6b), the summation of reflected light for all wavelengths will develop broadband reflection for a specific regime of the electromagnetic spectrum. Such a phenomenon is observed in the anisotropically reflecting ventral scales of the Chinese Cobra (*Naja atra*). The results are further discussed in Chapter 5.

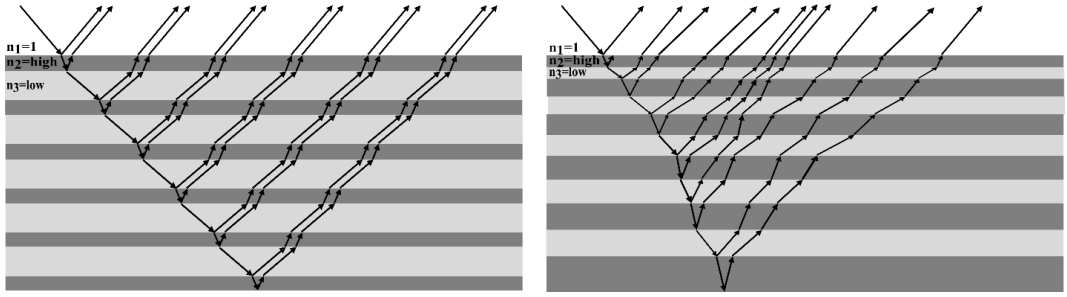

Figure 2.6: A Multilayer system with multiple interfaces developing constructive interference of light is optimized for (a) high reflection at specific wavelengths and (b) broadband reflection for a wavelength range. To develop high reflection for specific wavelength layer thickness is kept uniform. However, variation of this thickness will result in the reflection of light with a specific wavelength in accordance with the width of the subsequent layer. The combination of the reflected light might result in the formation of structural white.

Reflection at thin film and multilayer interfaces mostly depends on the angle of incidence. The interaction with visible light can result in a specific color depending on the layer thickness or white color when the layer thickness is varied in a multilayer pack. Interestingly high broadband reflection or white color can be also achieved in visible light through uniform scattering. Light scattering is described in the next section.

2.2.3 Scattering of light

The phenomenon of light scattering is explained as the deflection of light from its original direction of propagation due to the interaction with a scattering center. In general, scattering is of two types- elastic and non elastic scattering. Elastic scattering occurs when the sum of kinetic energy before and after the interaction remains constant. In inelastic scattering part of the energy

is converted into excitation energy. In this thesis, only elastic scattering is considered. The size of the scattering center in comparison with the incident light is important in describing the type of scattering.

Rayleigh scattering occurs when light interacts with small particles (about $< \frac{1}{10}\lambda$) in comparison with the wavelength. It is highly wavelength-dependent and the intensity is proportional to $\frac{1}{\lambda^4}$. Rayleigh scattering in a medium is limited to the short wavelength of light. In Mie scattering particle size is comparable to the wavelength of incident light. When particle size exceeds lambda, scattering is independent of wavelength. Geometrical optics is applied when the diameters of scattering particles are much larger than the wavelength (about 10λ). Often dimensionless size parameter x is used to define the type of scattering.

$$x = \frac{2\pi r}{\lambda} \qquad 2.20$$

where r is the radius of the scattering particle. For

$x \ll 1$, Rayleigh scattering

$x \gg 1$, geometrical optics

$x \approx 1$, Mie scattering

2.3 Materials

2.3.1 Snake scale

This thesis explores the underlying physics of the nano- and micro-structures in the snake scales, which optimize specific mechanical and optical properties in them. Several speculations were made on the functionalities of these structures. Therefore, the scales of numerous snake species from different geographical locations, habitats, and families were investigated to validate the assumptions. Snakes molt their scales regularly every three to four months. Thus abundant experimental samples were available without harvesting the living reptiles. No snakes were harmed while carrying out these experiments. The molted scales from captive snakes were collected by Guillaume Gomard from the Zeiss Innovation Lab @ KIT thanks to the contribution of different snake keepers (see details in Acknowledgments).

Ventral and dorsal scales of thirty-two snake species from different geographical locations, and habitats belonging to six different families were analyzed. Scales found on the back, abdomen, and eyes of the snake are called dorsal, ventral, and spectacle scales respectively. Snakes display a wide variety of habitats ranging from terrestrial, fossorial, arboreal, and semi-aquatic to aquatic. Most of the investigated scales belong to terrestrial species; however, scales

of arboreal species (*C. hortulana*) as well as of semi-aquatic species (*N. tessellata*) were also studied, altogether covering a broad range of habitats. Binomial and common names of all the investigated snake species along with their geographical locations and families are summarized in Table 2.1.

Table 2.1: Overview of the investigated species with their geographical locations, family, and habitat.

Binomial name	**Common Name**	**Family**	**Geographical Location of Origin**	**Habitat**
Crotalus atrox	Western Diamondback Rattlesnake	Viperidae	North America	Terrestrial
Pantherophis guttatus	Eastern Corn Snake	Colubridae		Terrestrial
Sisturus milarius barbouri	Dusky Pygmy Rattle Snake	Viperidae		Terrestrial
Crotalus lepidus klauberi	Banded Rock Snake	Viperidae		Terrestrial
Corallus hortulana	Amazon Tree Boa	Boidae	South America	Arboreal
Zamenis situla	European Ratsnake	Colubridae	Europe	Terrestrial
Natrix tessellata	Dice Snake	Colubridae		Semi-aquatic
Malpolon monspessulanus	Montpellier Snake	Psammophiidae		Terrestrial
Vipera ursinii rakosiensis	Hungarian Meadow Viper	Viperidae		Terrestrial
Vipera berus	Common European Viper	Viperidae		Terrestrial

Vipera aspis	Asp Viper	Viperidae		Terrestrial
Vipera seoanei	Seoane's Viper	Viperidae		Terrestrial
Vipera lotievi	Lotiev's Viper	Viperidae	Eastern Europe	Terrestrial
Vipera eriwanensis	Armenian steppe Viper	Viperidae		Terrestrial
Vipera renardi	Steppe Viper	Viperidae	Western and Central Asia	Terrestrial
Parias schultzei	Schultze's Pitviper	Viperidae	Asia	Arboreal
Tropidolaemus subannulatus	North Philippine Temple Pitviper	Viperidae		Arboreal
Trimeresurus flavomaculatus	Philippine Pitviper	Viperidae		Arboreal
Trimeresurus honsonensis	Hon Son Pit Viper	Viperidae		Arboreal
Naja atra	Chinese Cobra	Elapidae		Terrestrial
Antaresia perthensis	Pygmy Python	Pythonidae	Oceania	Terrestrial
Aspidites ramsayi	Woma Python	Pythonidae		Terrestrial
Morelia spilota	Carpet Python	Pythonidae		Mostly arboreal
Bitis arietans	Puff Adder	Viperidae	Africa and south-west Arabian Peninsula	Terrestrial

Echis pyramidum	Northeast African Carpet Viper	Viperidae	Africa	Terrestrial
Spalerosophis diadema	Diadem Snake	Colubridae		Terrestrial
Python regius	Ball Python	Pythonidae		Terrestrial
Bitis rhinoceros	West African Gaboon Viper	Viperidae	West Africa	Terrestrial
Bitis parviocula	Ethiopian Viper	Viperidae	East Africa	Terrestrial
Bitis cornuta	Many Horned Viper	Viperidae	South Africa	Terrestrial
Bitis rubida	Red Adder	Viperidae	South Africa	Terrestrial
Bitis armata	Southern Adder	Viperidae	South Africa	Terrestrial

2.3.2 Keratin

Snake scales are mostly composed of α-keratin and β-keratin [136]. Keratin also known as *scleroprotein* is a type of fibrous protein. Scales, hair, nails, feathers, horns, claws, hooves, and the outer layer of skin of some vertebrates are composed of keratin. The refractive index of keratin is around 1.55. Thus the snake scales are transparent in the visible light. However, the multicolor observed on different snake scales is created by the pigments or due to the interplay of light (mostly reflecting white scales) with the nano- and micro-structures embedded within the scales.

2.3.3 Melanin

The dorsal scales of the most analyzed snake scales were darker in color. In addition to camouflaging, the thermal melanism hypothesis predicts an ecological advantage of dark-colored animals in cold environments [71-74]. Enhanced growth rate, better body condition, longer activity, improved locomotion performance, and even higher fertility in the female ones are found in dark-colored snakes [79-82]. Snakes contain melanin within their scales. Thus it is assumed that the dorsal sides of snakes appear darker in color due to the absorption of melanin embedded within their scales. Melanin is an indole bichrome which is mostly responsible for the dark coloration of the brown and black scales [118]. Melanin has a broadband absorption spectrum in visible light.

2.3.4 Blue bee

The blue hairs of the female carpenter bee (*Xylocopa caerulea*) of the family Apidae were analyzed in this thesis. The blue hairs are mostly found on the head, thorax, and parts of the abdomen. Carpenter Bees of the genus *Xylocopa* often have bright-colored bodies and/or wings [94]. This vibrant color is important for their intraspecific recognition [94]. For the analysis, the bees were commercially purchased from an online shop [145].

2.3.5 Sample preparation

2.3.5.1 Snake scales

Molted scales were initially cut into small pieces and fixed on a glass substrate with two-component glue (UHU GmbH & Co., Germany) for the AFM imaging. For the SEM and CA measurements, the scales were attached to a silicon substrate with conductive adhesive tape (Fotostrip, Tesa AG, Germany). Some of them were also attached to glass substrates with the same glue. The internal structures of some of the scales were also analyzed. To image the scale cross-section, the scales were initially cut with a sharp razor blade. While cutting the scales the blade was not scratched over the scales; rather they were pressed on the scales to divide them into two halves. Through this process, the possibility of developing artifacts during sample preparation could be reduced by manifolds. The cross-section of snake scales was later fixed on a paper clip for imaging with the SEM. Temperature (21°C – 23°C) and humidity (50% - 70%) were well controlled during storage and measurements of all samples.

2.3.5.2 Blue hairs of female carpenter bee

The blue hairs were plucked from the head, thorax, and abdomen of the female carpenter bee with tweezers for optical microscopy, SEM imaging, and microphotometry analysis. For the imaging and spectroscopic analysis with microphotometry, the hairs were collected on a PTFE, Teflon foil which was wrapped around a glass slide. During the SEM imaging, the hairs were attached to the glass slide using two-component glue (UHU GmbH & Co., Germany). Similar to the snake scales internal structures of the hairs were also imaged with the SEM. Initially, the hairs were cut with a sharp razor blade and were later glued on the edges of a glass slide with two-component glue (UHU GmbH & Co., Germany) on the edges of a glass slide for imaging with the SEM. The hairs were attached in such that one half of the hair was attached to the glass and the other half was freely hanging in the air. Therefore, the cross-sections of the hairs were easily imaged.

2.4 Replication of snake scales

Some of the snake scales were replicated to validate the optical response of their nano- and micro-structures. A soft lithography technique using polydimethylsiloxane (PDMS) mold was used to fabricate replicas in polymethylmethacrylate (PMMA) material [119-120]. A schematic diagram of the replication process is displayed in Figure 2.7.

First, the scales were cleaned carefully with pressurized air. The samples were later attached to a silicon wafer with a double-sided adhesive tape (Fig 2.7a). A mixture of Sylgard Silicone Elastomer 184 and Sylgard Curing Agent 184 was prepared in a ratio of 10:1. The mixture was stirred evenly. To remove the air bubbles introduced due to stirring, the mixture was placed into an evacuated desiccator for 40 minutes. The wafer with the attached snake scales was collected into an aluminum container and the mixture was slowly poured on the snake scales (Fig 2.7b). In the next step, the aluminum container together with the mixture and wafer was carefully placed on a hot plate. The mixture was cured for 10 hours at a constant temperature of 45^0C. This prevented the snake scales from damaging. The hardened mold was separated from the snake scales and was cleaned by an ultrasonic bath with isopropanol. This removed the scale's remnants.

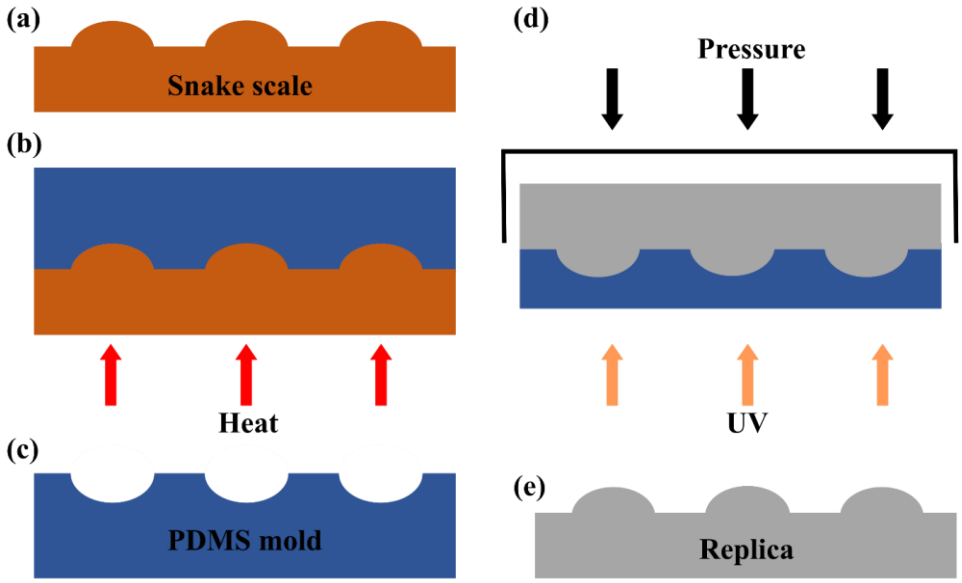

Figure 2.7: Schematic image of the soft lithography process. The snake scale structures are imprinted on PMMA replicas using a PDMS mold. (a) Snake scale with structures on the surface. (b) The mixture of Sylgard Silicone Elastomer 184 and Sylgard Curing Agent 184 is poured onto the scale surface. (c) The snake scales are peeled off from the PDMS after hardening the mixtures on a hot plate at 45 °C for 10 hours. (d) A PMMA droplet is dripped on the PDMS mold and is

pressed to avoid air bubbles. PMMA droplet along with the PDMS mold is allowed to cure for 24 hours. (e) Finally, the polymeric replica with a micro-fibril structured surface is acquired removing it from the PDMS mold.

A droplet of PMMA was dripped on the PDMS mold and a glass slide was carefully pressed into the PMMA droplet to avoid air bubbles on the resulting replica (Fig 2.7d). The PMMA was allowed to cure for 24 hours at room temperature. The snake scale replicas were finally obtained after separating from the PDMS mold (Fig 2.7e)

2.5 Surface characterization

2.5.1 Scanning electron microscopy

Snake scales, nano- and micro-structured polymeric foils, and hairs of blue carpenter bees were investigated by scanning electron microscopy (SEM). Both surface topography and the internal structure of the snake scales and bee hairs were analyzed. In a SEM, the sample is hit with the electrons emitted from an electron gun. These electrons interact with the sample surface and generate secondary electrons. These secondary electrons are collected by the detector to give a depiction of the surface. In this thesis, all the samples were imaged using a Zeiss Supra 60 VP SEM.

Electrons emitted by the cathode, pass through a hollow cylinder called the Wehnelt cylinder. Inside the cylinder, the electrons are accelerated by a voltage of 0.5 to 30 kV. The smallest beam cross section near the anode has a diameter of around 10-50 µm [122]. This spot size is too large to produce a sharp image. Therefore, the crossover is demagnified by the lens system consisting of one or two condenser lenses, apertures, and an objective which results in a reduced beam spot size of about 5-10 nm. The sample is placed on a stage below the microscope column. The sample surface is scanned line by line by beam deflection coils. Two deflection coils for x- and y- deflection are placed in front of the objective lens. Electrons interact with the sample and generate backscattered electrons, secondary electrons, cathodoluminscence/x-rays, Auger electrons, elastically scattered electrons, unscattered electrons, and inelastically scattered electrons. Information concerning the surface topology is contained in the low-energy secondary electrons. These electrons are collected by a detector located laterally above the specimen and an image of the surface is created. The microscope column and specimen chamber are evacuated to reduce the spreading and attenuation of the electron beam by gas molecules. Non-conductive samples suffer charge effects; therefore, non-conductive samples are often coated with an electrically conductive metal (mostly Ag or Au) to obtain high-resolution images. In this study, nonconductive snake scales, polymeric foils, and bee hairs were sputtered with silver at 45 mA

for 120 seconds which is assumed to develop a 10 nm thin layer of Ag on the sample surface. To visualize the internal arrangement of snake scales and hairs of blue carpenter bees, the samples were initially cut with a sharp razor blade. Later the cross section was sputtered with Ag to develop a 10 nm thick Ag coating which is necessary for the imaging. The cross sections were then imaged using SEM.

2.5.2 Atomic force microscopy

Atomic Force microscope (AFM) is one of the most indispensable and versatile tools for nano-scale imaging and tribology-related analysis. Alongside 3D topological imaging, AFM can be also used to measure contact (adhesion) and lateral forces (friction) [123-124]. SEM images provided a 2D depiction of the sample. Therefore AFM was further used to visualize the surface morphology in 3D. The AFM experiments were conducted with the Dimension Icon AFM from Veeco Inc., USA. The cantilevers, All-in-one-Al were purchased from BudgetSensors [143]. A schematic image of the AFM working principle is illustrated in Figure 2.8.

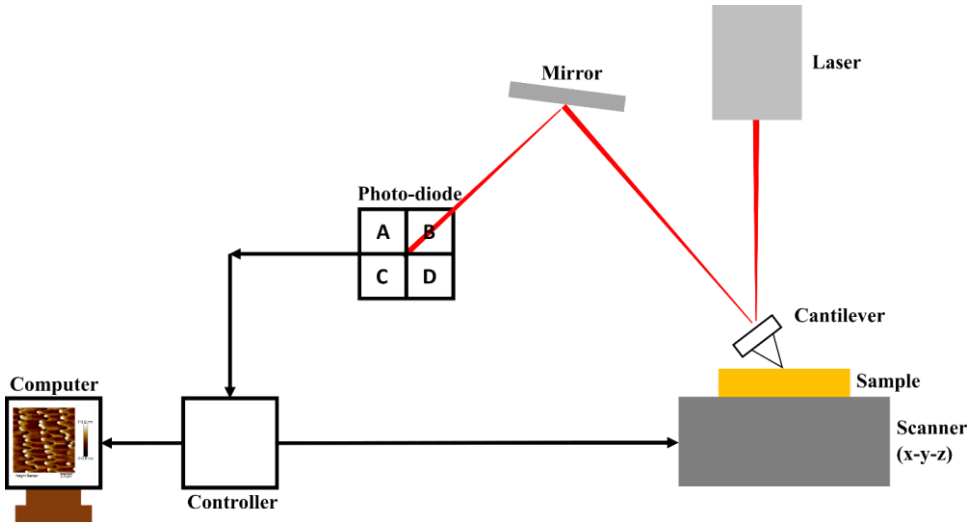

Figure 2.8: Working principle of an AFM. A cantilever with a sharp tip at one end records the bending (topography) or twisting (lateral force measurement) of the structured surface. Deflection of the cantilever (bending for topology and twisting for lateral force measurement) is recorded following the movement of the laser-focused on the backside of the cantilever. The laser is later guided into a photodiode and is finally presented on a screen. Figure has been adapted from [125].

Usually, a sharp pyramid-structured tip is attached to the end of a cantilever which measures the surface topography and lateral force of the sample. The laser beam is focused on the backside of the cantilever tip. The reflected laser beam is calibrated at the center of the photodiode. This laser beam detects the deformation of the cantilever (bending for topology and twisting for lateral force measurement) which is further modified to determine useful information. Initially, the sample is placed on a stage equipped with a controlled x-y-z scanner. The cantilever tip is then brought into contact with the sample surface.

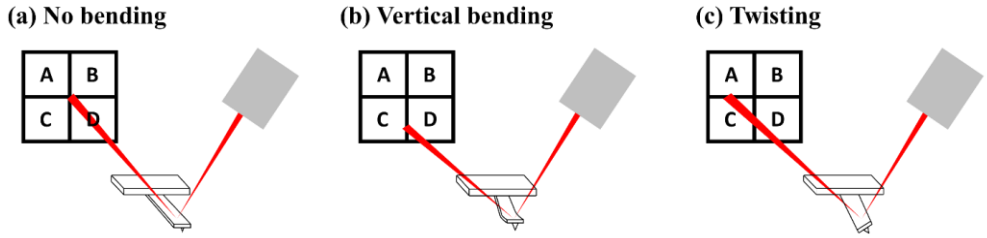

Figure 2.9: Deflection of cantilever leading to the displacement of laser on the photodiode. The laser focus on the backside of the cantilever is reflected onto the photodiode. (a) Before the deformation of the cantilever, the laser was at the central position of the photodiode, usually the state before initiating the measurement (b) The laser moves down with the cantilever vertically bending-associated with the topology measurement (c) The twisting of the cantilever causes the laser to move to the left-associated with the lateral force measurement. Figure has been adapted from [124].

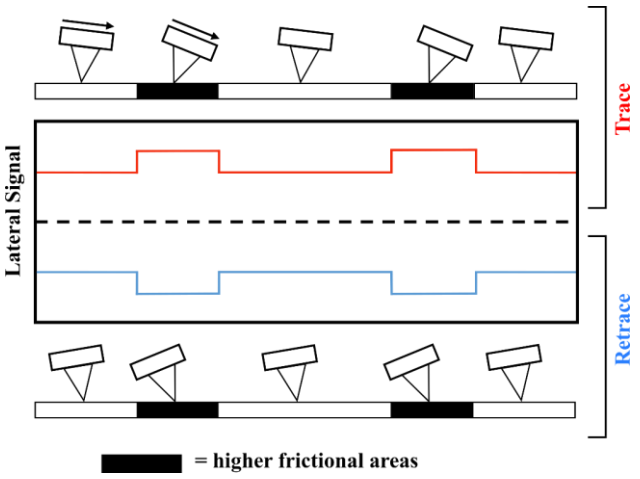

Figure 2.10: The principle of AFM tip measuring the lateral force (friction). The black areas represent the regions with higher friction in comparison with the white areas. When the AFM tip scans from the low friction area to the high friction area, the higher lateral signal is recorded as the tip twists more on the black regions (higher frictional areas). The frictional force of these two

regions can be compared by calculating the differences in lateral forces in trace and retrace directions. Figure has been adapted from [124].

An AFM can be run in several modes. In this thesis tapping and contact mode of the AFM were explored for the snake scales analyses. In contact mode, the cantilever continuously scans over the specific region of interest, and in tapping mode, the cantilever oscillates above the surface. When the cantilever is at rest, the cantilever neither bends nor twists (Fig 2.9a). No measurements are conducted in this stage. During the topography measurements, the bending of the cantilever is recorded. A vertical movement of the reflected laser beam is recorded on the photodiode (Fig 2.9b). During the lateral force measurements, the torsion (twisting) of the cantilever is recorded. The reflected beam on the photodiode moves laterally indicating the torsion of the cantilever (Fig 2.9c).

The basic principle of frictional force measurement using AFM is based on the lateral twisting of the cantilever. When the cantilever scans even over a homogeneous surface, its torsion is different in two different scanning directions [124]. In Figure 2.10, lateral force measurements on low and high-friction surfaces are shown. In contact mode, the cantilever twists while scanning over the sample surface. The twisting of the cantilever is larger when it measures on a high friction region in comparison with the low friction area. This increases the lateral signal. Such torsion is also observed when the scanning direction is reversed. Each scanning cycle of trace and retrace is called a friction loop [126]. Therefore, by calculating the lateral force difference associated with the twisting of the cantilever, the frictional force of a surface can be evaluated.

AFM records the torsion of the cantilever in terms of lateral signal. Therefore, a calibration procedure is needed to be introduced to convert deformation signals (deflection and torsion) to corresponding force (normal load and friction) [127]. Over the years, several force calibration methods have already been proposed [127-131]. In this work, the calibration procedure proposed by Schwarz *et al*. has been adopted [131]. In this method, deflection sensitivity and spring constant are crucial parameters for force calibration with which the normal load and friction force can be calculated as

$$\boldsymbol{F_{load} = \left(\frac{C_z}{S_{ver}}\right).(U_{ver} - U_{dis})} \qquad \textbf{2.21}$$

$$\boldsymbol{F_{fric} = \left(\frac{3C_{tor}}{4L^2 l}\right).\left(\frac{1}{mS_{ver}}\right).(\Delta U_{lat})} \qquad \textbf{2.22}$$

here,

U_{ver} - a set point which can be set manually

U_{dis} - threshold voltage at which the normal load is calibrated to be zero

ΔU_{lat} - voltage difference lateral signal in trace and retrace

S_{ver} - deflection sensitivity of the cantilever

m - correcting parameter of the displacement-dependent voltage between the laser moving in vertical and lateral directions in the photo-diode

C_z - spring constant

C_{tor} - torsional force constant

L - length of the cantilever

l - length of a tip at the cantilever end

For a cantilever with length L, width w, and thickness l, Young's modulus E and torsional modulus G are given by

$$\boldsymbol{C_z = \frac{Et^2w}{4L^3}} \qquad \textbf{2.23}$$

under the condition $t \ll w$, the torsional force constant is

$$\boldsymbol{C_{tor} = \frac{Gwt^3}{3}} \qquad \textbf{2.24}$$

Combining Equations friction force can be rewritten as.

$$\boldsymbol{F_{fric} = \left(\frac{3GL}{El}C_z\right).\left(\frac{1}{mS_{ver}}\right).(\Delta U_{lat})} \qquad \textbf{2.25}$$

In this work, $E = 1.69 \times 10^{11} N/m^2$ and $G = 5.09 \times 10^{10} N/m^2$ are collected from [131]. L and l are adopted from the BudgetSensors [143], m is calibrated by the experimental followed in [131]. S_{ver}, $C_{z,}$ and U_{dis} are determined from the thermal tune method integrated into the corresponding AFM software before every measurement. ΔU_{lat} is calculated from the AFM measurement results ("Friction-trace" and "Friction-retrace" signal in the corresponding AFM panel). Determining the values of all these parameters, the normal load and its corresponding friction force can be calibrated. During the analysis of every measurement, the obtained friction force is plotted versus the applied normal load. The friction coefficient is later calculated by calculating the slope of the curve.

The adhesion of a surface can be measured using the AFM by recording the force-distance curve [132]. Initially, the cantilever is fixed in x and y positions; then it is ramped in the z-direction. When the the tip reaches the sample surface the spring constant and deflection sensitivity of the cantilever are further explored to calculate the force between the cantilever tip and the sample surface. The theoretical basis of the force-distance curve is shown in Figure 2.11. In the following figure, a pyramidal-shaped AFM tip is considered.

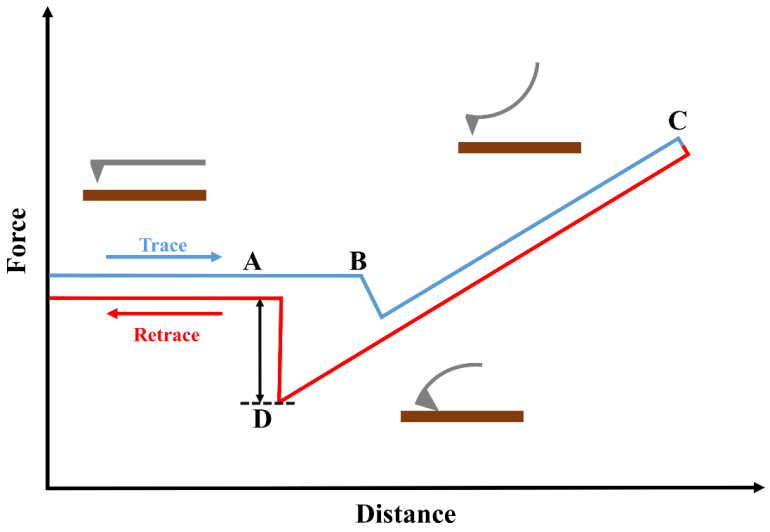

Figure 2.11: Force-distance curve showing an AFM tip measuring the adhesion of a surface. While approaching or retracting from a flat sample, the force on the AFM tip changes forming a pattern. Adhesion is the maximum force required to retract the cantilever tip from the sample surface (at D point). When the cantilever is relaxed above the sample surface (A point), the force on the cantilever is initialized as zero (in both trace and retrace directions). Figure has been adapted from [132].

In reference to Figure 2.11, the cantilever tip is relaxed over the sample surface during the process from point A to B. At point B tip goes down to the surface, and the resultant attractive forces (*e.g.* Van der Waals forces) between the sample surface and AFM tip pull the tip towards the surface. This phenomenon is often called the "snap-in" of the cantilever. The cantilever continues to force and the tip continues to move down until it reaches point C. At this point, the force is repulsive and causes a linear deflection of the cantilever. The moving direction reverses and the tip starts to retract from the sample surface. The process continues until the cantilever reaches point D and the "snap-out" is initiated as the force applied to the cantilever overcomes the tip-sample adhesion. In this process, the cantilever experiences another linear deflection in

the opposite direction. Finally, the tip moves up to the original point A, and the adhesion measurement cycle is finished. “Trace” (marked in blue) is defined as the approaching process from A to C and the retraction from C to A is called the “retrace” (marked in red).

2.5.3 Contact angle goniometer

Surface energy and adhesion force of solid materials can be analyzed through contact angle measurements. As already mentioned in Chapter 2.1.2 superhydrophobic surfaces show self-cleaning properties; therefore, contact angle measurements were conducted on snake scales in correlation with the nano- and micro-structures often found on their scale surface. The measurements were conducted with an OCA 40 system and the contact angle values were calculated by the corresponding SCA20 software (DataPhysics Instruments, Germany) with the Young-Laplace fitting method.

Initially, the samples were horizontally placed on a motion-controlled platform (x, y, and z direction). A deionized water droplet with a defined volume was dispensed on the sample surface with an actuator-driven syringe. The contour of the liquid and sample surface was extracted and analyzed during the dripping of the water droplet on the sample surface. The droplets were illuminated from the backside and were recorded by a camera during the process.

2.6 Optical microscopy and spectrophotometry

2.6.1 Optical microscopy

As already mentioned in the introduction, nanopores are found inside the hairs of the female carpenter bee which interact with the visible light to increase the reflection. Initially, the hairs were imaged with an optical microscope to assess the light-scattering abilities of the hairs in the visible regime. For the imaging microscope, Axioscope 5/7/Vario equipped with the Axiocam 305 color camera and the software ZEN core V 3.0 (all from Carl Zeiss Microscopy GmbH) were utilized.

2.6.2 UV-Vis-NIR spectrometry

Optical responses of the nano- and microstructures found on the snake scales were recorded using LAMBDA Ultraviolet-Visible-Near Infrared (UV-Vis-NIR) Spectro-photometer 950 from Perkin Elmer. The setup is equipped with a Spectralon® coated 150 mm integrating sphere. The setup uses a Deuterium light source for the ultraviolet (UV) and a halogen light source to emit visible (Vis) and near-infra-red (NIR) light. Thus the nominal spectral range is in the regime of 175 to

3300 nm. During the transmittance measurements, the spectrometer was calibrated by defining the transmittance in the air without placing any sample between the detector and the light source as 100% transmittance. The reflectance measurements were normalized with a diffuse reflectance standard Spectralon® from Labsphere.

During the measurement, a broadband light is initially guided through a slit. The light is then separated into different wavelengths using a movable diffraction grating. Thus the output light beam can be controlled by positioning the grating accordingly. Light of a specific wavelength is then incident on the sample using various mirrors. In conjunction with the integrating sphere both diffusive and total (diffusive + specular) or absolute light reflectance *R*, transmittance *T* can be measured. For separate measurements of transmittance *T* and reflectance *R* Kirchhoff's relationship applies as [144]

$$\mathbf{R + T + A = 1} \qquad \mathbf{2.26}$$

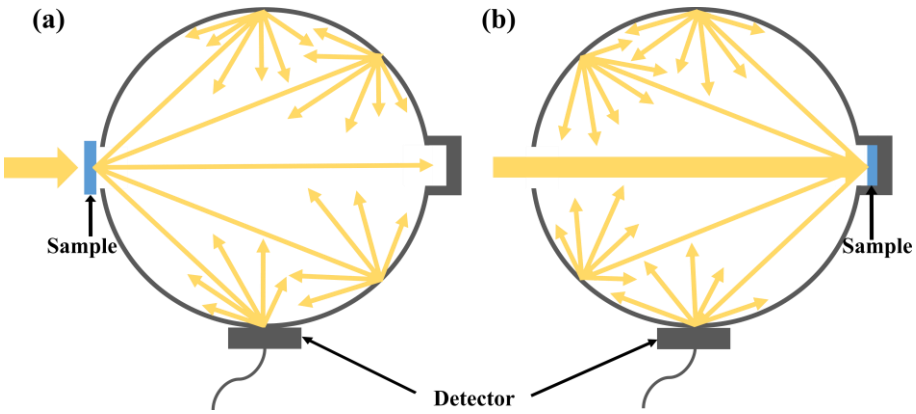

Figure 2.12: Integrating sphere with the sample placement for (a) transmittance and (b) reflective measurements. The intensity of transmitted and reflected light is uniform for any spatial angle due to the multiple scattering at the inner walls.

The experimental setup for transmittance and reflectance measurement is presented in Figure 2.12. For transmittance measurements, the sample is placed in front of the integrating sphere and the light passing through the sample is collected on the detector (Fig 2.12a). During the reflection measurement, the sample is placed at the exit port of the integrating sphere (Fig 2.12b). The light inside the sphere is scattered multiple times by the diffusive white walls of the sphere. Thus intensity inside the sphere becomes uniform at any spatial angle due to multiple scattering events.

2.6.3 Micro-photometry

Reliable measurements can be ensured with the UV-Vis-NIR Spectro-photometer. However, beam spot size could be reduced only in the range of 1mm. Therefore, for further reduction of spot size, micro-photometry was applied utilizing a microscope from Leitz Wetzlar, Germany. Xenon lamp was used to illuminate the sample. The tool was used to measure the reflectance of blue hairs of a female carpenter bee.

Incident light passes through a beam splitter and focuses on the sample through a 100X objective with a numerical aperture of NA= 0.95. Light reflected from the sample is then collected with the same objective. Impinging upon the beam splitter half of the light is directed towards a CCD camera (UI 3590 CP-C-HQ-R2, IDS, μeye), and the rest half is collected by a spectrometer (Ocean Insight QP AvaSpec-HS2048, Avantes, UK) via optical fiber (Avantes, UK). Layers of PTFE, Teflon foil was wrapped around a transparent glass slide. This wrapped glass slide was later used as a reference. The reference of this PTFE, Teflon foil wrapped around a glass slide was normalized as 100% reflection.

3 Multifunctionality of the Ventral and Dorsal Scales of Snakes

Snakes live in a wide variety of habitats, climates, and geographical locations. Interestingly, they optimize their ventral and dorsal scales to achieve multifunctional properties such as locomotion, thermoregulation, light scattering, color enhancement, water harvesting, developing anti-contaminating surfaces, and even sound production [35, 44-59, 62, 64-70]. They develop different nano- and micro-structures on or within the scales to achieve such properties. Focusing on locomotion, snakes optimize their ventral scales by growing different nano-structures on the scale surface to ease their locomotion [44-57]. These structures help them to achieve both frictionally anisotropic and frictionally isotropic surfaces which assist them in movement. Generally, snakes locomote using four different gaits- lateral undulation, sidewinding, concertina, and rectilinear. A snake can utilize all four locomotion traits depending on the habitat and requirements. Thus it is challenging to classify snakes based on their locomotion traits. In this chapter, a study is made on different nano-features on the scale surface in correlation with the locomotion traits of snakes. Following the previous studies [44-57], the results of this chapter further confirm that the surface textures optimize the locomotion of snakes. In general, a similarity is found in the nano-structures on their ventral scales. However, many differences are observed in the textures of their dorsal scales. A wide variety of structures with their dimensions ranging from nano- to micro-meter scale is found on their dorsal scale surface. In this chapter, a detailed analysis is also presented on the dorsal scales to understand how these nano- and micro-structures assist snakes to achieve multifunctional properties. The results indicate a universal function of ventral scales in assisting locomotion as well as diverse dedicated functions such as cleaning contaminations or reducing optical transmittance for dorsal scales. A short description of the snake species their families, habitats, and geographic locations were already presented in Chapter 2.

Snake scales have been studied for years to understand their multi-functionalities [34-59, 62-70]. Inspired by these properties, Weibin Wu started his investigations on snake scales in 2016 [142]. As the snakes molt typically every 3-4 months, not enough samples were available to finalize his study. With the availability of scales belonging to snake species from different geographical locations and habitats, I started my study in 2020 for further investigations. In this study, many physical theories are predicted to explain the functionality of these scales. The theories are validated through in-depth analysis of numerous snake species from different habitats and geographical locations. Therefore, in Chapters 3 and 7 some results have been adapted from

the thesis of Weibin Wu to summarize the findings [142]. At the end of these chapters, the results adapted from Weibin Wu's thesis are mentioned.

3.1 Images of scale ornamentations found on the ventral side

The nano-features frequently found on the ventral scales of snakes are often optimized for their locomotion [44-51, 55-57]. Generally, snake locomotion is divided into 4 types- lateral undulation, sidewinding, concertina, and rectilinear. Interestingly, some snakes can follow all four traits; however, sidewinders mostly restrict themselves to the sidewinding gear. Thus, Reiser *et al.* tried to classify snakes into sidewinding and non-sidewinding groups [57]. They observed distinctive features on the ventral scales specific to sidewinder and non-sidewinders. Being inspired by this study a detailed analysis is presented in this work on the ventral scales of snakes in correlation with their locomotion traits.

In Figures 3.1 and 3.2, SEM images of the ventral scales of investigated snake species are presented. SEM images belonging to snake species originating from North- and South America, Europe, and Western Asia are shown in Figure 3.1. Whereas, SEM images of snake species endemic to Asia, Oceania, and Africa are presented in Figure 3.2. Nano- and micro-structures are observed on the ventral scales of most snake species regardless of their geographic location or habitat. An exception is the flat surface topography without any prominent nano-pattern found on the scales of *E. pyramidum* (Fig.3.2j). Finger-like nano-structures are observed on the scales of most snake species. In this work, these features are defined as microfibrils. The microfibrils are oriented from head to tail direction of the snake body. The SEM images in Figures 3.1 and 3.2 are arranged in such a way that the head of the snake points toward the right. In most of the analyzed species, the microfibril pattern is observed. An in-depth analysis of these scales reveals three distinct patterns in these microfibrils: parallel-oriented, willow leaf-shaped, and hierarchical.

In reference to Figure 3.1 and 3.2 parallel oriented microfibrils are found on the ventral scales of Figure 3.1 (a) *C. atrox*; (b) *P. guttatus*; (f) *M. monspessulanus*; (g) *V. u. rakosiensis*; (h) *V. berus*; (i) *V. aspis*; (j) *V. seoanei*; (k) *V. lotievi*; (l) *V. eriwanensis*; (m) *V. renardi* and Figure 3.2 (a) *P. schultzei* and (e) *N. atra*. These microfibrils are quite shallow with a height of around 100 nm; however, the periodicity varies among the species. A periodicity in the range of 3-4 µm is observed on the scales of *P. guttatus*, *M. monspessulanus*, and *N. atra*. Increased periodicity within the range of 5 – 8 µm is observed on the scales of *C. atrox*, *V. berus*, *V. aspis*,

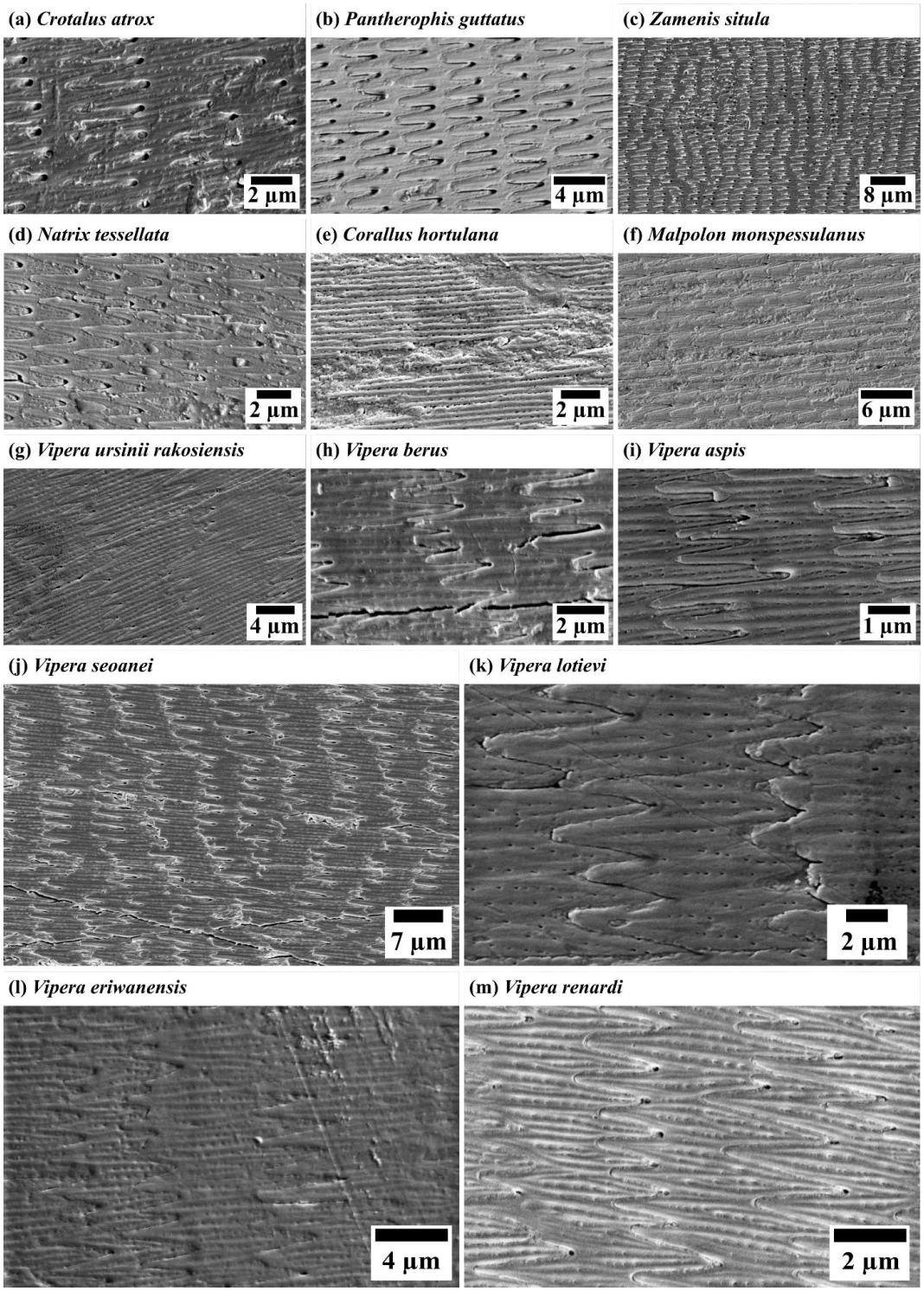

Figure 3.1: *SEM images of the microdermatoglyphic patterns on the ventral scales of snake species from North and South America, Europe, and Western Asia. Most species, i.e., (a) Crotalus atrox; (b) Pantherophis guttatus; (f) Malpolon monspessulanus; (g) Vipera ursinii rakosiensis; (h) Vipera berus; (i) Vipera aspis; (j) Vipera seoanei; (k) Vipera lotievi; (l) Vipera eriwanensis;*

and (m) Vipera renardi show parallel oriented microfibrils. Interestingly, the shape of microfibrils on (c) Zamenis situla and (d) Natrix tessellata resembles a willow leaf. In difference to the mentioned species, a ridge-like reticulate structure oriented along the longitudinal body axis is observed on (e) Corallus hortulana. SEM images in (b) and (f) are adapted from the PhD thesis of Weibin Wu [142]

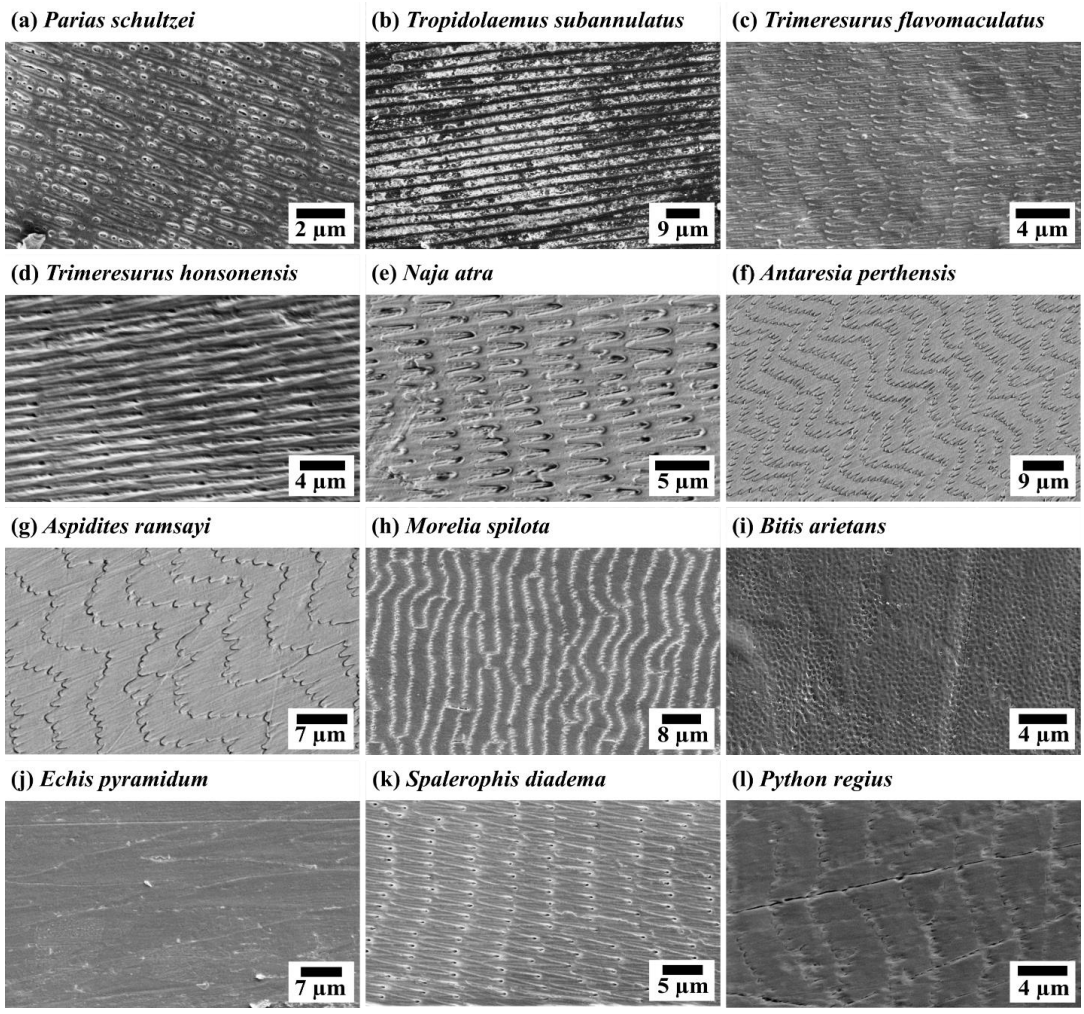

Figure 3.2: *SEM images of the microdermatoglyphic patterns on the ventral scales of snake species from Asia, Oceania, and Africa. Similar to some of the species presented in Figure 3.1, parallel-oriented microfibril patterns are also found on the ventral scales of (a) Parias schultzei and (e) Naja atra. Microfibril pattern in a shape similar to a willow leaf is observed on the scales of (c) Trimeresurus flavomaculatus; (d) Trimeresurus honsonensis and (k) Spalerosophis diadema. The hierarchical pattern is found on (f) Antaresia perthensis; (g) Aspidites ramsayi; (h) Morelia spilota and (l) Python regius. A ridge-like reticulate pattern oriented along the longitudinal body axis is found on (b) Tropidolaemus subannulatus. Nanopits are observed on (i) Bitis arietans and a flat surface with*

no apparent microstructure is found on (j) Echis pyramidum. SEM images in (e), (f), and (g) are adapted from the PhD thesis of Weibin Wu [142]

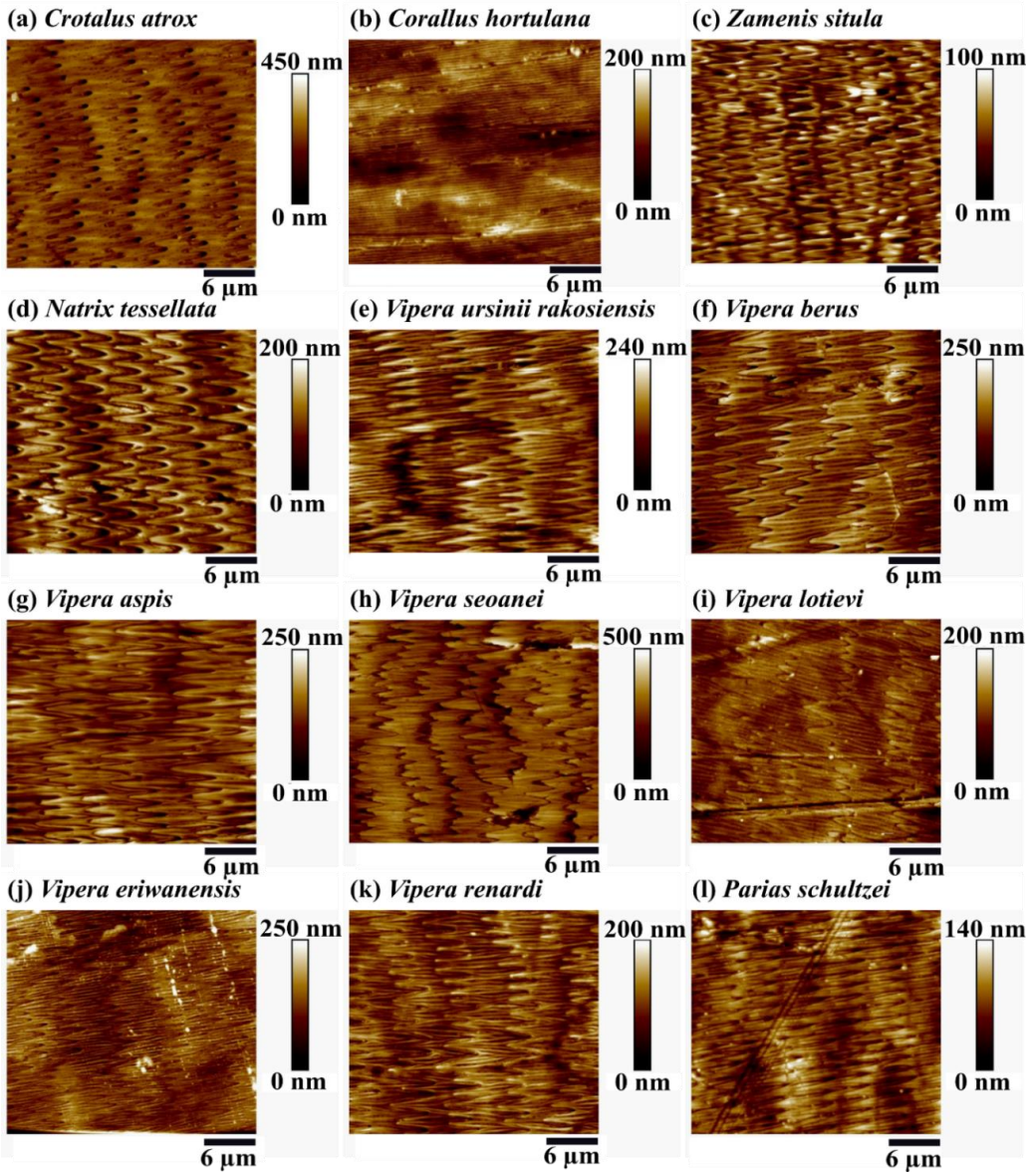

Figure-3.3: *AFM images of the ventral scales of (a) Crotalus atrox; (c) Zamenis situla; (d) Natrix tessellata; (e) Vipera ursinii rakosiensis; (f) Vipera berus; (g) Vipera aspis; (h) Vipera seoanei; (i) Vipera lotievi; (j) Vipera eriwanensis; (k) Vipera renardi; and (l) Parias schultzei show the parallel oriented microfibrils. Alongside microfibrils, nanoridges are found on the scales presented in (h), (i), and (l); both nanoridges and elliptical-shaped nanopits in (a), (e), (f), (g), (j) and (k). A ridge-like reticulate pattern is found on (b) Corallus hortulana. AFM scan area 30 µm.*

V. seoanei, *V. lotievi*, *V. eriwanensis*, *V. renardi*. Among the investigated species, the highest periodicity around 9 - 10 µm was measured on the scales of *V. u. rakosiensis*. This is the most commonly found microfibril pattern on the ventral scales.

Willow leaf-shaped microfibrils are found on the ventral scales of *Z. situla* (Fig 3.1c), *N. tessellata* (Fig 3.1d), *T. flavomaculatus* (Fig 3.2c), *T. honsonensis* (Fig 3.2d) and *S. diadema* (Fig 3.2k). The length and width of these structures are in the range of 1.5 to 4 µm and 0.6 to 1.5 µm respectively.

Reiser et al. showed that snake species showing microfibrils on the ventral scales tend to follow non sidewinding locomotion traits [57]. Our results show that microfibrils are observed on the ventral scales of these analyzed species. In addition, the dimensions of these structures are comparable to the species analyzed by *Reiser et al.*. Thus it can be assumed that these analyzed species are non-sidewinders as they develop microfibrils on their ventral scales. A ridge-like reticulate structure is observed on the scales of *C. hortulana* (Fig 3.1e) and *T. subannulatus* (Fig 3.2b). These ridges are also oriented from head to tail direction of the snake body. For the scales of *C. hortulana* and *T. subannulatus*, the width of these ridges is about 400 nm and 1.5 - 2 µm respectively. In 2010, Berthe *et al.* assumed that such ridges help snakes to climb (trees for example) [52]. They further showed that the ventral scales of *C. hortulana* develop frictional force anisotropy by these nanofeatures [52]. Here, the frictional force anisotropy is created due to the difference in friction force along the longitudinal and perpendicular directions of these ridges. High friction is observed across the perpendicular direction; whereas low friction along the longitudinal axis. In addition to *C. hortulana* it is assumed that the nano ridges on the scales of *T. subannulatus* are also optimized for snake climbing. As these ridges develop frictional force anisotropy it is concluded that the snakes belong to the group of non-sidewinders.

Numerous nanopits are observed on the ventral scales of *B. arietans* (Fig 3.2i). These nano-pits are about 50 nm in diameter and 30 nm in depth. This species utilizes the rectilinear locomotion trait. These nanopits do not develop frictional anisotropy, it rather develop a frictional isotropic surface which is fortunate for sidewinding locomotion [57]. Rectilinear locomotion involves the reorientation of the whole ventral scale. Thus, the contribution of frictional anisotropy by the microfibrils is probably unnecessary in this case which might result in the development of nanopits instead of microfibrils. Thus their development on the ventral scales of snakes showing the rectilinear locomotion traits remains an open research question.

A flat topography is observed on the ventral scales of *E. pyramidum*. A previous study reported that this species sidewinds occasionally [146]. As the species is a sidewinder, they should not require a frictionally anisotropic surface for locomotion. Thus, it is assumed that the snake chose to develop a flat topography instead of microfibrils on their ventral scales as it sidewinds.

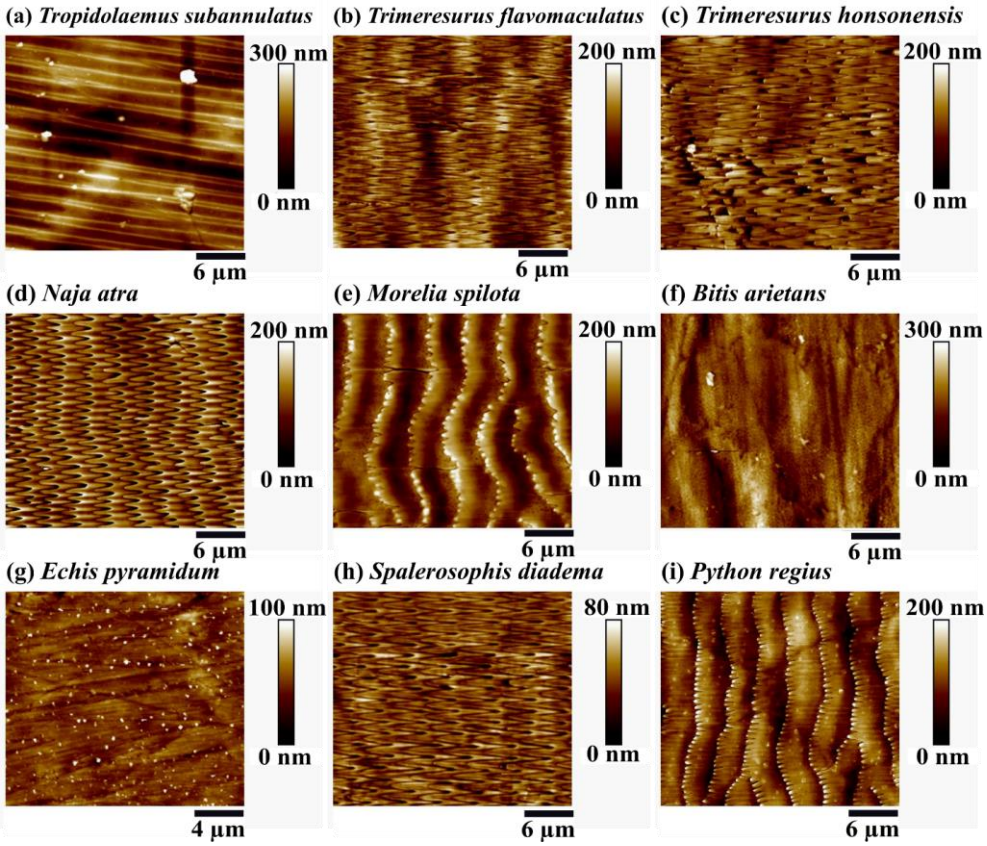

Figure 3.4: *The AFM images show ridge-like reticulate pattern on (a) Tropidolaemus subannulatus; parallel microfibrils on (b) Trimeresurus flavomaculatus; (c) Trimeresurus honsonensis; (d) Naja atra; (e) Morelia spilota; (h) Spalerosophis diadema and (i) Python regius. Alongside these microfibrils, ridges are also found on the scales of the species presented in (b); elliptical nanopits on (e) and (i). Nanopits are found on (f) Bitis arietans. When investigating the scales of (g) Echis pyramidum, it shows a very flat surface with no prominent nano- or micro-structure. AFM scan area 30 µm.*

It is widely accepted by the scientific community that the geometry and orientation of these microfibrils generate frictional anisotropy [44-51, 55-56]. To determine the size of the structures in three dimensions, AFM measurements were conducted on the ventral scales. The images are presented in Figures 3.3 and 3.4. Low friction is observed from the head to the tail

direction. Whereas, high friction from the tail to the head direction. This frictional force anisotropy is developed by the microfibrils which assist snakes in locomotion. In a recent study, this property was further verified using AFM, measuring across these nano-features with a sharp silicon cantilever [56].

Microfibrils found on the scales of *Z. situla* (Fig 3.3c) and *S. diadema* (Fig 3.4h) showed a height of around 20-30 nm. Height in the range of 40-60 nm is observed on the scales of *N. tessellata* (Fig 3.3d), *V. u. rakosiensis* (Fig 3.3e), *V. lotievi* (Fig 3.3i), *V. eriwanensis* (Fig 3.3j), *T. flavomaculatus* (Fig 3.4b), *P. schultzei* (Fig 3.3l), and *N. atra* (Fig 3.4d). Microfibrils on *V. berus* (Fig 3.3f), *V. aspis* (Fig 3.3g), *V. seoanei* (Fig 3.3h), *V. renardi* (Fig 3.3k) and *T. honsonensis* (Fig 3.4c) are much more prominent and a height around 80-90 nm is observed on these species. *M. spilota* (Fig 3.4e) and *P. regius* (Fig 3.4i) showed a height of around 120-150 nm. Shallow microfibrils are observed on the scales of *C.* atrox (Fig 3.4a). In the AFM image nanopits are observed alongside these microfibrils. These nanopits are about 300 nm in diameter. The depth of these nanopits is in the range 300-350 nm which is much higher in comparison with the ones found on the ventral scales of other snake species.

The ridge-like reticulate pattern observed on the scales of *C. hortulana* (Fig 3.3b) and *T. subannulatus* (Fig 3.4a) showed heights around 70 and 120 nm respectively. Studies show that these features assist snakes in climbing [52]. Such height information might reflect the locomotion ability of different species. Interestingly such ridges were also observed on the scales of *C. atrox*, *V. u. rakosiensis*, *V. berus*, *V. aspis*, *V. seoanei*, *V. lotievi*, *V. eriwanensis*, *V. renardi*, *P. schultzei*, and *T. flavomaculatus* alongside the microfibril pattern. The width of these ridges varies in the range of 300 to 600 nm. In general, these ridges are quite shallow and the height varies in the range of 20 to 60 nm. In accordance with the microfibrils, these ridges are also oriented in head-to-tail direction. As the width and height of the nano-ridges are comparable to the dimensions of ridges found on the scales of *C. hortulana*; it can speculated that these structures also help these snakes to climb.

In addition to the microfibrils and ridges, shallow nanopits are found on the scales of *C. atrox*, *V. u. rakosiensis*, *V. berus*, *V. aspis*, *V. eriwanensis*, *V. renardi*, *M. spilota*, and *P. regius*. The major axes of these elliptical nanopits are about 1.5 times those of the minor axes. These pits are around 200 to 400 nm in diameter with a depth of about 10 to 70 nm. These nanopits generate frictionally isotropic surfaces which assist sidewinding locomotion [57]. A snake can follow all four locomotion gears when necessary. Thus it is assumed that nanopits on the scales might help

these non-sidewinders in sidewinding locomotion. Similar to the SEM images, no prominent structure is observed on the scales of *E. pyramidum* (Fig 3.4g).

Usually length and mass of snakes have a positive relationship [133]. These physical properties vary among the species. This study further confirms that the height and periodicity of the microfibrils vary among the species. Microfibrils with heights of 20 nm (*Z. situla*) and even as high as 150 nm (*P. regius*) were recorded. The physical properties (mass and length) and dimensions of these microfibrils vary among the species. It was speculated that there is a relation between the physical properties and microfibril dimensions. To consider the effect of both mass and length, their ratio is plotted vs. the height of the microfibrils in Figure 3.5. The length and mass of these investigated species are collected from the works of Feldman *et al*. [133]. Interestingly, an increase in microfibril height is observed with the increase in mass-length ratio. The analysis indicates that heavier snakes develop more pronounced microfibrils. This effect might have a direct impact on increasing the frictional anisotropy to ease locomotion.

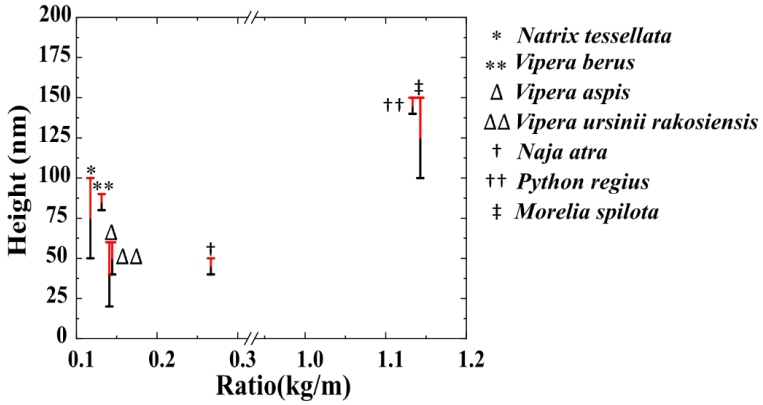

Figure 3.5: *Height of the nanostructures vs. mass-length ratio. As a general trend, an increase in height is observed with the increase in mass-length ratio.*

Microfibrils found on the ventral scales develop lower frictional force while moving forward and higher frictional force while moving backward. The results in Figure 3.1-3.4, indicate that the height and periodicity of these structures vary among the species. In a recent publication, Wu *et al.* showed that higher microfibril tips induce higher frictional anisotropy [56]. Therefore, these naturally grown microfibrils with varying dimensions might have a significant effect in optimizing locomotion. The results in Figure 3.5 indicate that the height of the microfibrils increases with the increase in mass-length ratio. To further investigate this optimization a comparative study is made on the frictional anisotropy of the ventral scales of some snake species

and the mass-length ratio of the subsequent species. The frictional forces were measured on the scales from head to tail and tail to the head direction.

Weibin Wu already analyzed the friction force of three snake species using the AFM [56]. In this thesis, the frictional force and the frictional force anisotropy of the snake scales were measured and analyzed following the methodology established by Weibin Wu [56,142]. An AFM tip measured against (trace) and along (retrace) the nano-features to record the topological and frictional force information. Thus measurements were conducted both in the direction from head to the tail (along the microfibrils) and tail to the head (against the microfibrils) direction of the snake body. Details about the measurement technique were presented in Chapter 2, Section 2.5.2.

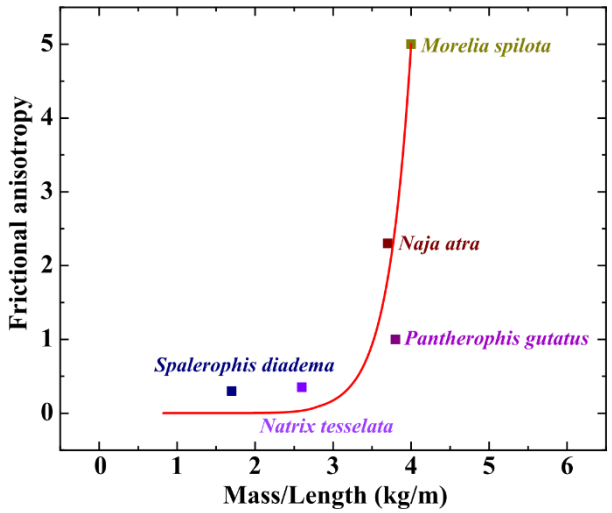

Figure 3.6: *Frictional anisotropy vs. mass-length ratio for selected snake species. The anisotropy increases with the increase in mass-length ratio.*

The comparative analysis shows that snake scales develop higher frictional force from the tail-to-head direction (against the microfibrils) and lower frictional force in head to head-to-tail direction (along the structure). The anisotropy is obtained by comparing the friction forces recorded against and along the microfibrils. Here, frictional anisotropy is defined as the ratio of friction coefficient obtained while measuring against and along the microfibrils meaning from tail to head and head to tail direction of the snake species.

A comparative study is made on the frictional anisotropy of scales belonging to five different snakes and their subsequent mass length ratio. Results presented in Figure 3.6 indicate that the frictional anisotropy increases with the increase in mass-length ratio. This increase in anisotropy is related to the increase in height of these microfibrils. The red line is not a

mathematical curve, rather it is used to guide the reader's eye to identify the relation between frictional anisotropy and mass-length ratio. Results indicate that the heavier snakes optimize their microfibrils accordingly to generate higher frictional anisotropy.

Nano-features found on the ventral scales are optimized for specific snake locomotion. These finger-like projections defined as microfibrils are quite shallow (height around 120-150 nm) and their height and periodicity vary among the species. Interestingly, height and frictional anisotropy of the ventral scales increase with the increase in mass-length ratio of the subsequent snake species. Thus it further confirms that these naturally grown structures are optimized to ease snake locomotion.

3.2 Imaging of scale ornamentations found on the dorsal side

In the previous studies, it was already suggested that snakes optimize their dorsal scales to achieve optical, thermoregulatory, water harvesting properties and even to produce sound [35, 62, 64-70]. Therefore, the surface topography of dorsal scales of investigated snake species was also examined to understand if the nano- and micro-structures are optimized to achieve any specific functionality.

Much diversity is observed in the dorsal scale pattering. The geometry of these structures varied a lot among the species. The SEM and AFM images are presented in Figures 3.7, 3.8, 3.9, and 3.10. Ridge-like reticulate patterns are observed on the scales of *C. atrox* (Fig 3.7a), *P. guttatus* (Fig 3.7b), *N. tessellata* (Fig 3.7e), *V. berus* (Fig 3.7g), *V. u. rakosiensis* (Fig 3.7j), *V. lotievi* (Fig 3.7k) and *V. eriwanensis* (Fig 3.7l). To relate to the multi-functionality of these ridges, a 3D depiction of these scales was necessary. Therefore, AFM analyses were conducted on the scales of *C. atrox* (Fig 3.9a), *N. tessellata* (Fig 3.9d), *V. u. rakosiensis* (Fig 3.9f), *V. berus* (Fig 3.9g), *V. lotievi* (Fig 3.9j) and *V. eriwanensis* (Fig 3.9k). The ridges are about 0.5 µm in width and show a height of around 300 - 500 nm. Such ridges are also observed on the dorsal scales of *T. subannulatus* (Fig 3.8b and 3.10b). Pronounced structures with a height and width of around 2.5 µm are observed on this species. It is already speculated that these ridges on the ventral side of *C. hortulana* might assist snakes in locomotion; the ridges on their dorsal scales are much more prominent. Thus it is assumed that these ridges help snakes to climb or to curl around the branches of the trees.

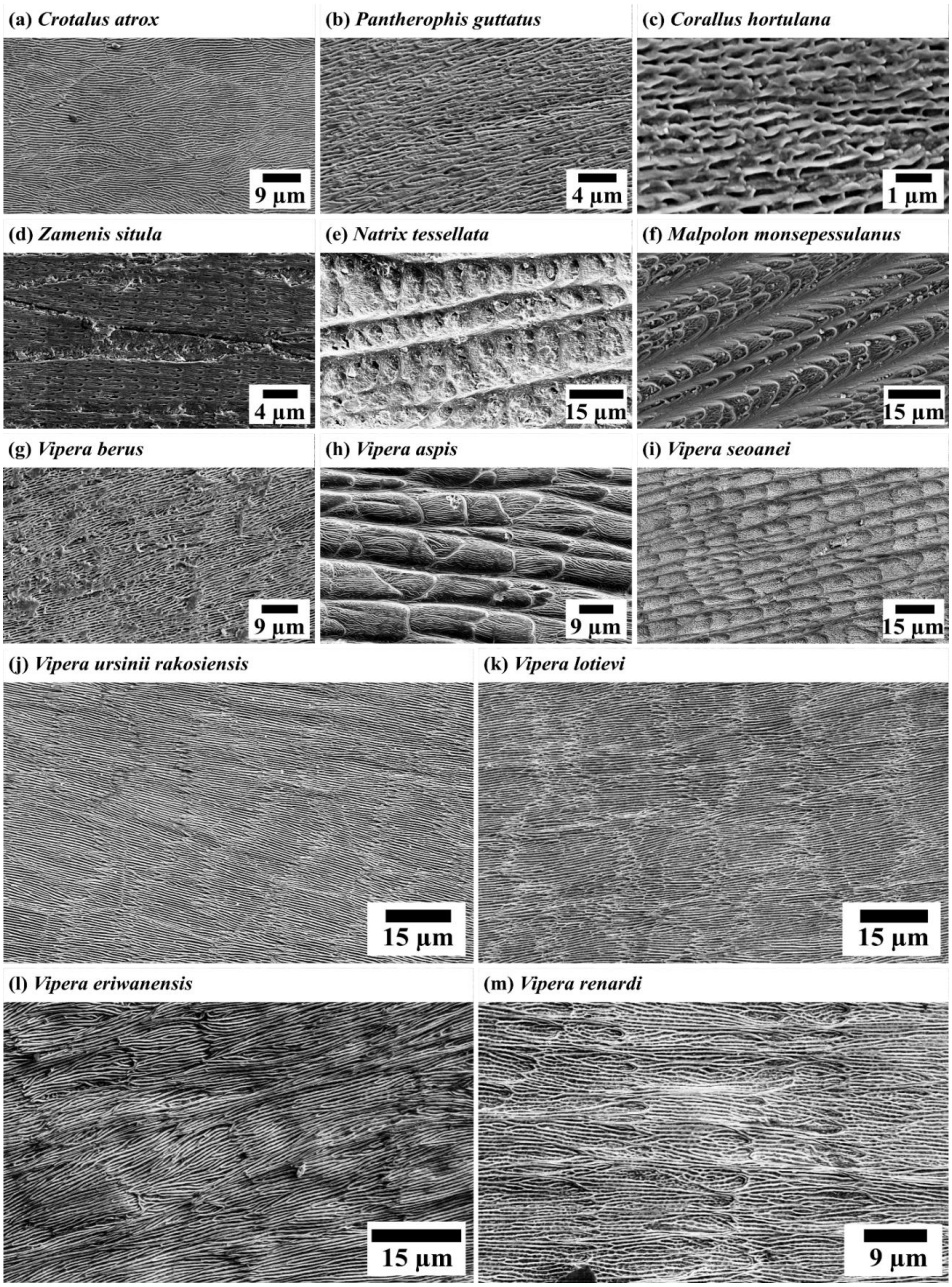

Figure 3.7: *SEM imaging of the dorsal scales of the snake species of North, South American, European, and Western-Asian origin is presented. A ridge-like reticulate pattern with no substructure is found on (a) Crotalus atrox; (b) Pantherophis guttatus; with a reticulate substructure on (e) Natrix tessellata; (j) Vipera ursinii rakosiensis; (g) Vipera berus; (k) Vipera lotievi; (l) Vipera eriwanensis; Canaliculated patterning with cross-hatching ribs on (f) Malpolon monspessulanus; cross-hatching ribs with reticulate substructure on (h) Vipera aspis; (i) Vipera seoanei (m) Vipera renardi. Polygonal juxtaposed pattering on (c) Corallus hortulana. Lamellate*

imbricate with echinate substructure on (d) Zamenis situla. Some of these terms to describe the pattern types follow Reference [42].

Among the investigated species, a major type of lamellate imbricate pattern is observed in seven species. Much diversity is found in the substructure. The echinate pattern is found on the scales of *Z. situla* (Fig 3.7d and 3.9c), *P. regius* (Fig 3.8l and 3.10i), *A. perthensis* (Fig 3.8f), and *A. ramsayi* (Fig 3.8g). Among these *Z. situla* belongs to the Colubridae family; whereas the rest belong to the family of Pythonidae. Interestingly, a difference is also observed in their geographical locations. *A. perthensis* and *A. ramsayi* belong to the Oceania region; however, *Z. situla* and *P. regius* are European and African snakes. This result indicates that the micro-patterns of snake species might be similar regardless of their difference in family or geographical locations. Periodicity in the range of 3.5-4 µm is observed for the structures found on the scales of *Z. situla* and *P. regius*. However, much height difference is observed among these two species. Height of 15-20 nm and 150 nm is measured on the scales of *Z. situla* and *P. regius* respectively. An echinostriate pattern is found on the Asian snake species *N. atra.* These microfibrils showed a height and periodicity around 50 to 100 nm and 3.5 to 4 µm respectively (Fig 3.8e and 3.10e).

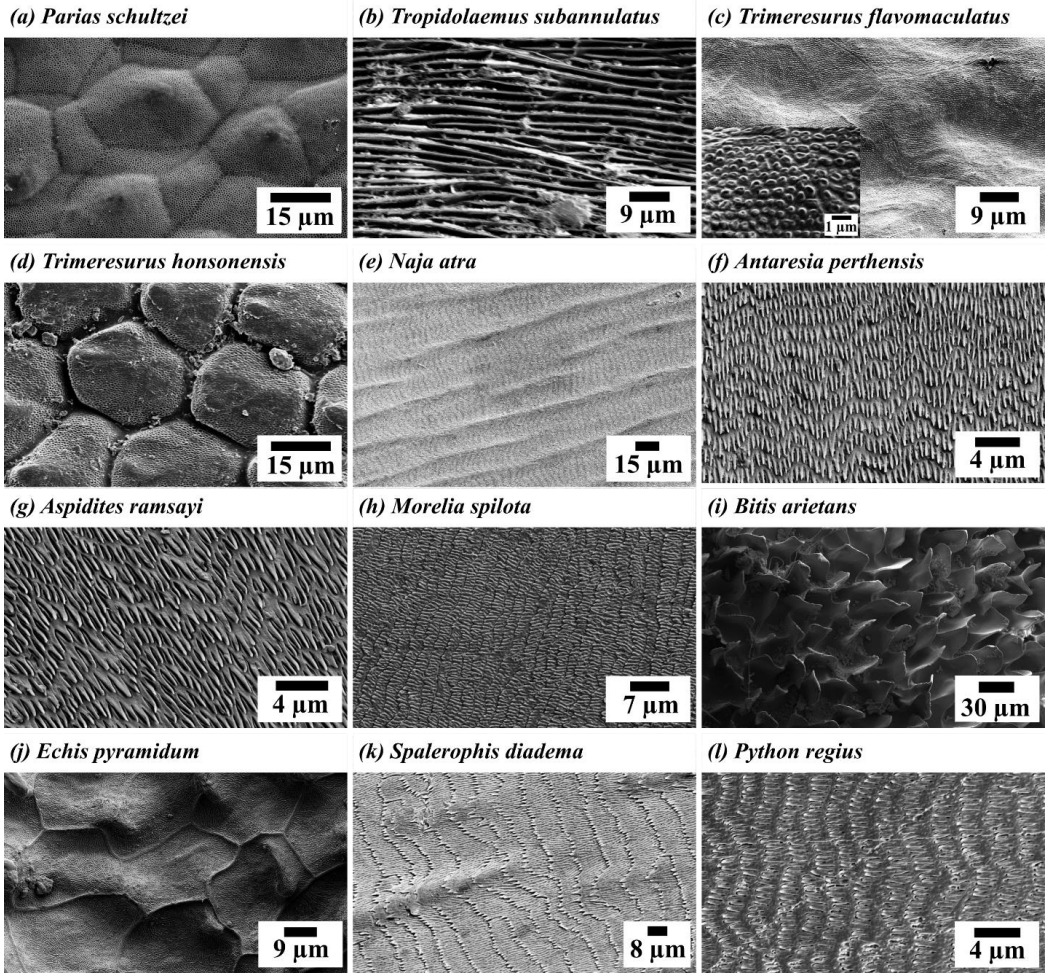

Figure 3.8 *SEM images of the investigated snake species in Asia, Oceania, and Africa. Dome-shaped microstructure with porous nanostructure is found on (a) Parias schultzei; and (d) Trimeresurus honsonensis. A ridge-like reticulate pattern with reticulate substructure on (b) Tropidolaemus subannulatus. Lamellate imbricate pattern with echinate substructure are found on (f) Antaresia perthensis (g) Aspidites ramsayi (l) Python regius; echinostriate (e) Naja atra; papillate-(h) Morelia spilota; reticulate and echinate-(k) Spalerosophis diadema. Foveated with raised cell borders observed on (c) Trimeresurus flavomaculatus (nibble-like substructure shown in the inset) and (i) Bitis arietans. Verrucate and polygonal juxtaposed reticulate microstructuring on (j) Echis pyramidum. Microstructures found on the dorsal scales of P. schultzei, T. honsonensis, T. flavomaculatus, and B. arietans are almost perpendicular to the scale's surface. Therefore the scales were tilted by* 30^0 *while imaging.*

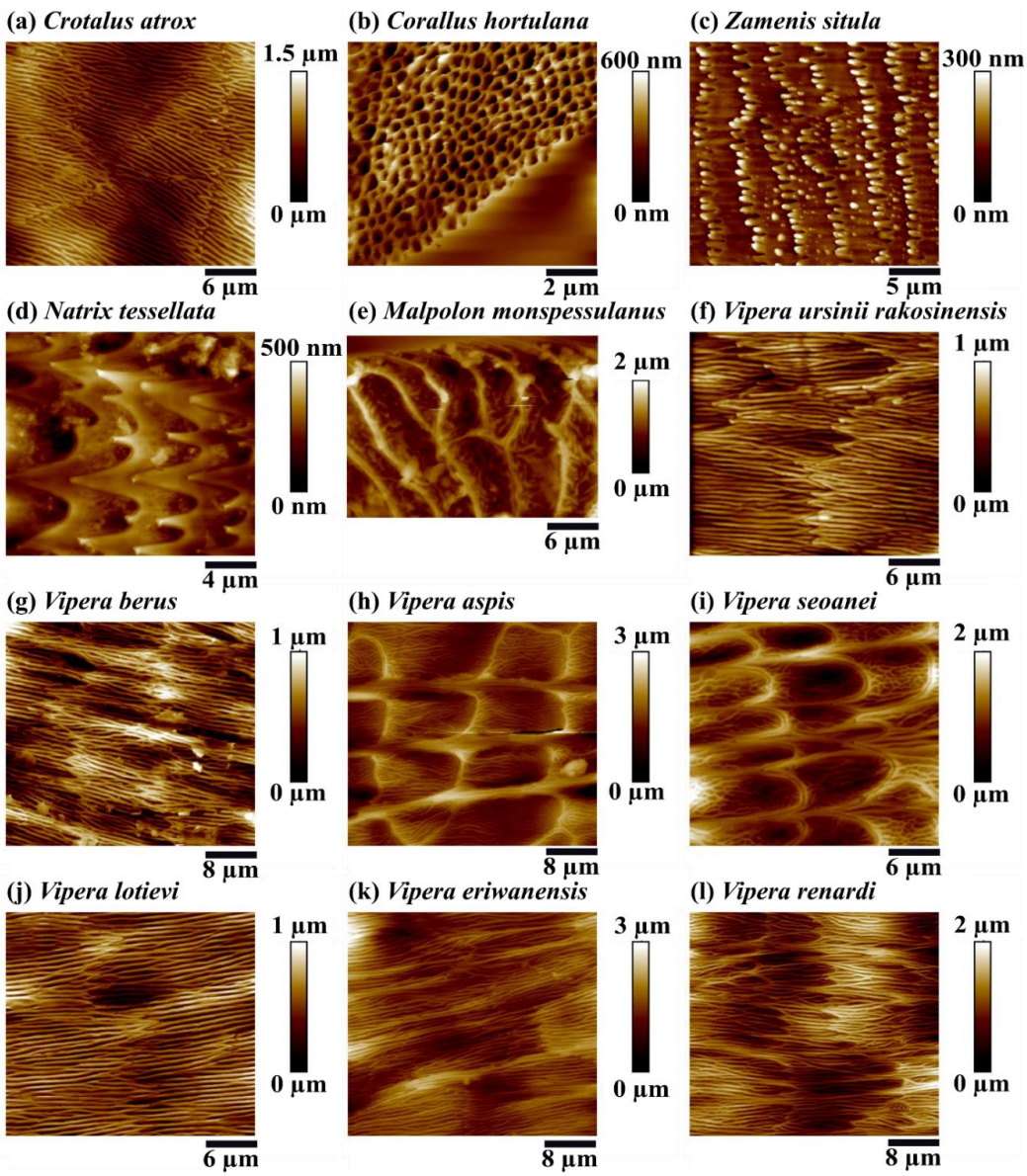

Figure 3.9: *The AFM images present in detail the ridge-like reticulate pattern on (a) Crotalus atrox; (d) Natrix tessellata; (f) Vipera ursinii rakosiensis; (g) Vipera berus; (j) Vipera lotievi and (k) Vipera eriwanensis. Polygonal juxtaposed structuring on (b) Corallus hortulana and lamellate imbricate echinate pattering on (c) Zamenis situla. Canaliculated cross-hatching ribs are found on (e) Malpolon monspessulanus; (h) Vipera aspis; (i) Vipera seoanei and (l) Vipera renardi. Scan area in (b) 10 µm; (d) 20 µm; (c) 25 µm; (a), (e), (f), (i), (j) is 30 µm; (g), (h), (k), (l) 40 µm*

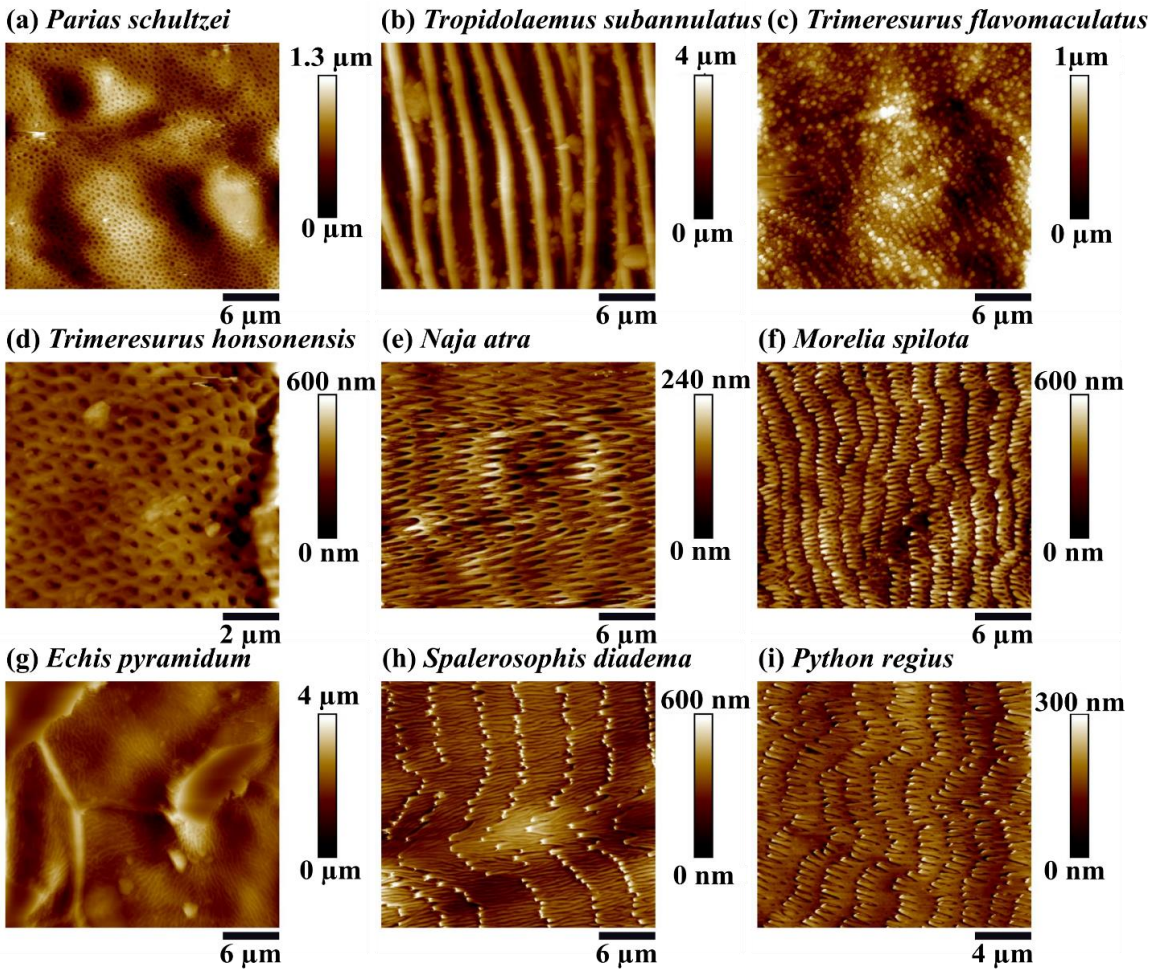

Figure 3.10: *AFM images reveal the nanostructured pits on (a) Parias schultzei; (d) Trimeresurus honsonensis; nibbles on (c) Trimeresurus flavomaculatus; ridge-like structure on (b) Tropidolaemus subannulatus; verrucate and polygonal patterning on (g) Echis pyramidum. Lamellate imbricate major structure with substructure, echinostriate-(e) Naja atra; papillate-(f) Morelia spilota; reticulate and echinate-(h) Spalerosophis diadema; echinate-(i) Python regius is observed. Scan area in (d) 10 µm; (i) 20 µm; (a), (b), (c), (e), (f), (g), (h) 30 µm.*

M. spilota belonging to the Pythonidae family and originating from the Oceania region is different from *A. perthensis* and *A. ramsayi* and shows a papillate substructure. The height and periodicity of these structures are measured to be around 250 - 400 nm and 2.5 µm respectively (Fig 3.8h and 3.10f). Interestingly, both reticulate and echinate substructures with a height of 250 - 450 nm and a periodicity of 5 to 6 µm are observed on the scales of *S. diadema* (Fig 3.8k and 3.10h).

Canaliculated patterns with crosshatching ribs are found on the scales of *V. aspis* (Fig 3.7h and 3.9h), *V. seoanei* (Fig 3.7i and 3.9i), *and V. renardi* (Fig 3.7m and 3.9l). Much pronounced microfibrils are observed on the dorsal side of these species. These micro-structures have a periodicity and height of around 10-12 µm and 1 µm respectively. Alongside these parallel-oriented microfibrils extending from head to tail direction, nano-ridges are also observed. These ridges have a width of around 0.5 µm and a height in the range of 200-500 nm. Interestingly, *M. monspessulanus* from the family of Lamprophiidae show similar micro-features on their dorsal scales (Fig 3.7f and 3.9l).

In contrast to the ridges, lamellate imbricate patterns and canaliculated polygonal juxtaposed or honeycomb-like features are found on the scales of *C. hortulana* (Fig 3.7c and 3.9b). These pits are 250-300 nm in depth and about 1 µm in diameter. Polygonal juxtaposed structures with numerous ridges are also observed on the scales of *E. pyramidum*. These ridges have a height of around 2.5 µm (Fig 3.8j and 3.10g). Dorsal scales of *P. schultzei* (Fig 3.8a and 3.10a) and *T. honsonensis* (Fig 3.8d and 3.10d) show dome-shaped micro-structures. Numerous nanopits are observed on the surface of these micro-domes. These nanopits show a depth of 150-350 nm when they are measured with an AFM. Foveated with raised cell borders are observed on the scales of *T. flavomaculatus* (Fig 3.8c and 3.10c). These nibble-like nanofeatures observed in addition to these primary structures are about 150-250 nm in both diameter and height. Pillar-like structures with a height of around 30 µm are observed on the scales of *B. arietans* (Fig 3.8i). Microstructures found on dorsal scales of *P. schultzei, T. honsonensis, T. flavomaculatus,* and *B. arietans* are perpendicular to the scale's surface. Therefore the scales were tilted by 30^0 while imaging. The detailed classification of the major and sub-structures of the scales is summarized in Table 3.1.

In general, nano- and micro-ridges are observed on the dorsal scales of most snake species excluding *P. schultzei, T. flavomaculatus, T. honsonensis, B. arietans, E. pyramidum,* and *C. hortulana*. These nanoridges found on the ventral scales assist snakes in climbing [52]. As similar structures are found on the dorsal scales it can be assumed that these structures might help snakes to curl around trees to avoid slipping. Phadnis *et al.* showed that some snakes use their dorsal

scales for rainwater harvesting [103]. Their results further indicated that nano-ridges on their structures assist them in water harvesting as they show high contact angles. Similar nanoridges are also observed on the dorsal scales of most snake species. Besides, micro-structures with comparable height and width are observed on the dorsal scales of some snake species which might result in high contact angles. Thus the wetting properties of the dorsal scales are further analyzed in comparison with the ventral scales to understand the effect of surface textures.

3.3 Wettability analysis of the ventral and dorsal scales

Wettability can be controlled by developing random textures on the surfaces. In nature, different biological systems develop hierarchical nano- and micro-structures on the surface to tailor wetting properties. In 1997 Barthlott *et al.* showed that micro-structures on the leaves of the Lotus plant promote the self-cleaning properties of these leaves [11]. These micro-structures on the leaf surface decrease adhesion force due to the reduction in contact area resulting in the reduced surface energy [11]. This decreased surface energy results in high water contact angles (CA) and low roll-off angles. Such high contact angles and low roll-off angles enhance the wet self-cleaning properties of textured surfaces [11]. Topological analysis of the ventral and dorsal scales reveals nano- and micro-structures on the surface. These structures might affect the wetting properties of these scales. In 2019, Phadnis *et al.* showed that the water harvesting mechanism on the dorsal scales of *C. atrox* is enhanced when in contact with the nano-ridges found on the scale surface [101]. A high contact angle of around 120° was recorded. This high contact angle resulted in the accumulation of water on the snake's body and enhanced the water harvesting process.

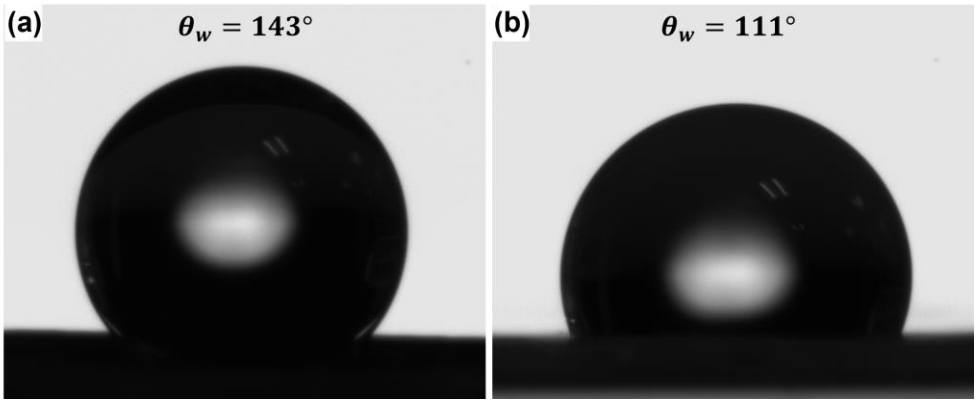

Figure 3.11: *Water contact angle measurement on (a) dorsal and (b) ventral scales of Sisturus miliarius barbouri with 1 µL droplet volume.* (The figure is adapted from the thesis of Weibin Wu [142]).

Inspired by this study the wettability of the snake scales was measured to understand if their scale textures promote wet self-cleaning or water harvesting properties. The results of CA

measurements are summarized in Table 3.1. In general, a higher contact angle is observed on the dorsal scales in comparison with the ventral scales. This could be attributed to the pronounced nano- and micro-structures on their scale surface.

Figure 3.11 shows a 1 µL water droplet on the dorsal and ventral surface of *S. miliarius* revealing the corresponding contact angle of 143° and 111°, respectively. The higher value found on the dorsal scale reveals that the dorsal scale of *S. miliarius* is more hydrophobic than the ventral ones. Figure 3.11 is adapted from the PhD thesis of Weibin Wu [142]

For the investigated snake species, an average CA over 140° is observed on the scales of *B. arietans* and *V. aspis.* Such high CAs could be related to the micro-structures on the dorsal scales. CAs around 130° to 140° were recorded on the dorsal scales of *P. guttatus, M. monspessulanus, P. schultzei, T. flavomaculatus, A. perthensis, A. ramsayi* and *M. spilota*. CAs between 120° and 130° were recorded on the dorsal scales of *C. atrox, C. hortulana, V. u. rakosiensis, N. atra* and *S. diadema*. The size of the dorsal scales of *Z. situla, N. tessellata, V. berus, V. seoanei, V. lotievi, V. eriwanensis, V. renardi, T. subannulatus, E. pyramidum* and *P. regius* were less than 1mm. Thus contact angle measurements on these small scales could not be conducted with the available equipment. This variation in the CAs across the species could be attributed to the difference in nano- and micro-structures on the dorsal scales.

In general, CAs around 110° were recorded on the ventral side of the investigated snake species. The reduced CA in comparison to dorsal scales can be attributed to the reduced aspect ratio (ratio of the height and periodicity) of these microfibrils. Further reduced CAs were recorded on the scales of *B. arietans* (59°), *T. subannulatus* (60°), *T. flavomaculatus* (97°), *P. regius* (98°) and *C. hortulana* (98°). Water droplets spread on the ventral scales of *B. arietans* and *T. subannulatus* the moment a droplet was dripped on the scale surface. Therefore, the results confirm that scale ornamentations on these scales resulted in a hydrophilic surface with a low contact angle. Hierarchical structures on dorsal snake scales are superior to the microfibril structure found on the ventral scales. These high values suggest that some snakes carefully decorate their dorsal scales to achieve high contact angles. However, these values are not high enough to conclude that these structures assist snake scales to achieve self-cleaning properties. However, these CAs are comparable to CA observed on the dorsal scales of *C. atrox* [101]. Thus it can be assumed that the surface textures might help snakes to harvest water on their scales.

Table 3.1: *Overview of the measured micro-ornamentation pattern and water CAs of the twenty-five investigated snake species, sorted by the geographic location of the studied specimens. The terms used to describe the patterns follow the work of Price [42]. All scales featuring a transmission peak at 250 nm are marked with an † (related to section 3.4).*

Binomial name	**Family**	**Geographic range**	**Micro-ornamentation**			**Water CA**	
			Ventral scale	**Dorsal scale**		**Ventral scale**	**Dorsal scale**
				Major pattern type	**Subtype**		
Crotalus atrox	Viperidae	North America	Parallel orientated microfibrils	Ridge-like reticulate pattern	-	110 ± 1°	129 ± 4°
Pantherophis guttatus	Colubridae		Parallel orientated microfibrils	Ridge-like reticulate pattern	-	108 ± 1° ++	133 ± 2° ++
Corallus hortulana	Boidae	South America	Ridge-like reticulate pattern†	Polygonal juxtaposed†	-	98 ± 8° ++	121 ± 4° ++
Zamenis situla	Colubridae	Europe	Willow leaf shaped microfibrils†	Lamellate imbricate†	Echinate	108 ± 4°	*
Natrix tessellata	Colubridae		Willow leaf shaped microfibrils†	Ridge-like reticulate pattern†	Microfibril pattern	108 ± 5°	*
Malpolon monspessulanus	Psammophiidae		Parallel orientated microfibrils	Canaliculated	Cross-hatching ribs	118 ± 5° ++	130 ± 7° ++
Vipera ursinii rakosiensis	Viperidae		Parallel orientated microfibrils	Ridge-like reticulate pattern	-	106 ± 4°	123 ± 2°

Vipera berus	Viperidae		Parallel orientated microfibrils	Ridge-like reticulate pattern	-	106 ± 3°	*
Vipera aspis	Viperidae		Parallel orientated microfibrils	Canaliculated†	Cross-hatching ribs and reticulate	111 ± 1° ++	141 ± 4° ++
Vipera seoanei	Viperidae		Parallel orientated microfibrils†	Canaliculated†	Cross-hatching ribs and reticulate	107 ± 3°	*
Vipera lotievi	Viperidae	Eastern Europe	Parallel orientated microfibrils	Ridge-like reticulate pattern†	-	112 ± 1°	*
Vipera eriwanensis	Viperidae		Parallel orientated microfibrils†	Ridge-like reticulate pattern†	-	105 ± 2°	*
Vipera renardi	Viperidae	Western and Central Asia	Parallel orientated microfibrils†	Canaliculated†	Cross-hatching ribs and reticulate	108 ± 1°	*
Parias schultzei	Viperidae	Asia	Parallel orientated microfibrils†	Dome shaped†	Porous	107 ± 3°	134 ± 2°
Tropidolaemus subannulatus	Viperidae		Ridge-like reticulate pattern†	Ridge-like reticulate pattern†	-	60 ± 7°	*
Trimeresurus flavomaculatus	Viperidae		Willow leaf shaped microfibrils†	Foveated with raised cell border†	Nibble	97 ± 7°	138 ± 6°

Trimeresurus honsonensis	Viperidae		Willow leaf shaped microfibrils†	Dome shaped†	Porous	103 ± 2°	125 ± °
Naja atra	Elapidae		Parallel orientated microfibrils	Lamellate imbricate	Echinostriate	111 ± 1° ++	122 ± 4° ++
Antaresia perthensis	Pythonidae	Oceania	hierarchical microfibrils	Lamellate imbricate	Echinate	110 ± 2° ++	135 ± 5° ++
Aspidites ramsayi	Pythonidae		Hierarchical microfibril	Lamellate imbricate	Echinate	102 ± 6° ++	133 ± 4° ++
Morelia spilota	Pythonidae		Hierarchical microfibrils	Lamellate imbricate	Papillate	108 ± 2° ++	134 ± 6° ++
Bitis arietans	Viperidae	Africa and south-west Arabian Peninsula	Porous surface with nanoholes	Foveated with raised cell border	Reticulate and porous	59 ± 3°	145 ± 3° ++
Echis pyramidum	Viperidae	Africa	Flat surface with no structure†	Verrucate and polygonal juxtaposed†	Reticulate	*	*
Spalerosophis diadema	Colubridae		Willow leaf shaped microfibrils†	Lamellate imbricate†	Reticulate and echinate	109 ± 2°	126 ± 5° ++
Python regius	Pythonidae		Hierarchical microfibrils	Lamellate imbricate	Echinate	98 ± 4°	*

† Optical transmission peak at 250 nm

- No structure found

* Scales were too small (diameter of single scale < 1 mm) to conduct reliable measurements

++ Contact angle data collected from the PhD thesis of Weibin Wu

3.4 Optical properties of the ventral and dorsal scales

Nano- and micro-features sometimes enhance the optical properties of structured surfaces. In the topographical analyses, both nano- and micro-structures are observed on the ventral and dorsal scales of snakes. Therefore, the optical properties of the scales were recorded in the wavelength range of 200-800 nm to determine if these structures respond to UV and visible light.

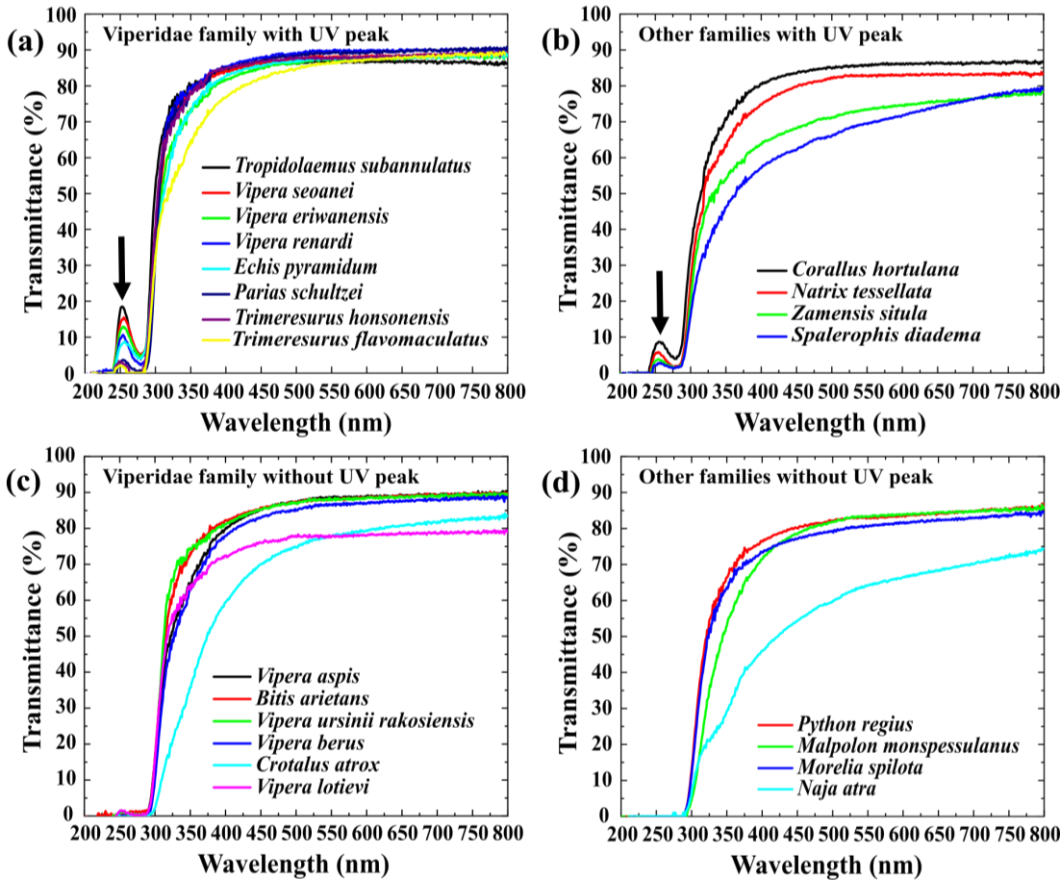

Figure 3.12: *Optical transmittance of the ventral scales measured in the UV and visible range. Almost half of the measured spectra show an additional transmittance peak in the UV close to 250 nm (see arrow in (a, b)). To allow for easy comparison, all spectra showing a UV transmittance peak are plotted for the snake species belonging to (a) Viperidae and (b) other families. Spectra without the UV transmittance peak is plotted for snake species belonging to (c) Viperidae and (d) other families.*

Figure 3.12 presents the transmittance properties of the ventral scales. In general, the examined scales showed transparency in the range of 70-90% for visible light. Interestingly, a UV transmittance peak is recorded close to 250 nm for some species. To allow an easy comparison

the optical response of the species belonging to Viperidae and other families which showed the UV peak are plotted in Figure 3.12a) and 3.12b). Transmittance curves without the peaks in the UV regime for species belonging to Viperidae and other families are presented in Figure 3.12c) and 3.12d) respectively.

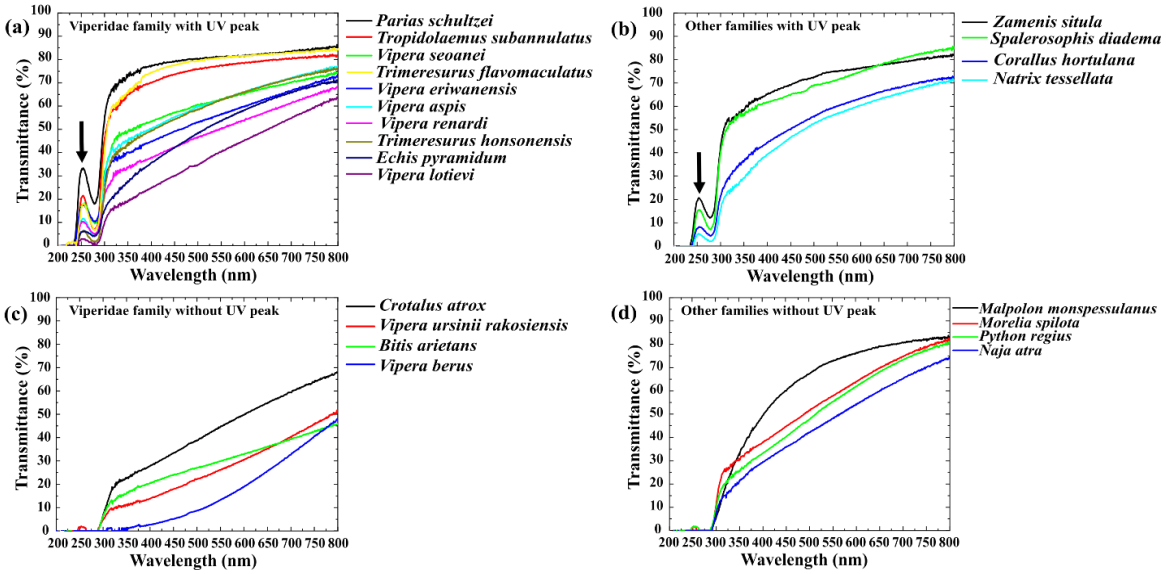

Figure 3.13: *Optical transmittance of the dorsal scales measured in the UV and visible ranges. For ease of analysis, the spectra of the species showing the UV peak (black arrow) are divided into (a) the Viperidae family and (b) other families. The spectra without UV peaks are shown in (c) for the Viperidae family and in (d) for other families.*

Most of the examined ventral scales are transparent in the visible light. However, reduced transmittance is observed for the ventral scales of *V. lotievi*, *C. atrox*, *N. atra*, *Z. situla*, and *S. diadema*. As a general trend transmittance of these scales reduced to 50% in wavelength range of 300-400 nm. It indicates that these scales are transparent even in UV light. However, a 50% transmission cut-off is observed at higher wavelengths for *M. monspessulanus* (344 nm), *C. atrox* (427 nm), *N. atra* (423 nm), and *S. diadema* (437 nm). This might be caused by the absorption of melanin which could be present within the scales or reflection. The optical transmittance of the dorsal scales of some snake species was also measured. The results are summarized in Figure 3.13. Interestingly, similar to the ventral scales, UV transmittance peaks are also observed on the dorsal scales of some snakes. Species belonging to Viperidae and other families with the UV transmittance peak are plotted in Figure 3.13a and 3.13b, respectively; whereas spectra without peaks for the species belonging to Viperidae and other families are presented in Figure 3.13c and 3.13d, respectively.

In general, the optical transmittance of the dorsal scales is lower in comparison with the ventral scales. Transmittance is even as low as 50% for most of the scales in visible light. However, 50% transmittance cut-off is observed for lower wavelength for the scales of *P. schultzei* (297 nm), *T. subannulatus* (305 nm), *Z. situla* (307 nm), *T. flavomaculatus* (304 nm), and *S. diadema* (313 nm). It indicates that these scales are more transparent than the other dorsal scales.

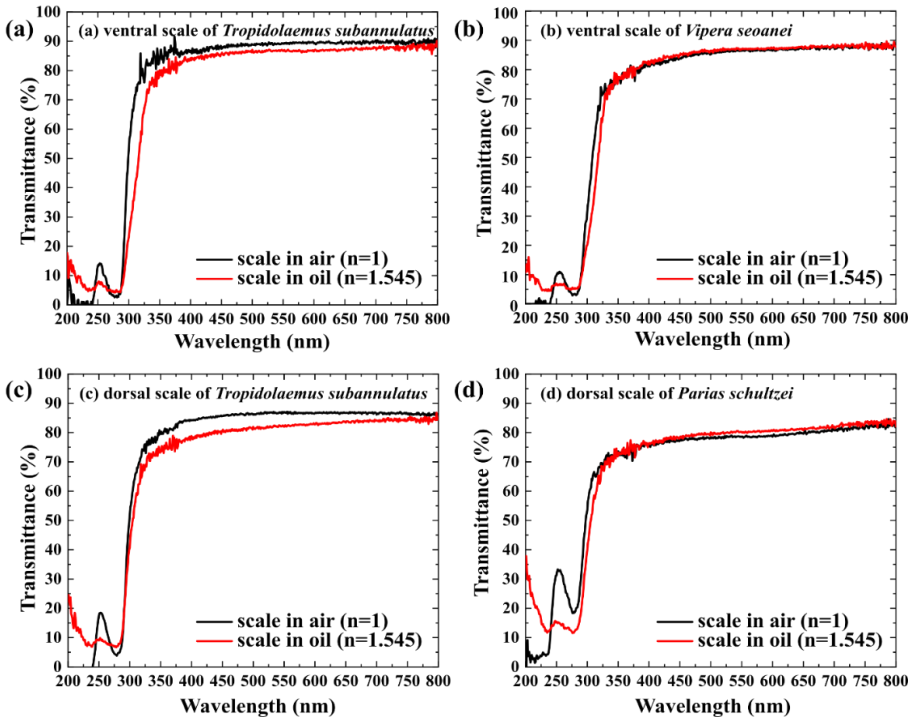

Figure 3.14: *Transmittance measurement of some arbitrarily chosen scales in the air (black line) and index-matching oil (n=1.545, red line). The UV peak close to 250 nm vanishes or greatly reduces when measured in oil. (a) Ventral scale of T. subannulatus. (b) Ventral scale of V. seoanei. (c) Dorsal scale of T. subannulatus. (d) Dorsal scale P. schultzei.*

The overall decrease in transmittance for the dorsal scales might be caused by the absorption of melanin. In 2020, Martínez-Freiría *et al.* suggested that the dark dorsal scales of some snake species control the thermoregulation within the snake body [77]. Therefore, the results also conclude that the dorsal scales showed reduced transmittance due to the absorption by melanin which is fortunate for thermoregulation within the snake body [75-82].

Regardless of the body location, UV transmittance peaks are observed on both dorsal and ventral scales of some snake species. However, these peaks are more enhanced on the dorsal scales in comparison with the ventral scales. The topological analysis confirms that nano-pits found on the dorsal scales are much deeper and denser in comparison with the ones found on the

ventral scales. The highest transmittance peak is observed for the dorsal scales of *P. schultzei*, which might be facilitated by the nanopits found on the scale surface with a depth of 250-350 nm (Fig.3.5a and Fig.3.7a). However, these UV peaks are also observed on the scales which did not show any nano-pits (ventral scales of *T. honsonensis* or *S. diadema*). Therefore, it is assumed that this UV peak might be a material property that might be additionally enhanced by the nano-structures on the scale surface.

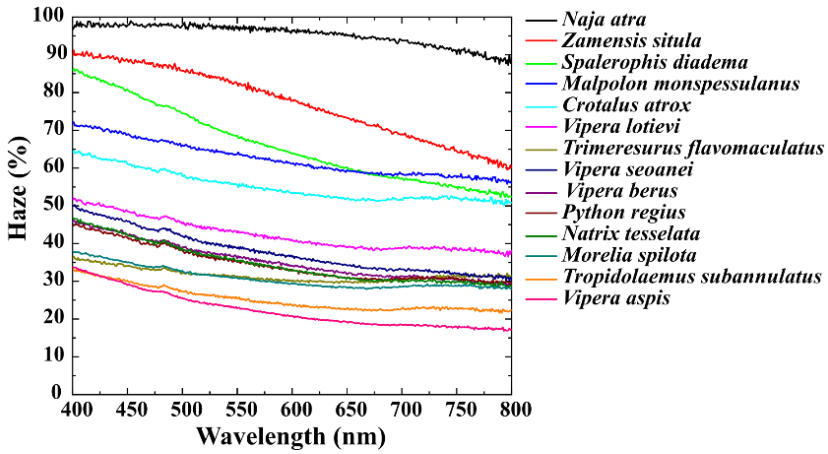

Figure 3.15: *Haze vs. wavelength measured in the range of 400-800 nm. Ventral scales which showed microfibrils are only considered for this investigation. Much variation is observed in the optical property which is attributed to the dimensions of these nano-patterns.*

To verify this speculation, the optical transmittance of the ventral scales of *T. subannulatus* (Fig 3.14a) and *V. seoanei* (Fig 3.14b) and dorsal scales of *T. subannulatus* (Fig 3.14c) and *P. schultzei* (Fig 3.14d) was measured in air and refractive index matching oil. The scales were first measured in the air; then drops of index-matching oil were poured on the scale surface. Snake scales are mostly composed of α-keratin and β-keratin [134]. Thus, an index matching oil of 1.545 was used to estimate the refractive index of the snake scales based on the refractive index of snake spectacles (1.5) [135]. The results show that the transmittance peaks of all the analyzed scales reduced when measured in oil. However, it is not reduced to zero which might be caused if the refractive index of index matching oil does not match completely with the effective refractive index of snake scales. The transmittance peak around 250 nm is observed on the dorsal and ventral scales of different snake species. These peaks are observed on the scales where microfibril patterns with nanopores are observed, and it was also observed on the dorsal scales where instead of nanopores or microfibril ridge-like structures are observed. No specific type of surface texture can be associated with the origin of this peak. Thus it is assumed that this UV transmittance peak is a material property that is observed in the low-pigmented scales and

much reduced in the high-pigmented scales. It can be further concluded that UV peaks are not observed on the darker scales as melanin absorbs highly in the UV regime [136]. In the context of the current experiments, the results indicate that the peak around 250 nm is indeed a material property that might be enhanced by the nano-structure on the scale surface. However, these peaks are mostly observed in the low-pigmented scales and much reduced in the high-pigmented scales. As melanin absorbs highly in the UV regime [136], it can be assumed that the peaks are reduced due to the high absorption of melanin within the high-pigmented scales.

In general, scales are transparent in the visible regime. Dark-colored dorsal scales are mostly developed due to the absorption of melanin within the scales. In reference to SEM and AFM images diverse surface topography is found on the ventral and dorsal scales. Such nano- and micro-structures might result in diffusive light transmission. As it is quite inevitable that the texturing on dorsal scales will result in the diffused transmission of light, diffused transmittance of the ventral scales was only recorded. In optics, the degree of this diffused transmittance (or reflection) is often defined as Haze which is the ratio of diffused transmittance (or reflection) to the summation of diffused and specular transmittance (or reflection) [137-138]

$$\textbf{Haze} = \frac{\textbf{diffused transmittance}}{\textbf{diffused transmittance+specular transmittance}} \quad \textbf{(3.1)}$$

here, the angular threshold of light diffusion is considered at 8^{o}.

The haze property was measured on the ventral scales which showed a microfibril pattern. The response of *N. atra*, *Z. situla*, *S. diadema*, *M. monspessulanus*, *C. atrox*, *V. lotievi*, *T. flavomaculatus*, *V. seoanei*, *V. berus*, *P. regius*, *N. tessellata*, *M. spilota*, *T. subannulatus* and *V. aspis* is presented in Figure 3.15a. Haze around 90-95 and 20-30% is observed on the scales of *N. atra* and *V. aspis* in the visible light. The difference could be related to the variation of periodicity of these microfibrils as the height of these nano-features is around 100 nm for all the examined species. Besides, the tilted microcavities found within the ventral scales of *N. atra* might result in the increased haze. A detailed analysis is made on the ventral scales of *N. atra*. The results are presented in Chapter 5. It is assumed that the difference in scattering might be caused by the difference in periodicity (varying in the range of 3-11 μm) of these microfibrils.

In summary, it is demonstrated that snake scales are optimized for specific functionalities. For example, nanofeatures on the ventral scales of most snakes assist in snake locomotion. The pattern of these structures differs depending on the locomotion trait of the specific snake species. Different nano- and micro-structures are also observed on the dorsal scales. Dimensions of these structures range from nano- to micro-meter scales. The specific functionality of these structures

is yet to be found; however, the structures on the dorsal scales showed higher contact angle properties. However, the contact angle values are not high enough to conclude that snakes develop self-cleaning properties on their dorsal. The nanofeatures on the ventral scales show a low contact angle of around 110^{o}. Lower values are observed on the scale surfaces with numerous nanopits. Hydrophilic properties might be observed on the scales, but it should not be very effective for the snakes as the ventral scales are in constant contact with the ground or trees. In general, the ventral scales are transparent in the visible light. Reduced transmittance is observed on the dorsal scales, which might be caused due to the melanin within the scales. In general, it can be concluded that the snakes modify their scales to survive in their respective habitat. In addition to locomotion snakes also modify their scales to achieve specific optical properties.

Results that have been adapted from the PhD thesis of Weibin Wu.

Ventral and dorsal scales of numerous snake species have already been studied in the PhD thesis of Weibin Wu [142]. To validate assumptions some of his results are also presented here. SEM images of the ventral scales of *Pantherophis diadema* (Fig 3.1b), *Malpolon monspessulanus* (Fig 3.1f), *Naja atra* (Fig 3.2e), *Antaresia perthensis* (Fig 3.2f), and *Aspidites ramsayi* (Fig 3.2g) and contact angles of the ventral and dorsal scales of *Corallus hortulana*, *Vipera aspis*, *Malpolon monspessulanus*, *Pantherophis guttatus*, *Antaresia perthensis*, *Aspidites ramsayi*, *Morelia spilota*, and *Naja atra* have been reproduced from the PhD thesis of Weibin Wu [142]. In addition, contact angles of the ventral scales of *Bitis arietans* and dorsal scales of *Spalerosophis diadema* have been reproduced from his thesis [142].

A shortened version of this chapter was published as the conference proceeding "On the structural and optical properties of the Hungarian Meadow Viper (Vipera ursinii rakosiensis)" by KM S. Reza, W. Wu, M. M. Romel, R. Thelen, G. Gomard, H. Hölscher, Proc. SPIE 12481, Bioinspiration, Biomimetics, and Bioreplication XIII, 1248106 (2023)

A shortened version of this chapter will be published as the article, "On the multi-functionality of snake scales: structural properties, wettability, and spectral transmittance of dorsal and ventral scales by the example of twenty-five snake species" by W. Wu, KM S. Reza*, F. Buck, S. Yu, R. Thelen, H. Hölscher, G. Gomard (*both authors equally contributed)*

4 Nanopores Creating Broadband Reflection in Snake Scales

Ventral scales of the snakes are often optimized for efficient snake locomotion through evolution [44-57] and the results presented in Chapter 3 confirm that. In addition to such startling properties, snakes sometimes optimize their ventral scales to fortunate optical and thermoregulatory properties [58-59]. For example, some snakes living in equatorial regions with hot and humid climates and superficially conductive substrates develop white venters [58-59]. Recent studies reported that such reflecting white scales help snakes avoid overheating [59]. In principle, such reflecting white scales can be produced by pigments or through light manipulation by the nano- or microstructures. However, these previous studies do not explain the physical mechanism through which snakes achieve such surfaces. In this chapter, the underlying physics of such white surfaces is discussed. The properties of the reflecting white scales were compared with the transparent or translucent scales. The results evidence that nanopores found inside the reflecting white ventral scales scatter in the UV, visible, and near-infrared regimes. As they reflect near-infrared light, it is assumed that these scales are optimized for efficient thermoregulation within the snake body. In opposite to this, an amorphous structure with no nanopores is found inside the transparent or translucent scales. Interestingly, these scales are also transparent in the UV and near-infrared regimes.

4.1 Imaging of the ventral scales

Surface topology, internal structure, and optical properties of the ventral scales of five African vipers of the genus *Bitis* are analyzed in this work. As these snakes belong to the same genus and geographical origin, they are more closely related to each other. Among them, the Red Adder (*Bitis rubida*), the Southern Adder (*Bitis armata*), and the Ethiopian Viper (*Bitis parviocula*) are only found in South Africa. The Puff Adder (*Bitis arietans*) is found in South Africa and other African countries. The West African Gaboon Viper (*Bitis rhinoceros*) is endemic to West Africa. Details about the species were already presented in Chapter 2.

Investigations of the reflecting white scales of *B. rubida* are presented in Figure 4.1. Photographs of the examined snake species and their ventral scales are displayed in Fig 4.1a) and b), respectively. Molted ventral scales were placed on white paper with a printout of the KIT logo and imaged with a digital camera. In this way, the optical properties of the scales can be easily judged by the naked eye. The photographs confirm that the logo cannot be read through the reflecting white scales of *B. rubida*. The high reflection and strong scattering of the scales hide

the logo underneath it. To study the surface topography, SEM and AFM imaging were conducted on the scale surface. SEM (Fig 4.1c) and AFM (Fig 4.1d) images reveal a ridge-like reticulate pattern on the scales. These structures are oriented from head to tail direction of the snake's body. These ridges have a width and height of around 500 nm and 40-50 nm respectively. Similar ridge-like reticulate patterns are also observed on the transparent or translucent ventral scales of *Corallus hortulana* and *Tropidolaemus subannulatus* (see Fig 3.11 of Chapter 3). The width and height of the ridges observed on the ventral scales of *C. hortulana* are comparable to the ones found on the ventral scales of *B. rubida*. As similar patterns are found on both transparent or translucent and reflecting white scales; it can be assumed that these nanofeatures do not scatter light.

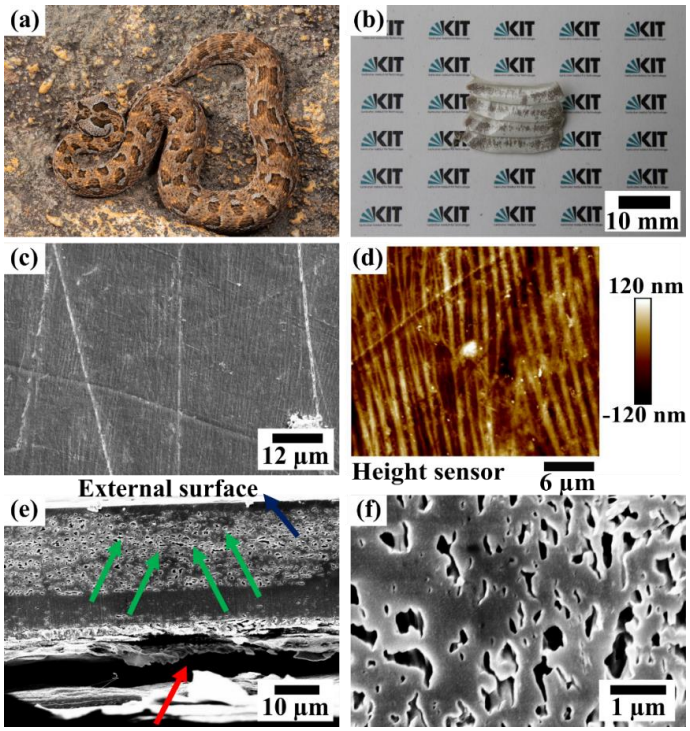

Figure 4.1: *Photographs of* ***(a)*** *the snake B. rubida* ***(b)*** *and its reflecting white ventral scales placed on white paper with the printout of the KIT logo. The logo is hidden by the reflecting white ventral scales.* ***(c)*** *SEM* ***(d)*** *and AFM images of the external surface indicate a shallow ridge-like reticulate structure.* ***(e)*** *SEM imaging of the cross-section reveals the nanopores (marked with green arrows) underneath the external surface. The red arrow indicates the air gap found between the layers of the scales. The blue arrow indicates the external surface* ***(f)*** *Magnified SEM image shows that these nanopores have a random geometry with a typical length of around 0.5 µm.*

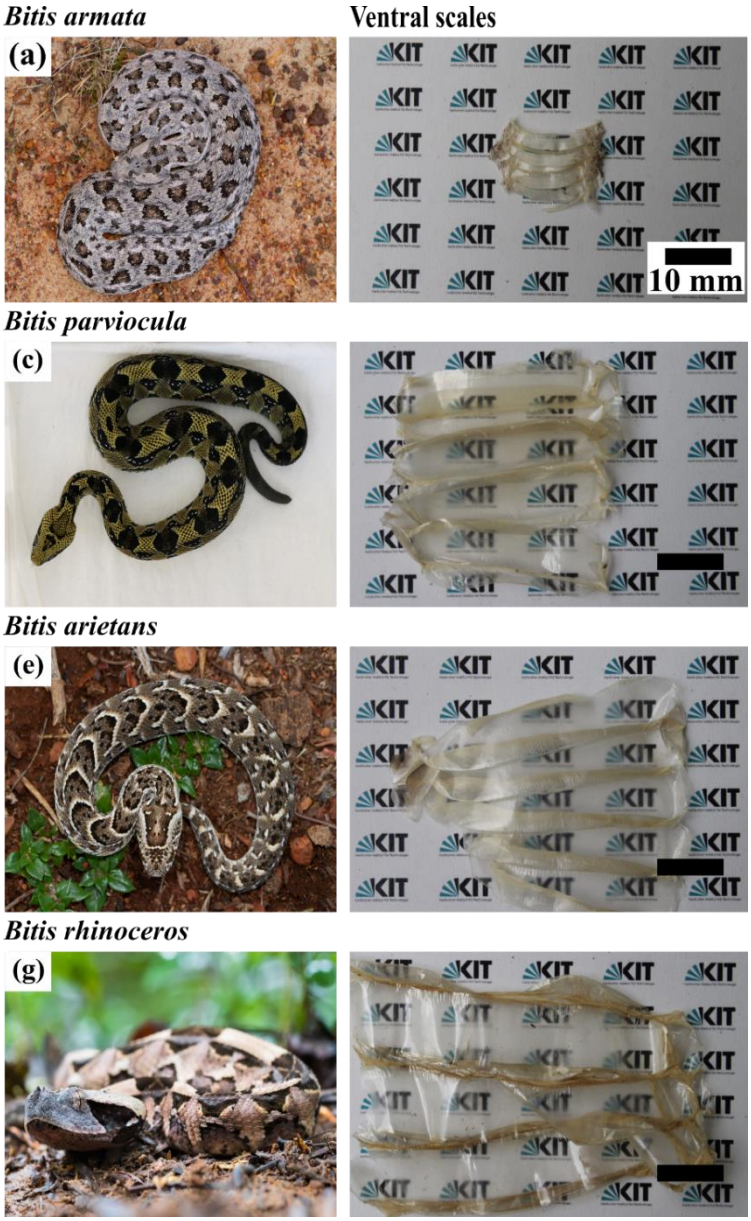

Figure 4.2: *Photographs of the four snake species and their ventral scales placed on white paper with the printout of the KIT logo of* ***(a)*** *B. armata;* ***(b)*** *B. parviocula;* ***(c)*** *B. arietans; and* ***(d)*** *B. rhinoceros. Similar to the scales of B. rubida, the scales of B. armata have high reflection in the visible light and the logo cannot be read through these scales. However, the scales of B. parviocula, B. arietans, and B. rhinoceros are mostly transparent or translucent and the logo is visible through the scales.*

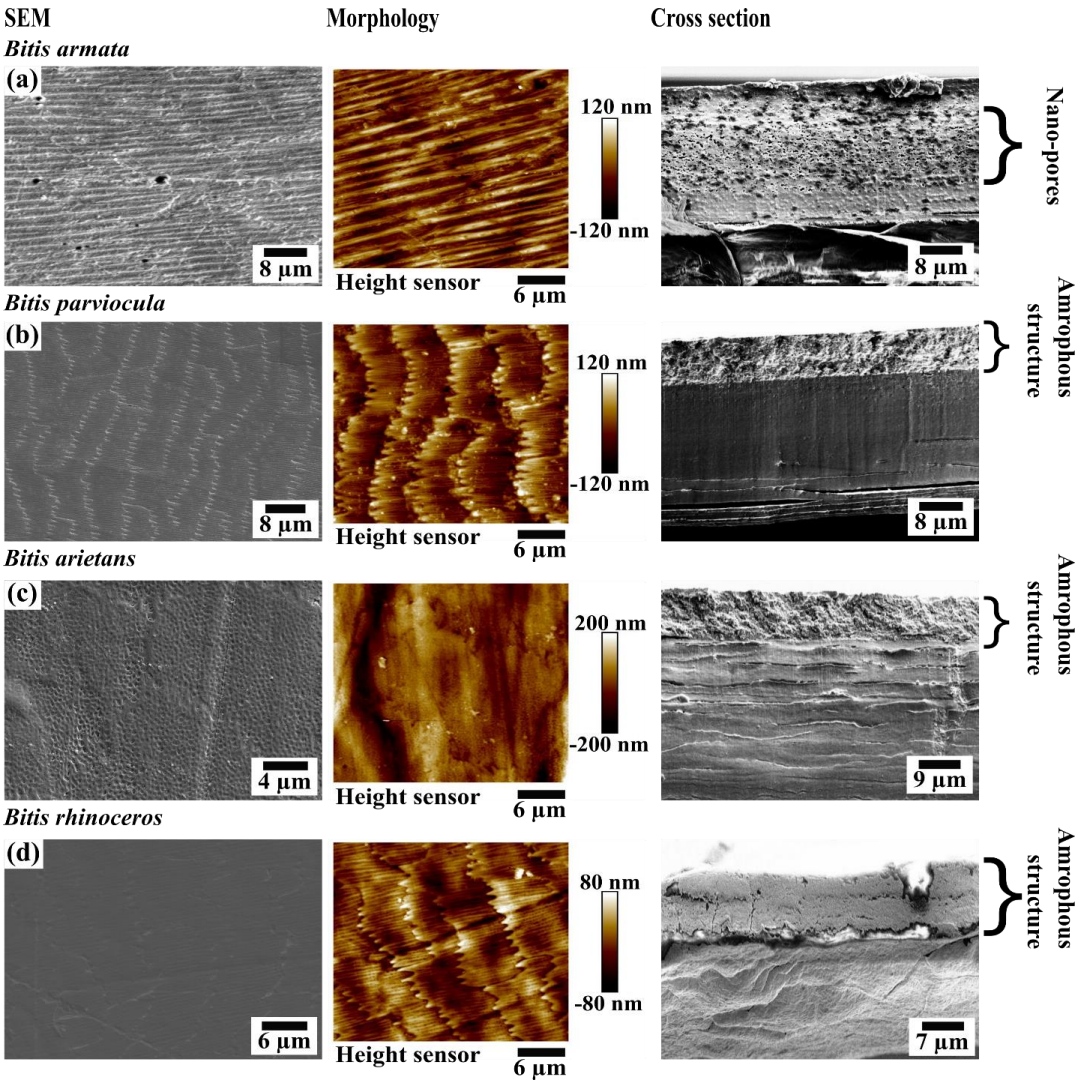

Figure 4.3: *SEM and AFM images of the surface topography and cross-section SEM image of the ventral scales of* ***(a)*** *B. armata;* ***(b)*** *B. parviocula;* ***(c)*** *B. arietans; and* ***(d)*** *B. rhinoceros Similar to B. rubida a ridge-like structure is found on the scale surface of B. armata. Microfibrils are observed on the scales of B. parviocula and B rhinoceros. In difference, numerous nanopits are found on the scale surface of B. arietans. In the cross-section image, numerous nanopores are found underneath the reflecting white surface of B. armata. However, an amorphous structure with no nanopores is observed within the transparent or translucent ventral scales of B. parviocula, B. arietans, and B. rhinoceros.*

As the surface topography images do not explain the physics behind the optical appearance the scales' inner structure was analyzed. They were cut with a sharp razor blade and the cross-sections were imaged with SEM. Images of these cross sections are presented in Fig 4.1e) and f). The results indicate that these scales are double-layered with an air gap between them

(the air gap is marked with a red arrow). Snakes usually molt their scales every 3-4 months. This air gap might be an artifact of the molted scales which might help them during the molting process.

Interestingly, just underneath the external surface (indicated by a blue arrow), numerous nanopores (indicated by green arrows) are found. The magnified SEM image of these nanopores (Fig 4.1f) shows their random geometry. They are mostly oriented disorderly with no periodic pattern. These nanopores to some extent appeared elliptical. The length of the structures was around 0.5 µm along the major and minor axes of these ellipses.

The inner structure of the reflecting white scales resembles the structure found in white beetles which produce their intense white color by nano-structures [139]. In 2014, Buressi *et al.* showed that the nanopores found inside the scales of white beetles scatter the visible light to develop the white surface through retro-reflection [139]. As similar nanopores are also observed within the reflecting white scales of *B. rubida*, it is assumed that the reflecting white surface is produced due to the interaction of light with the nanopores. To validate the assumption, the topology and internal structure of the transparent or translucent scales of *B. parviocula*, *B. arietans*, and *B. rhinoceros* were analyzed. In addition, the reflecting white scales of *B. armata* were also investigated for further authentication. The results are presented in Figs 4.2 and 4.3, respectively. Photographs of the snake species *B. armata*, *B. parviocula*, *B. arietans*, and *B. rhinoceros* are shown in Fig 4.2 a), b), c), and d) respectively. The scales of the species were again photographed on white paper with the printout of the KIT logo. The photographs indicate the difference in optical properties of these scales that appear to the naked eye. The logo is hidden underneath the reflecting white scales; whereas it can be easily read through the transparent or translucent scales. Images presented in Fig 4.3 reveal the surface textures and internal structures of these scales. Interestingly, similar to the scales of *B. rubida*, a ridge-like reticulate pattern is observed on the scales of *B. armata* (Fig 4.3 a). Usually, such nano-ridges assist snakes in climbing [52]. Microfibril patterns are observed on the scales of *B. parviocula* (Fig 4.3b) and *B. rhinoceros* (Fig 4.3d). In reference to the previous studies and the results presented in Chapter 3, it is assumed that these microfibrils assist them in locomotion [44-51, 53-57]. In addition to nano-ridges and microfibrils, nanopits are also observed on the ventral scales of snakes [57]. Studies confirm that such nanofeatures are optimized for sidewinding locomotion traits [57]. Similar to the structure found on other sidewinding snakes, numerous nanopits are observed on the scale surface of *B. arietans* (Fig 4.3c). In general, these structures do not enhance the reflectance property but rather optimize the locomotion. The SEM images showing the surface textures for the scales of *B. arietans* are also presented and discussed in Section 3.1 of Chapter 3.

Cross-sections of these scales were analyzed to further validate the assumption that the white color is produced due to light scattering by these nanopores. Similar to the internal structures of *B.* rubida, numerous nanopores were found underneath the external surfaces of *B. armata* (Fig 4.3a). Dimensions of these nanopores are comparable to the ones found within the scales of *B. rubida*. In opposite to this, a solid structure with no nanopores (commonly defined as an amorphous structure) is observed in the transparent or translucent ventral scales of *B. parviocula* (Fig 4.3b), *B. arietans* (Fig 4.3c), and *B. rhinoceros* (Fig 4.3d). The results indicate that nanopores are found in the reflecting white ventral scales of *B. rubida* and *B. armata*. In contrast, amorphous structure is found in the transparent or translucent ventral scales of *B. parviocula*, *B. arietans*, and *B. rhinoceros*. The results confirm that the nanopores found inside the reflecting white scales scatter visible light to develop such surfaces.

4.2 Optical properties of the ventral scales

In previous studies, it was stated that these reflecting white venters help snakes achieve thermoregulatory properties [58-59]. Therefore, the optical response of the scales was recorded in the UV, visible, and near-infrared wavelength ranges to visualize the overall optical properties of these reflecting white and transparent or translucent scales.

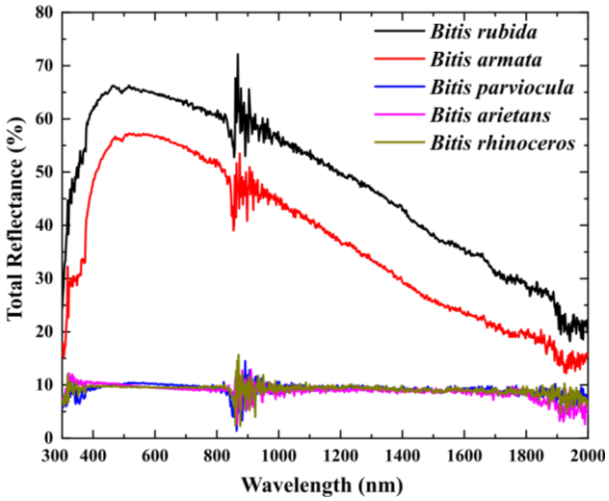

Figure 4.4: *Optical responses of the ventral scales of B. rubida, B. armata, B. rhinoceros, B. arietans, and B. parviocula are recorded in the wavelength range of 300-2000 nm. Total reflectance around 55-65% is observed for the porous ventral scales of B. armata and B. rubida in the range of 400-1050 nm. Higher reflection is also observed in the range of 300-400 nm for the porous scales. The reflection gradually decreases with the increase in wavelength and reduces*

to around 20% at 2000 nm. However, amorphous ventral scales of B. rhinoceros, B. arietans, and B. parviocula show a low reflection of 8-10% in the range entire spectrum of consideration.

Reflecting white scales of *B. rubida* and *B. armata* showed total reflectance around 55-65% in the wavelength range of 400-1050 nm. With the further increase in wavelength, the reflection reduces to the lowest value around 20% at the wavelength of 2000 nm. Interestingly, higher reflection is also observed for these scales in the range of 300-400 nm. It indicates that these nanopores reflect UV light in addition to visible and near-infrared light. In opposite to this, a lower reflection of around 8-10% is recorded for the scales of *B. parviocula, B. arietans,* and *B. rhinoceros* in the entire spectrum of interest (300-2000 nm). The noise around 900 nm is an artifact that is created due to the switching of the detectors of the LAMBDA 1050 UV-Vis-NIR spectrometer (PerkinElmer Inc., USA).

In summary, nanopores are found within the reflecting white ventral scales of snakes. These nanopores scatter light when incident upon the scales. Random geometry of these nanopores intensifies this scattering. Thus a broadband reflection is observed due to the scattering of light by these nanopores through retro-reflection. These reflecting white ventral scales are found on some species living in the equatorial region. The results indicate that snakes living in such hot and humid climates tend to optimize the thermoregulatory properties of their ventral scales by developing these nanopores as they reflect near-infrared light. In opposite to this, an amorphous structure is found in the transparent or translucent scales. This comparative study evidences that the nanopores found in the reflecting white scales interact with light to develop such surfaces.

A shortened version of this chapter will be published as the article, "Nanopores in ventral snake scales cause white venters in the genus Bitis" by KM S. Reza, L. M. Borgmann, J. Chen, H. Gunstheimer, R. Thelen, G. Gomard, U. Lemmer, G. Gomard, and H. Hölscher.

5 Micro-cavities Developing Anisotropically Reflecting Ventral Scales in Snakes

Due to the limited choice of materials many creatures in nature often optimize their optical appearance by the virtue of nano- and micro-structures. Some snakes such as the Chinese Cobra (*Naja atra*) develop anisotropically reflecting ventral scales. The results presented in this chapter indicate that numerous tilted microcavities are embedded within these anisotropically reflecting scales. These tilted microcavities interact with visible light to achieve such surfaces. Some snakes living in hot and humid climates prefer to develop white reflecting venters to avoid overheating [59]. Results presented in Chapter 4 confirm that nanopores found inside these scales scatter visible and near-infrared light to enhance thermoregulatory properties within the snake body. As the ventral scales of *N. atra* also appear whitish to the naked eye; the optical properties of the scales were recorded in visible and near-infrared regimes. Interestingly, the scales reflect both visible and near-infrared light. This might be caused due to the interaction of microcavities with the incident light. In opposite to this, the transparent scales do not show any anisotropic reflectance or higher reflection in the visible or near-infrared regimes. The results verify that tilted microcavities within the ventral scales of the Chinese Cobra develop anisotropically reflective surfaces that reflect near-infrared light.

5.1 Topological analysis of the scales

In this work, a comparative study is made on the surface topology, internal structure, and optical properties of the anisotropically reflecting scales of the Chinese Cobra (*Naja atra*) and the transparent or translucent scales of the Carpet Python (*Morelia spilota*). The details of the snake species were already provided in Chapter 2. This comparison helps to explain the mechanism through which *N. atra* develops such surfaces.

The scales of the two snakes were placed on white paper with the printout of the KIT logo in the background. Thus, the optical properties of these scales can be easily compared by the naked eye. During the photography, the position of the camera was fixed and the scales were tilted by 45^{o} from head to tail and from tail to head direction of the snake body. In the photographs, the scales are oriented such that the head of the snake points towards the right side. The scales of *N. atra* are mostly brown in color (Fig 5.1a) which might be caused due to the presence of melanin within the scales. These scales already appear whitish when photographed without any rotation.

Reflection of these scales increases when they are tilted by 45° from head to tail direction. Interestingly, the reflection of these scales reduces when they are tilted by 45° along the tail-to-head direction. Reflection of the scale reduces and they appear much darker due to the enhanced absorption by melanin within the scales.

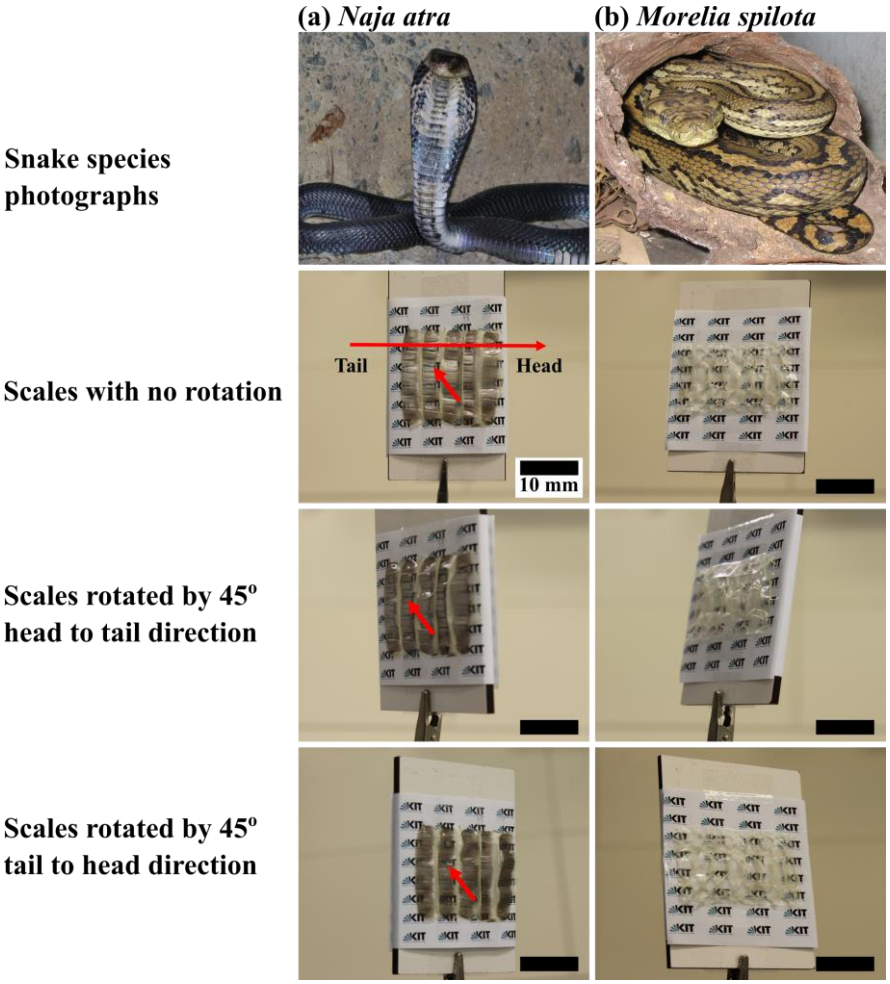

Figure 5.1: *Photographs of snake species and ventral scales of (a) Naja atra and (b) Morelia spilota. The scales were photographed on a white background with a printout of the KIT logo. The reflection of the scales of N. atra varies when the scales are tilted in the direction from head to tail direction. In the photographs, the scales are oriented such that the head of the snake points towards the right side. In the photographs, the scales were rotated from head to tail direction and tail to head direction. Interestingly, the reflection increases and decreases when rotated by 45^0 along the head-to-tail and tail to the head direction of the snake body respectively. The red arrow in the photographs indicates the difference in reflection appears to the naked eye when the scales are tilted accordingly. In difference to the scales of N. atra, much-reduced reflection is observed*

for the transparent or translucent scales of M. spilota. The reflection did not vary when tilted from head to tail or from tail to head direction.

The printout is not visible through scales of *N. atra* in all three of these photographs which is caused by both light reflection by the micro-cavities and absorption by melanin. The red arrow in the photographs indicates the difference in reflection appears to the naked eye when the scales are tilted accordingly. In opposite to this, the logo can be easily read in all three photos through the transparent or translucent scales of *M. spilota* (Fig 5.1b). The reflection of these transparent or translucent scales does not vary when they are tilted from head to tail or from tail to head direction.

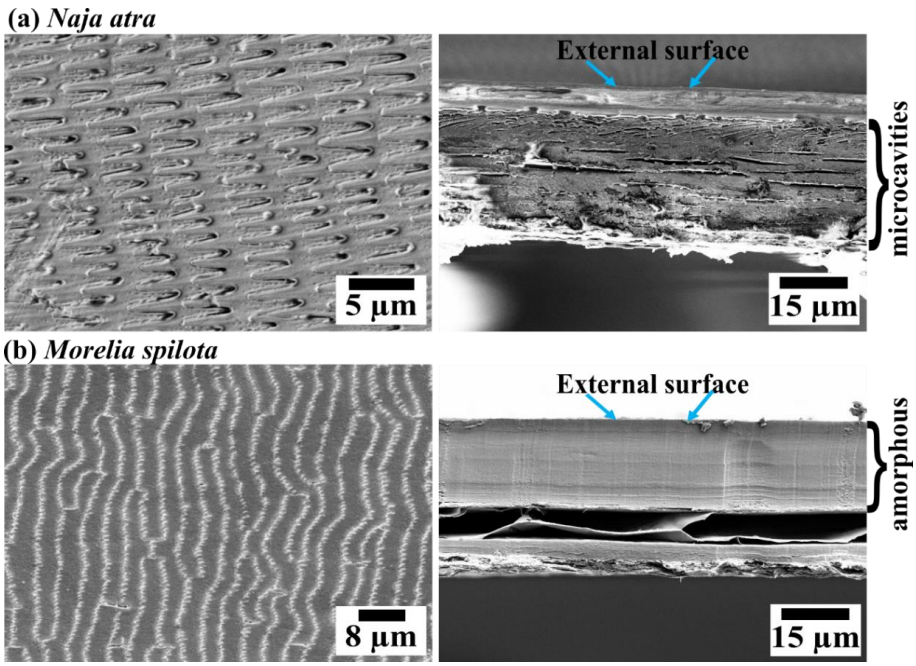

Figure 5.2: *SEM images of the surface topography and the cross-section of the ventral scales of (a) Naja atra and (b) Morelia spilota. Similar to ventral scales of other species (discussed in Chapter 3), microfibrils are observed on the scale surface. Interestingly, alternate layers of tilted micro-cavities are found within the anisotropically reflecting scales of N. atra. In opposite to this, an amorphous structure without any microcavities is observed in the transparent or translucent scales of M. spilota. A thicker microcavity is found embedded deeper into the scale. The blue arrows in the cross-section SEM images indicate the external surfaces of the subsequent scales.*

To understand the underlying physics of such optical appearance the scales were analyzed with the SEM. Figure 5.2 presents the surface topography of the scales of both *N. atra* (Fig 5.2a) and *M. spilota* (Fig 5.2b). The microfibrils aligned along the head-to-tail direction of the snake

body are observed on both of these scales. Here, the SEM images are oriented such that the head points toward the right side of the images. Microfibrils found on the scales of *N. atra* and *M. spilota* have periodicity around 3 µm and 5 µm, respectively. Ventral scales of numerous snake species belonging to different families, habitats, and geographical locations are already presented in Chapter 3 to confirm that these nano-structures are optimized to ease snake locomotion. The SEM images presented in Figure 5.1 are already presented in Chapter 3.

As similar surface textures are observed on both anisotropically reflecting and transparent or translucent scales, it is assumed that the microfibrils do not develop such an optical phenomenon. Therefore, the internal structures of the scales were further investigated. The scales were cut with a sharp razor blade and the subsequent cross-sections were imaged using SEM. The microscopic images show that both of these scales are about 40 µm thick. In the cross-section of *N. atra* (Fig. 5.2a), alternate layers of tilted micro-cavities are observed. The thickness of these micro-cavities found underneath the external surface varies in the range of 1-1.5 µm. In general, snake scales are composed of keratin [135]. This compact structure with alternate layers of titled micro-cavities and keratin might interact with visible light to develop such anisotropically reflecting surfaces. To verify this assumption cross-sections of the transparent or translucent scales of *M. spilota* were also imaged with the SEM. An amorphous structure with no micro-cavities is observed in the transparent or translucent scales of *M. spilota* (Fig. 5.2b). However, a cavity around 7-8 µm in thickness is found deeper into the layer. As the length and thickness of this cavity are not comparable to the wavelength of visible light, this cavity should not interact with the visible light to modify the optical properties. The blue arrows in the cross-section images of these scales indicate the external surfaces of the scales.

5.2 Optical properties of the scales

Generally, the ventral scales of snakes appear transparent or translucent to the naked eye. Transmittance of most of the scales presented in Figure 3.12d) of Chapter 3 is observed in the range of 70-90%. A reduced transmittance of around 40-45% is observed for the ventral scales of *N. atra*. It is assumed that absorption by the melanin and enhanced scale reflection have resulted in a decrease in the transmission for these scales. To visualize the optical appearance of the scales blocking the back reflection, the bottom surfaces of the scales were painted with black ink and attached to a glass slide. The top surface of the glass slide on which the scales were attached was also painted with black ink. The ink was sticky enough to attach the scales on the glass slide. The edges of the glass slide were also painted with black ink. This process allowed to measure the reflectance of the top surface of the scale as the reflection of the bottom surface was absorbed by

black pigment. To compare the optical properties, the process was repeated on the transparent or translucent scales of *M. spilota*. The scales were characterized in the wavelength range of 400-800 nm with a UV-Vis-NIR spectrometer. In reference to Fig 5.1, a difference in the reflection is observed for the scales of *N. atra* when they are tilted from head to tail and from tail to head directions. Therefore, the scales were rotated in accordance with the light source to record the response of these micro-cavities. Scales attached to the black painted glass slide were attached to the sample holder which was later collected inside the integrating sphere. As the light source of the LAMBDA 1050 UV-Vis-NIR spectrometer (PerkinElmer Inc., USA) cannot be rotated, the sample holder along with the scale attached glass slide were rotated from 10^{o} to 45^{o} with a step of 5^{o}. This allowed the measurement of the optical response of these microcavities when the light is incident on the scale surface from different angles resembling the tilting of the scales in accordance with a fixed light source.

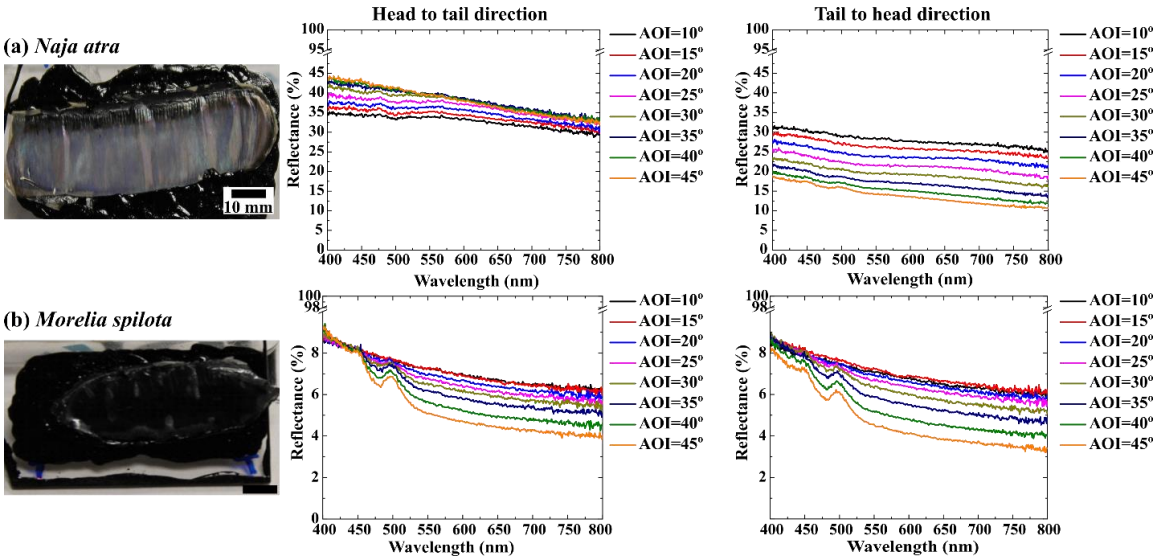

Figure 5.3: *Photographs of the ventral scales of (a) N. atra and (b) M. spilota attached on glass slides. The bottom surfaces of the scales and glass slides were painted with black ink which was sticky enough to attach the scales to the glass slides. The edges of the glass slides were also painted with black pigment to avoid unwanted scattering within the integrating sphere. The photographs (tilted by around 30^{0}) already indicate the difference in the physical appearance of the scales which is further enhanced due to the absorption by the rear surface. The reflectance was measured in the wavelength range of 400-800 nm varying light incident angle from 0^{o} to 45^{o} by a step of 5^{o}. The reflection increased for the scales of N. atra with the increase in the angle of incidence when measured from head to tail direction. However, it reduces with the increase in incidence angle when measured from tail to head direction. In opposite to this, for the scales of*

M. spilota the reflection reduces with the increase in angle of incidence regardless of the direction of measurement.

A total reflection of around 4% to 8% is recorded for the transparent or translucent scales of *M. spilota* in the visible range. The reflection decreased with the increase in light incidence angle when measured from both head to tail and tail to head direction. Thus no reflection anisotropy is observed on the amorphous scales where no micro-cavities are observed.

Higher reflection is observed for the ventral scales of *N. atra*. The reflection varied between 20% and 45% in the wavelength range of 400 nm to 800 nm with the variation in incidence angle when measured from different directions. The reflection increases when measured from head to tail direction with the increase in incidence angle. However, reflection decreases with the increase in the angle of light incidence when measured from tail to head direction. The overall reflection is higher when measured along the head-to-tail direction in comparison with the reflectance recorded when measured in the other direction.

For better visualization of the anisotropic reflectance property of the scales of *N. atra*, reflectance at 500 nm is plotted against the angle of incidence in Figure 5.4. The results are compared with the optical response of amorphous scales of *M. spilota* for better understanding. The reflection increases with the incidence angle when measured from head to tail direction (Fig 5.4a). However, it reduces with the increase in light incidence angle when measured from the tail to the head direction (Fig 5.4 b). In difference to the response of anisotropically reflecting scales, no difference in the reflection is observed with the increase in the angle of incidence for the transparent or translucent scales of *M. spilota* when measured from different directions.

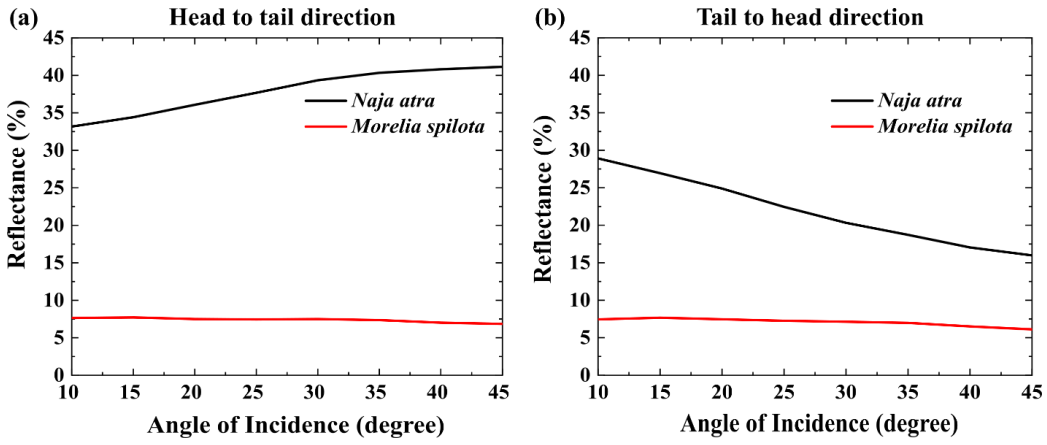

Figure 5.4: *Reflectance vs. Angle of incidence at the wavelength at 500 nm for the ventral scales of N. atra and M. spilota when measured from (a) head to tail; (b) tail to head; directions. For*

the scales of N. atra, reflectance increases with the increase in angle of incidence when measured from head to tail direction. However, the reflection reduces with the increase in the incidence angle when measured from tail to head direction. No difference in reflectance is observed for the scales of M. spilota when measured from different directions.

Sometimes, snakes develop white ventral scales to avoid overheating in hot and humid climates [59]. Results presented in Chapter 4, already confirm that nanopores found inside the ventral scales interact with the visible light to develop such reflecting white surfaces. In addition, these scales reflect near-infrared light possibly to avoid overheating. These nanopores have a random geometry. In general, they are elliptical in shape with a diameter of around 500 nm. In the scales of *N. atra* anisotropically reflecting surfaces are developed due to the interaction of light with the tilted micro-cavities found underneath the external surfaces of scales. These cavities are about 1 µm in thickness. As the width of these micro-cavities is comparable to the diameter of the nanopores found in the reflecting white scales, the optical response of the scales was also recorded in the near-infrared light. A comparative study is made with amorphous transparent or translucent scales of *M. spilota* to understand the response of these micro-cavities to near-infrared light.

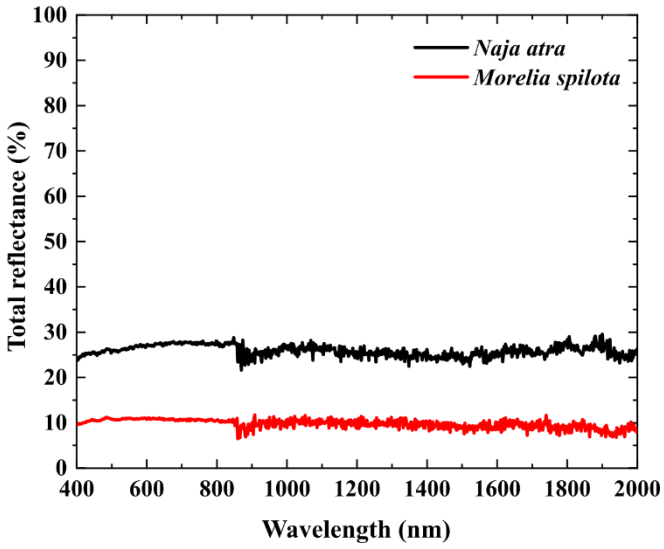

Figure 5.5: *Total reflectance of the ventral scales of Naja atra and Morelia spilota. Higher reflection is observed for the scales of N. atra in comparison to the scales of M. spilota. This higher reflection in the visible and near-infrared light might be caused due to the interaction of light with the microcavities embedded within the scales of N. atra. In opposite this low reflection of around 8-10% is recorded for the amorphous transparent or translucent scales of M. spilota in the entire spectrum of consideration.*

In Figure 5.5 the total reflectance of the ventral scales of *N. atra* and *M. spilota* is presented in a wide spectral range from 400 nm to 2000 nm. Reflection around 8-10% is observed for the transparent or translucent scales of *M. spilota* in visible and near-infrared light. However, a higher reflection of around 25% is observed for the anisotropically reflecting scales of *N. atra* in the entire spectrum of consideration. The results indicate that microcavities found inside the scales of *N. atra* reflect both visible and near-infrared light which might enhance the overall thermoregulatory properties of the snake body.

In summary, some Chinese Cobras develop anisotropically reflecting ventral scales. This work indicates alternate layers of micro-cavities found within the scales interact with the visible light to develop such an optical appearance. A significant difference in reflectance is observed when scales are tilted from head to tail and from tail to head direction. The results further show that these microcavities reflect near-infrared light. Comparative analysis with the transparent or translucent scales confirms that alternate layers of tilted microcavities found within the scales of some snake species are optically responsive to visible and near-infrared light.

A shortened version of this chapter is in preparation as the article, "Micro-cavities Developing Anisotropically Reflecting Scales in Snakes" by KM S. Reza, M. Ahmed, G. Gomard, U. Lemmer, and H. Hölscher

6 Differences in Surface Topography of the Snake Scales with the Variation in Appearance

Snakes often modify their body scales to perform multifunctional activities. Results presented in Chapters 3, 4, and 5 discuss some ventral scale optimizations that snakes adopt to ease locomotion and enhance optical and thermoregulatory properties within their body. Interestingly, some snakes also optimize the dorsal scales. These cold-blooded ectotherms often appear dark in color. In addition to camouflaging, the thermal melanism hypothesis predicts an ecological advantage of dark-colored animals in cold environments [71-74]. However, melanistic snakes are often vulnerable to their predators due to the increase in detectability [75-78]. However, enhanced growth rate, better body condition, longer activity, improved locomotion performance, and even higher fertility in the female ones are found in dark-colored snakes [79-82]. Thus a tradeoff remains in detectability and melanism. To address this natural phenomenon, many snakes develop a "Zigzag pattern" on the dorsal side. The scales within the zigzag pattern often appear darker in color than the neighboring scales. In 2020, Martínez-Freiría *et al.* conducted an extensive analysis of the dorsal scale within the zigzag pattern of 39 Eurasian Vipers [77]. They investigated if these dark-colored scales within the pattern are optimized for thermoregulatory functions. Their study stated that increased pigment concentration of the dark scales is fortunate for snakes to enhance their heat absorption. In 2013, Spinner *et al.* assumed that the microstructures along with the nano ridges found on darker dorsal scales reduce reflection resulting in enhanced thermoregulation within the snake body [65]. However, their spectroscopic analysis does not consider the absorption of melanin in the visible light.

For further investigations, dorsal scales of snake species showing zigzag patterns on their dorsal side are analyzed in this work. A comparative study is made on the dark- (defined as high-pigmented scale) and the neighboring light-colored (low pigmented scales) colored scales to determine if the scale textures have an impact in enhancing the optical and thermal properties of these species. The results show that nano- and micro-structures found on the scale surface differ with the variation in pigment concentration. The height of the microstructures found on the high-pigmented scales is higher than the ones found on low-pigmented scales. In agreement with the previous studies, lower reflection was recorded for the high-pigmented scales in comparison with the low-pigmented scales in the visible light. However, a higher reflection was measured on the high-pigmented scales in comparison to the low-pigmented scales when measured in near-

infrared light. The optical properties of the replicas prepared in PMMA material from the high and low-pigmented scales are comparable. However, higher reflectance was recorded for the replicas prepared from high-pigmented scales in both visible and near-infrared light in comparison with the replicas prepared from low-pigmented scales. Therefore, it is assumed that the enhanced micro-structures of the high-pigmented scales do not reduce reflection. Rather it increases reflection in a broad spectrum.

6.1 Micro-ornamentation of the dorsal scales

In this chapter, the analysis results of dorsal scales of the Dusky Pygmy Rattle Snake (*Sisturus militaries barbouri*), West African Gaboon Viper (*Bitis rhinoceros*), Ethiopian Viper (*Bitis parviocula*), Many Horned Viper (*Bitis cornuta*), Red Adder (*Bitis rubida*), Southern Adder (*Bitis armata*), and Puff Adder (*Bitis arietans*) are presented. The zigzag pattern is found on the dorsal scales of these species. Similar to the species investigated by Martínez-Freiría *et al.* the scales within the zigzag pattern are rich in melanin in comparison with the neighboring scales [77].

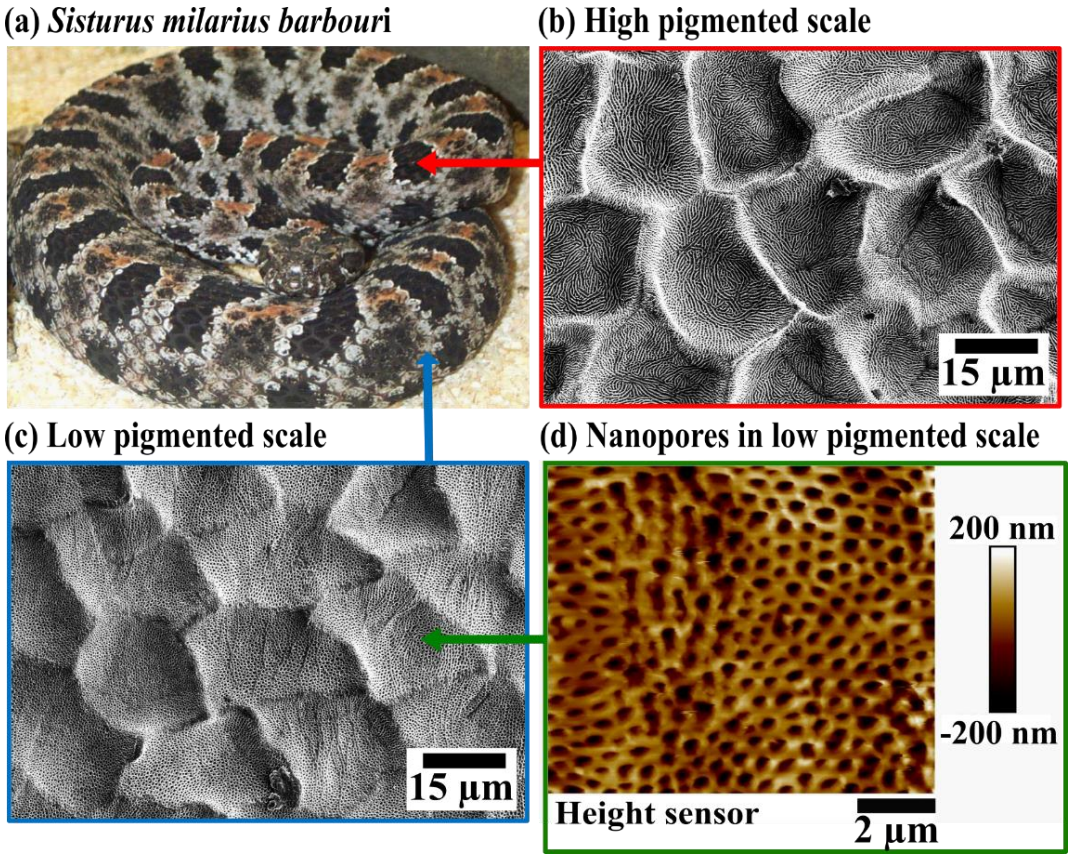

Figure 6.1: *(a) Photograph of the snake species, Dusky Pygmy Rattle Snake (Sisturus milarius barbouri). The photograph already indicates the high-pigmented scales within the zigzag pattern. SEM images of the (b) high and (c) low pigmented dorsal scales reveal micro-cavities on the*

scale's surface. As the micro-cavities are almost perpendicular to the scale surface the samples were tilted by 30^0 during the measurements. The SEM images already indicate the difference in depth of these microcavities with the variation in pigment concentration. Microfibrils are found within the microcavities of the high-pigmented dorsal scales; whereas nano pits are observed within the microcavities of low-pigmented scales. (d) The AFM images of the low pigmented reveal that the nanopits are about 800-1000 nm in diameter and 250-300 nm in depth.

In Figure 6.1, the results of *S. m. barbouri* are presented. The photograph of the species (Fig 6.1a) shows the zigzag pattern on their dorsal scales. The scales within the pattern are darker in comparison with the other scales. To further investigate surface textures the scales were imaged with the SEM. The microscopic images show the naturally grown nano- and micro-structures on the scales. Micro-cavities are found on both high (Fig 6.1b) and low (Fig 6.1c) pigmented scales. These micro-cavities are almost perpendicular to the scale surface. Therefore, to have a better depiction, scales were tilted by 30^0 while imaging. These cavities are mostly elliptical. The length and width of the major and minor axes of such ellipses are about 20-30 µm and 15-20 µm respectively. However, the depth of these micro-cavities differs with the variation in pigment concentration. Micro-cavities found on high-pigmented scales have a depth of around 10-12 µm; whereas the depth is 5-6 µm for the ones found on the low-pigmented scales.

In addition to these micro-structures, nano-ridges are also observed within the micro-cavities of high-pigmented scales. These ridges are about 0.5 µm thick. In difference to high-pigmented scales, instead of nano ridges, numerous nano-pits are found on the low-pigmented scales. These nanopits were further imaged with an AFM and the diameter and depth around 800-1000 nm and 250-300 nm were recorded, respectively (Fig 6.1d). Therefore, a difference in the structure of both nano and micro-structures is found with the variation in pigment concentration of the scales. Interestingly, these differences in the nano- and micro-textures are found even on a single scale with variation in pigment concentration. Figure 6.2 summarizes the observations on single dorsal scales of *S. m. barbouri*. Here, only the upper (Fig 6.2b) and lower (Fig 6.2e) halves of the scales are highly pigmented and the other halves are low pigmented. Deeper micro-cavities with nanoridges are found on high-pigmented regions of the scales (Fig 6.2a and 6.2d). However, micro-cavities with reduced depth and nano-pits are found on the low-pigmented regions of the scales (Fig 6.2c and 6.2f). This investigation indicates that regardless of their location on a scale (upper or lower half) a difference in structures is observed with the variation in pigment concentration.

The SEM images of the high and low-pigmented scales of *S. m. barbouri* indicate that the nano- and micro-structures differ significantly with the variation in pigment concentration. To further confirm these findings, high and low-pigmented scales of *B. rhinoceros*, *B. parviocula*, *B. cornuta*, *B. rubida*, *B. armata*, and *B. arietans* were also examined. The photographs of the snake species- *B. rhinoceros* (Fig 6.3a), *B. parviocula* (Fig 6.3b), *B. cornuta* (Fig 6.3c), *B. rubida* (Fig 6.3d), *B. armata* (Fig 6.3e) and *B. arietans* (Fig 6.3f) show the zigzag pattern on their dorsal scales. Similar to the scales of *S. m. barbouri*, high-pigmented scales are found within the zigzag patterns of these species. SEM images of the high- and low-pigmented scales of the subsequent snake species indicate the difference in nano- and micro-structures.

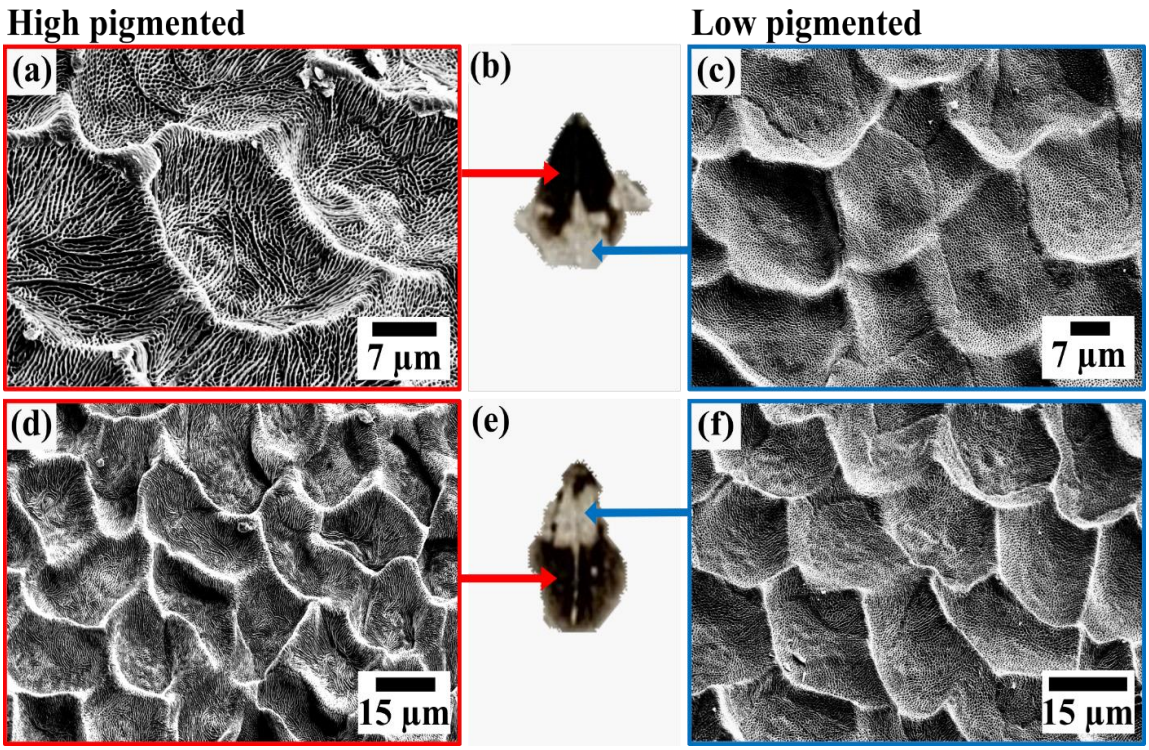

Figure 6.2: *Photographs of the scales on a white background. (b) The upper and (e) lower halves of the scales have a high content of melanin. SEM images in (a) and (d) indicate deeper micro-cavities and nano-ridges on the high-pigmented regions of the scales. Micro-cavities with reduced depth and nano-pores are found in the low-pigmented regions of the scales in (c) and (f). The photographs and SEM images reveal that structural difference is observed with the variation of melanin content regardless of their position in the scales (upper or lower half). As the micro-cavities are almost perpendicular to the scale surface the samples were tilted by 30^0 during the measurements.*

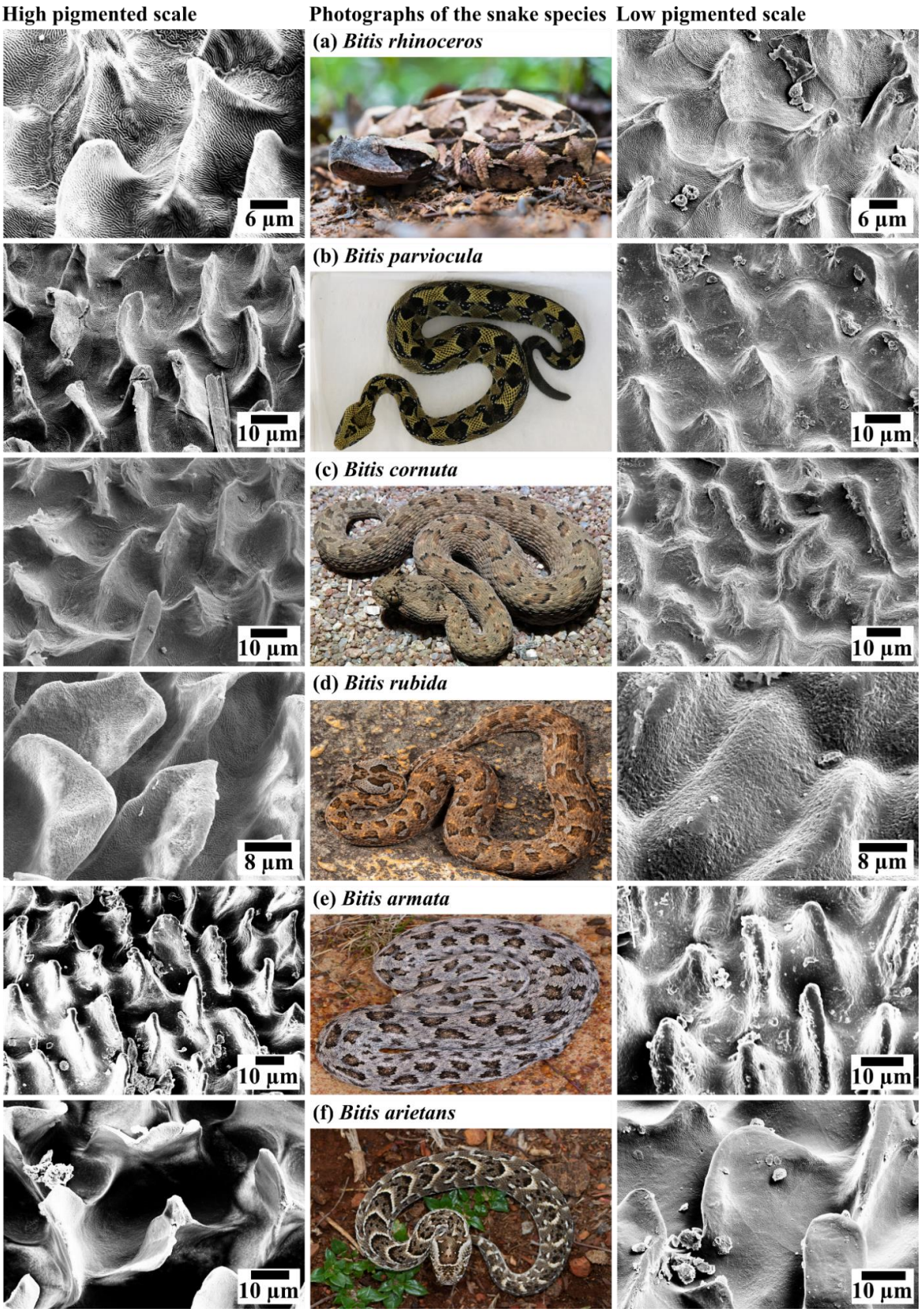
High pigmented scale
Photographs of the snake species
Low pigmented scale
(a) Bitis rhinoceros
6 µm
6 µm
(b) Bitis parviocula
10 µm
10 µm
(c) Bitis cornuta
10 µm
10 µm
(d) Bitis rubida
8 µm
8 µm
(e) Bitis armata
10 µm
10 µm
(f) Bitis arietans
10 µm
10 µm

Figure 6.3: Photograph of snake species, SEM images of the high and low pigmented dorsal scales of (a) Bitis rhinoceros (b) Bitis parviocula (c) Bitis cornuta (d) Bitis rubida (e) Bitis armata (f) Bitis arietans indicate the difference in surface textures with the variation in pigment concentration. The scales within the pattern have a high content of melanin in comparison with the neighboring scales. Nano-ridges are observed on the micro-domes of high pigmented scales of B. rhinoceros, B. parviocula, B. cornuta, and B. rubida. In addition to micro-domes, nanopits are found on the low pigmented scales of B. rhinoceros, B. parviocula, B. cornuta, B. rubida and B. arietans. As the micro-cavities are almost perpendicular to the scale surface the samples were tilted by 30^0 during the measurements.

In difference to the micro-cavities found on the scales of *S. m. barbouri*, dome-shaped micro-structures are observed on the high and low-pigmented scales of *B. rhinoceros, B. parviocula, B. cornuta, B. rubida, B. armata,* and *B. arietans*. The width of these micro-domes is comparable among the high and low-pigmented scales. However, the height of the micro-domes varies with the difference in pigment concentration. The height of these micro-domes found on the high-pigmented scales is much higher than the ones found on the low-pigmented scales. Nano pits are found on the low pigmented scales alongside the micro-domes on some of these species. In addition to the micro-domes, nano-ridges are observed of high pigmented scales of *B. rhinoceros, B. parviocula, B. cornuta,* and *B. rubida*. In opposite to this, nanopits are found on the micro-domes of low-pigmented scales of *B. rhinoceros, B. parviocula, B. cornuta, B. rubida,* and *B. arietans*.

The results indicate that the nano-and micro-features found on the scale surface differ with the variation in pigment concentration. However, this difference is not common to all snakes with a zigzag pattern on the dorsal side. For example, a difference in surface texturing is not found on the high and low-pigmented dorsal scales of Rock Rattle Snake (*Crotalus lepidus klauberi*). Photographs of the snake species indicate the zigzag pattern on the dorsal scales (Fig 6.4a). Similar to the other species, the scales within the zigzag pattern are darker in color in comparison with the neighboring scales. High and low-pigmented scales were further analyzed with the SEM. In difference to the other species, microstructures are not observed on the scale surface. Instead of micro-cavities or micro-domes, only nanoridges are observed on both high (Fig 6.4b) and low (Fig 6.4c) pigmented scales. The scales were further characterized with an AFM. Nano ridges found on both high and low-pigmented scales showed a width of around 500 nm. However, a height difference is observed. These nanoridges found on the high-pigmented

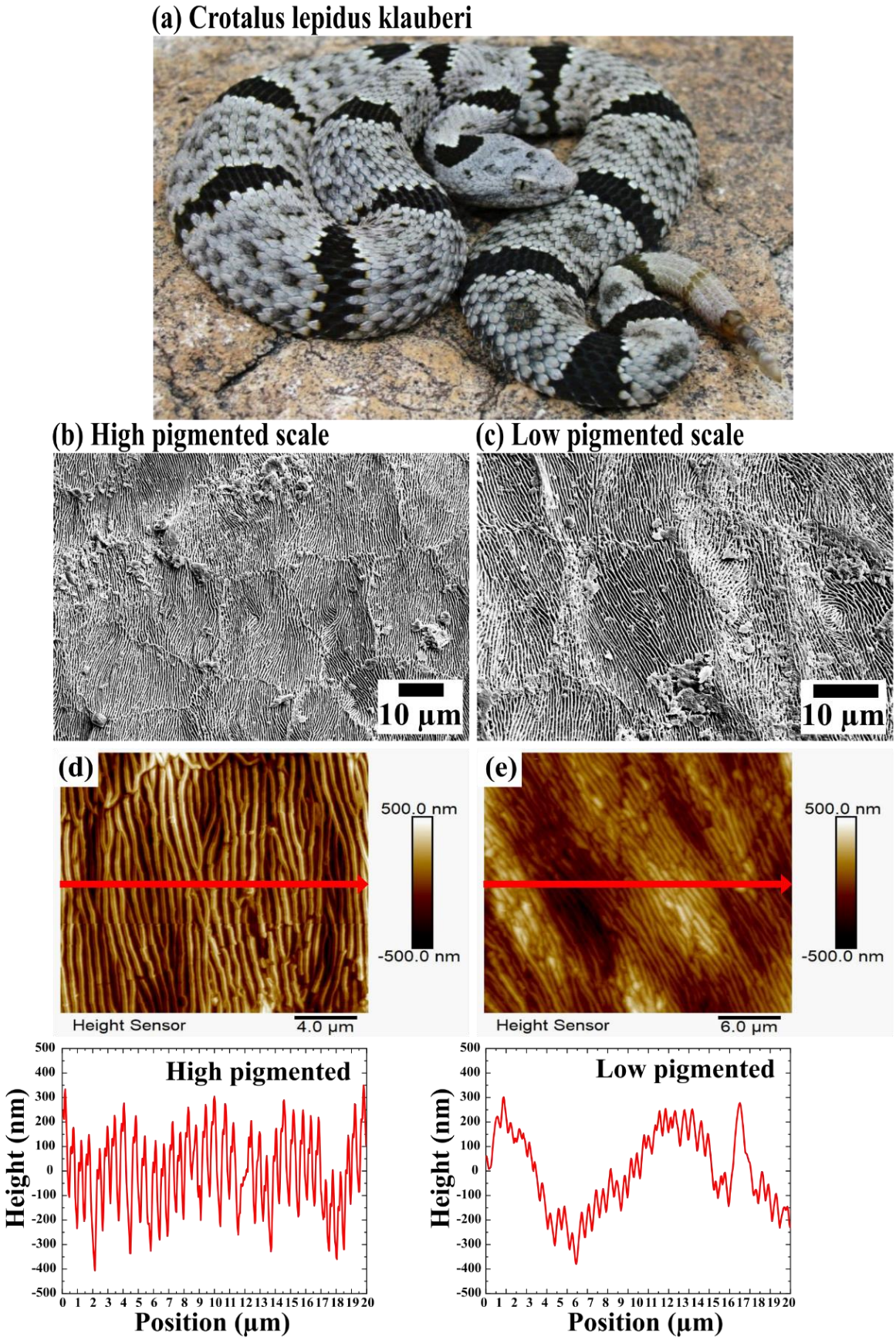
(a) Crotalus lepidus klauberi
(b) High pigmented scale
(c) Low pigmented scale
10 µm
10 µm
(d)
(e)
500.0 nm
-500.0 nm
500.0 nm
-500.0 nm
Height Sensor
4.0 µm
Height Sensor
6.0 µm
High pigmented
Low pigmented
Height (nm)
Position (µm)
Height (nm)
Position (µm)

Figure 6.4: *(a) Photograph of Rock Rattle Snake (Crotalus lepidus klauberi) showing the zigzag pattern of high and low pigmented scales on their dorsal side. SEM images of the (b) high and (c) low pigmented scales indicate the nano ridges on the scale surface. These ridges are about 0.5 µm in width. In difference to the other species, no micro-structures are observed on these scales. AFM images of the (d) high and (e) low pigmented scales reveal that the height of these nanoridges differs with the variation in pigment concentration. The ridges of the high and low pigmented scales have a height of around 400 nm and 200 nm respectively. AFM scan area (d) 20 µm; (e) 30 µm*

scales (Fig 6.4 d) showed a height around 400 nm; whereas the one found on the low-pigmented scales (Fig 6.4 e) showed a height around 200 nm. In general, a difference height of these nanoridges is observed with the difference in pigment concentration.

6.2 Optical properties of the high and low pigmented dorsal scales

Photographs of snake species indicate that the dorsal scales within the zigzag pattern are rich in melanin. In previous studies, it was predicted that these pigmented scales are optimized for heat absorption within the snake body [77]. Topological analyses reveal the structural difference between high and low-pigmented scales. To further verify if these scales are optimized for efficient heat absorption, optical responses of these scales were recorded in the wavelength range of 400-2000 nm. The results are presented in Figure 6.5.

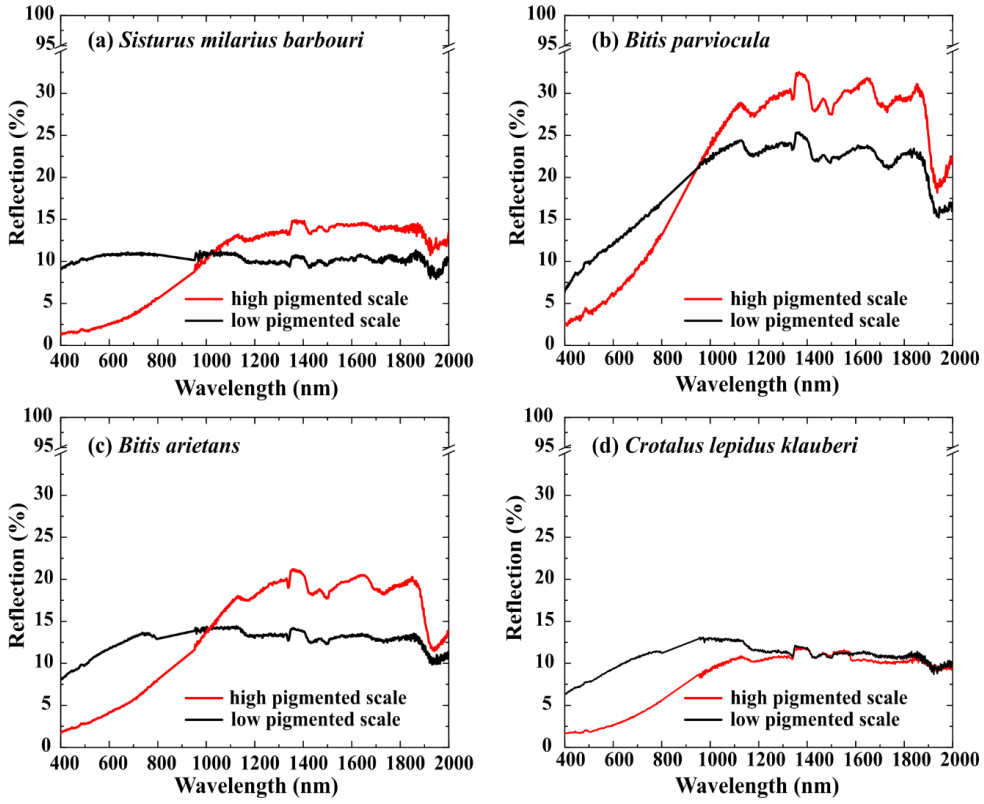

Figure 6.5: *Reflectance properties of the high and low pigmented dorsal scales of (a) Sisturus milarius barbouri (b) Bitis parviocula (c) Bitis arietans and (d) Crotalus lepidus klauberi. In general, lower reflectance is observed for the high-pigmented scales in comparison with the low-pigmented scales in the wavelength range of 400-1000 nm. In opposite to this, higher reflection is observed for the high-pigmented scales in the wavelength range of 1000-2000 nm. No difference is observed for the high and low pigmented scales of C. l. klauberi in this wavelength regime.*

The optical responses of high and low pigmented scales of *S. m. barbouri*, *B. arietans*, *B. parviocula,* and *C. l. klauberi* are shown in Figure 6.5a), b), c), and d). When characterized in the wavelength range of 400-1000 nm, lower reflection was recorded for the high-pigmented scales in comparison to the low-pigmented. However, in the wavelength range of 1000-2000 nm higher reflection was recorded for the high-pigmented scale in comparison with the low-pigmented scales of *S. m. barbouri*, *B. arietans,* and *B. parviocula*. Interestingly, no difference in the spectrum is observed for high and low-pigmented scales of *C. l. klauberi* in the wavelength range of 1000-2000 nm. In reference to the SEM images, no micro-structures are found on the high or low-pigmented scales of *C. l. klauberi*. Interestingly, no micro-structures are found on the dorsal scales of this species and no difference in optical response was recorded in the near-infrared regime. Thus it can be assumed that the difference in optical properties observed in the low and high-pigmented scales of *S. m. barbouri*, *B. parviocula,* and *B. arietans* in the wavelength range of 1000-2000 nm is mostly caused due to the difference in depth or height of the micro-cavities or micro-domes found on their scale surface.

6.3 Topological and optical properties of the replicas

Melanin has high absorption in the visible regime [138]. Thus this reduction of reflection for the high pigmented scales in the visible light could be attributed to the absorption by melanin within the scales. Interestingly, a difference in the nano- and micro-structure is also observed with the variation in pigment concentration. To verify if the nano- and micro-features have an effect in tailoring the optical properties, replicas of high and low-pigmented scales of *S. m. barbouri* were prepared in PMMA material. The optical properties of these scales were further recorded in visible and near-infrared light.

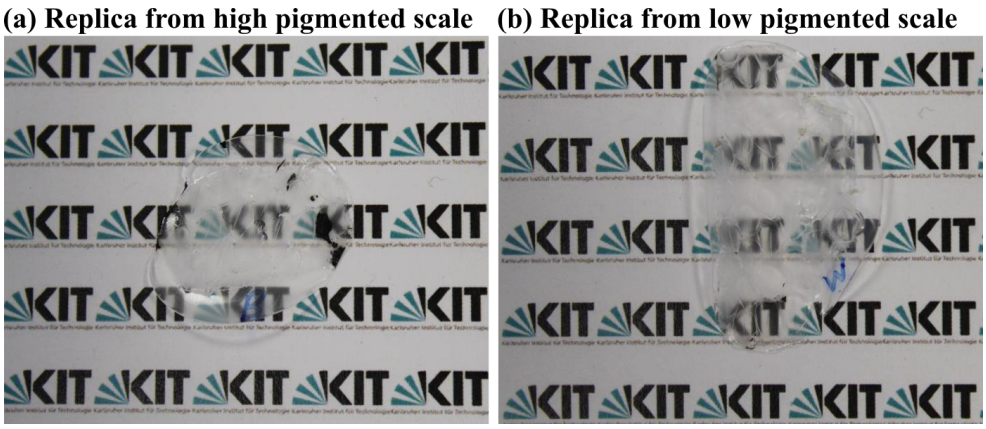

Figure 6.6: *Photographs of replicas prepared in PMMA material from (a) high and (b) low pigmented scales. The replicas are transparent or translucent to the naked eye.*

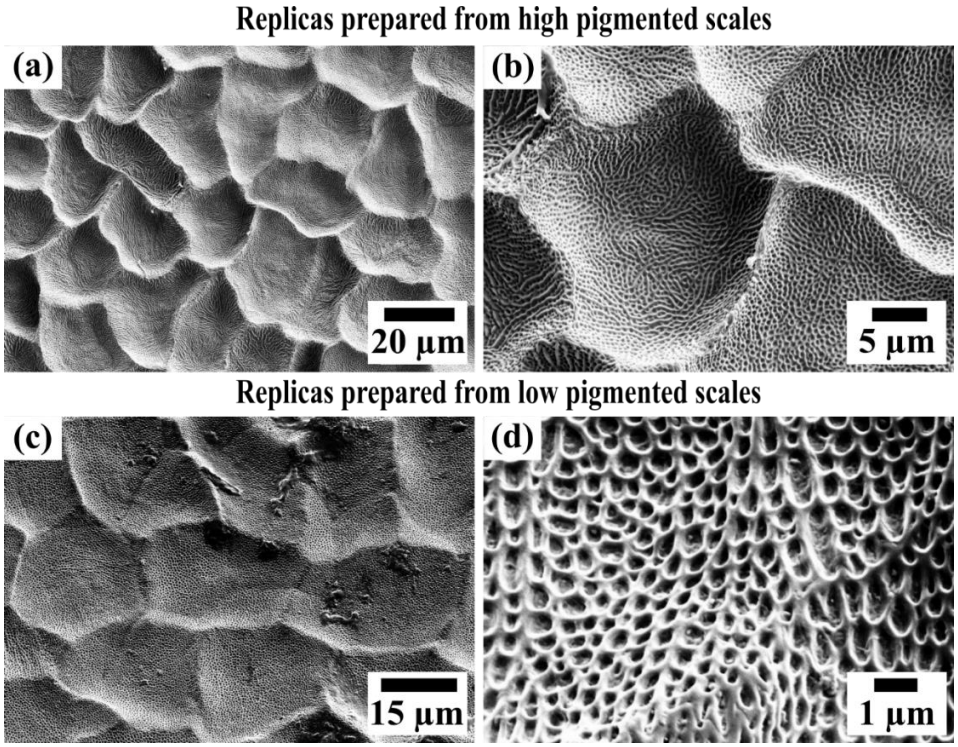

Figure 6.7: *SEM images of replicas prepared in PMMA material from high (a, b) and low (c, d) pigmented scales. The nano- and micro-structures are well imprinted on the replicas. Similar to the natural scales depth of the micro-cavities prepared from high pigmented scales is deeper than the ones prepared from low pigmented scales. Nanoridges and nano pits are also well imprinted on the high and low-pigmented scales respectively. As the micro-cavities are almost perpendicular to the surface of the replicas the samples were tilted by* 30^0 *during the imaging.*

Replicas were prepared from the high and low-pigmented scales of the *S. m. barbouri* using the soft imprint lithography technique described in Chapter 2. Through this process, the naturally grown textures on the scale surface were developed in PMMA material. Photographs of the replicas are shown in Figure 6.6. The replicas are placed on white paper with the printout of the KIT logo in the background during the photography. Replicas prepared from both high (Fig 6.6a) and low (Fig 6.6b) pigmented scales are transparent or translucent to the naked eye. For further analysis, the replicas were investigated with the SEM. The results are presented in Figure 6.7. The images indicate that the nano- and micro-structures are well imprinted on the replicas. As expected, micro-cavities in the replicas of high-pigmented scales (Fig 6.7a) are deeper than the ones found on the replicas of low-pigmented scales (Fig 6.7c). Alongside these micro-cavities, nanoridges and nanopits found on the natural scales are also imprinted on the replicas prepared from high (Fig 6.7b) and low (Fig 6.7d) pigmented scales. As the micro-cavities are almost perpendicular to the scale surface the samples were tilted by 30^0 during the imaging.

The SEM images indicate that the structures are well imprinted on the replicas. To verify if these surface textures have an effect in optimizing the optical properties, the replicas were characterized in the wavelength range of 400-2000 nm. The spectra were further compared with the spectrum of reference PMMA. Here, the reference PMMA has no surface textures. The results are presented in Figure 6.8. Higher reflection is observed for the replicas prepared from both high and low-pigmented scales in comparison with the reference PMMA in the visible and near-infrared light. In difference to the natural scales, higher reflection is observed for the replicas prepared from high-pigmented scales in comparison with the ones prepared from low-pigmented scales in both visible and near-infrared light. However, reduced reflection is observed for the high-pigmented natural scales in comparison with the low-pigmented natural scales in visible light (fig 6.5a).

The results indicate that nano- and micro-structures found on the high-pigmented scales interact with visible and near-infrared light to increase the reflection. These results contradict the previous study where it was assumed that the nano-and micro-structures found on the high-pigmented scales interact with the light to reduce reflection [65]. Much noise was observed around 900 nm due to the switching of the detectors of the LAMBDA 1050 UV-Vis-NIR spectrometer (PerkinElmer Inc., USA). Thus the data between 800-900 nm is not plotted.

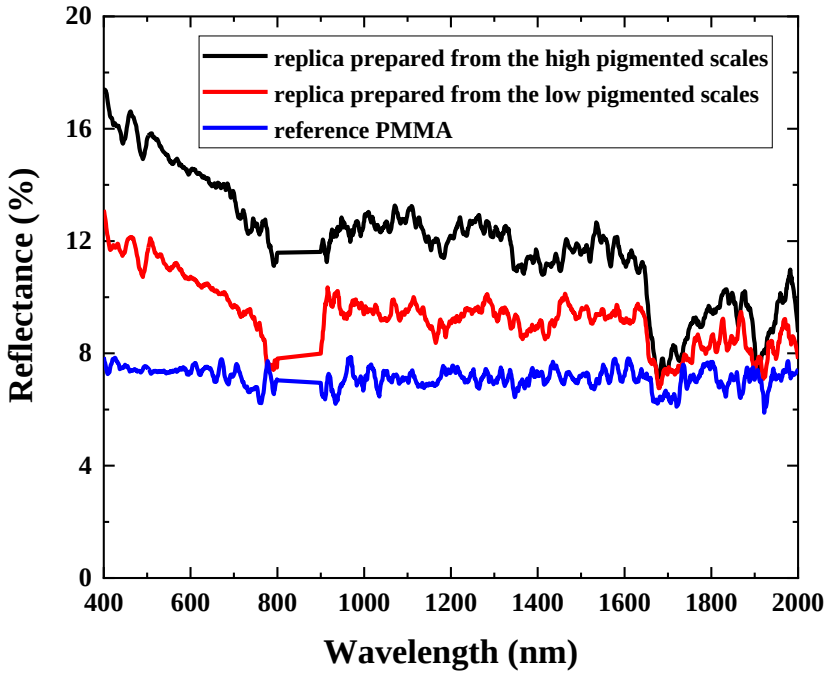

Figure 6.8: *Reflection of the replicas prepared from high and low-pigmented scales of S. m. barbouri and reference PMMA. The reflection increases for the replicas in comparison with the reference PMMA in both visible and near-infrared light. Higher reflection is observed for the replicas prepared from high-pigmented scales in comparison with the ones prepared from low-pigmented scales. This indicates that nano- and micro-structures found on high-pigmented scales increase the reflection. Much noise was observed around 900 nm due to the switching of the detectors of the LAMBDA 1050 UV-Vis-NIR spectrometer (PerkinElmer Inc., USA). Thus the data between 800-900 nm is not plotted.*

Differences in nano- and micro-structures are observed with the variation in pigment concentration of the dorsal scales. The previous study indicates that the optical properties of the high-pigmented dorsal scales are optimized for enhanced thermoregulatory properties of the snakes [65]. However, the results presented in this thesis show that the nano- and micro-structures imprinted on high-pigmented scales increase reflection. Therefore, it can be assumed that the intense dark color is produced by melanin and the micro-structures might not have an effect in reducing the reflection.

The replicas shown in Figure 6.6 are prepared by Junchi Chen from Light Technology Institute, Karlsruhe Institute of Technology, Germany.

7 Micro-ornamentation and Spectral Transmittance of Spectacle Scales

Millions of years of evolution have optimized the ventral and dorsal scales of snakes to perform multifunctional activities. Results presented in Chapters 3, 4, 5, and 6 highlight the optimizations of these nano- and micro-structures to ease snake locomotion and to achieve optical and thermoregulatory properties. Interestingly, the eyes of snakes are covered by scales, too. Such scales are also observed in fossorial lizards and most geckos which are called brille or spectacles [85]. They are mostly transparent and provide mechanical protection to the cornea, minimize evaporative water loss, and are assumed to protect against solar radiation [87-89].

Snakes locomote in direct contact with the ground with unavoidable dust or other contaminants. As snakes do not have any extremities to clean their spectacles, in this work it was speculated that snakes might have developed nano- and micro-structures on their spectacles to promote self-cleaning. As nature typically optimizes surface textures to achieve multiple functionalities; it was further speculated that spectacles are modified through evolution to enhance light capturing to the retina. Observations and analysis indicate that the spectacles have tiny to no surface structures. The wetting properties of the spectacles indicate low contact angles. Such lower values do not promote wet self-cleaning properties following the principle of the Lotus Effect. The spectacle scales are transparent in visible light; however, the transparency is comparable to the ventral scales of some species (fig 3.12a). Thus it confirms these structures often found on the spectacle surface are not also optimized to enhance the vision of snakes. The results indicate that these scales do not promote specific functionality or optical properties. Therefore, the benefits to snakes for the development of such structures on the spectacles are yet to be understood.

Snake scales have been studied for years to understand their multi-functionalities [35, 44-59, 62, 65-70]. Inspired by their properties Weibin Wu started his investigations on snake scales in 2016. As the snakes molt in around 3-4 months enough samples were not available to summarize his findings. Besides, only two spectacle scales are available from one completely shaded skin. With the availability of scales belonging to snake species from different geographical locations and habitats, I extended this study in 2020 by further investigations. In this study, many physical theories have been predicted to explain the functionality of scales. The theories have been validated through in-depth analysis of numerous snake species. Therefore, in this chapter,

some results have been adapted from the thesis of Weibin Wu to summarize the findings [142]. At the end of this chapter, the results that have been adapted from Weibin Wu's thesis are referenced.

7.1 Surface topology of the spectacles

In this work, the spectacles of 18 snake species from 5 different families were examined to understand if the structures on the scales are optimized to achieve wet self-cleaning or enhanced optical properties. These species live in a wide variety of habitats and different geographical locations. A detailed overview of them was already provided in Chapter 2. This comparative analysis across 5 different families and habitats further generalized this study. In addition to the topological analysis, wettability and optical measurements were conducted on some of these species.

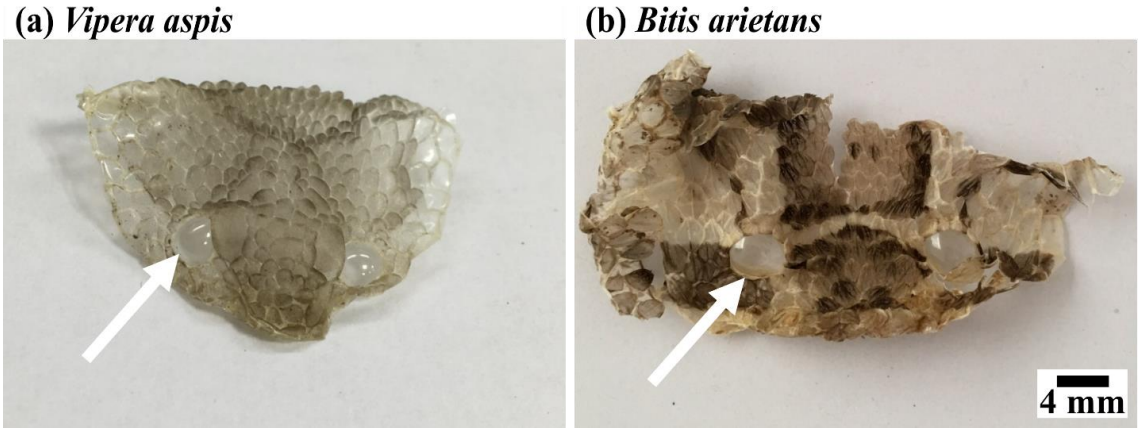

Figure 7.1: *Photographs of the molted head scales of (a) V. aspis and (b) B. arietans. The spectacles (marked by white arrows) are much more transparent than the other head scales. The spectacles of B. arietans (about 5 mm in diameter) are a little larger than the ones of V. aspis (about 4 mm in diameter)* (The figure has been reproduced from the thesis of Weibin Wu [142]).

Figures 7.1 and 7.2 have been reproduced from the PhD thesis of Weibin Wu [142]. Figure 7.1 shows the photographs of the head scales along with the spectacles (marked with white arrows) of *V. aspis* and *B. arietans*. They already indicate that the spectacles are more transparent in comparison with the other head scales. Besides, they are slightly larger than the other scales and of round shape. The dark coloration of the other head scales is most likely caused by the absorption by melanin embedded within the scales.

In general, the spectacles of all examined species appeared smooth to the naked eye; however, tiny nanofeatures are observed on the scale surface when examined in detail with high-resolution microscopy. SEM images in Fig 7.2 a) and b) display the surface topography of the central region and edges of the spectacles. Figure 7.2 b) shows an SEM image recorded close to the edge of the spectacle. Here, the polygonal structures are stretched perpendicular to the spectacle radius direction. Their overall size close to the edge of the spectacle is about 40 µm to 60 µm in length and 5 µm in width. Stitching micro-features in hexagon and polygon shapes with a

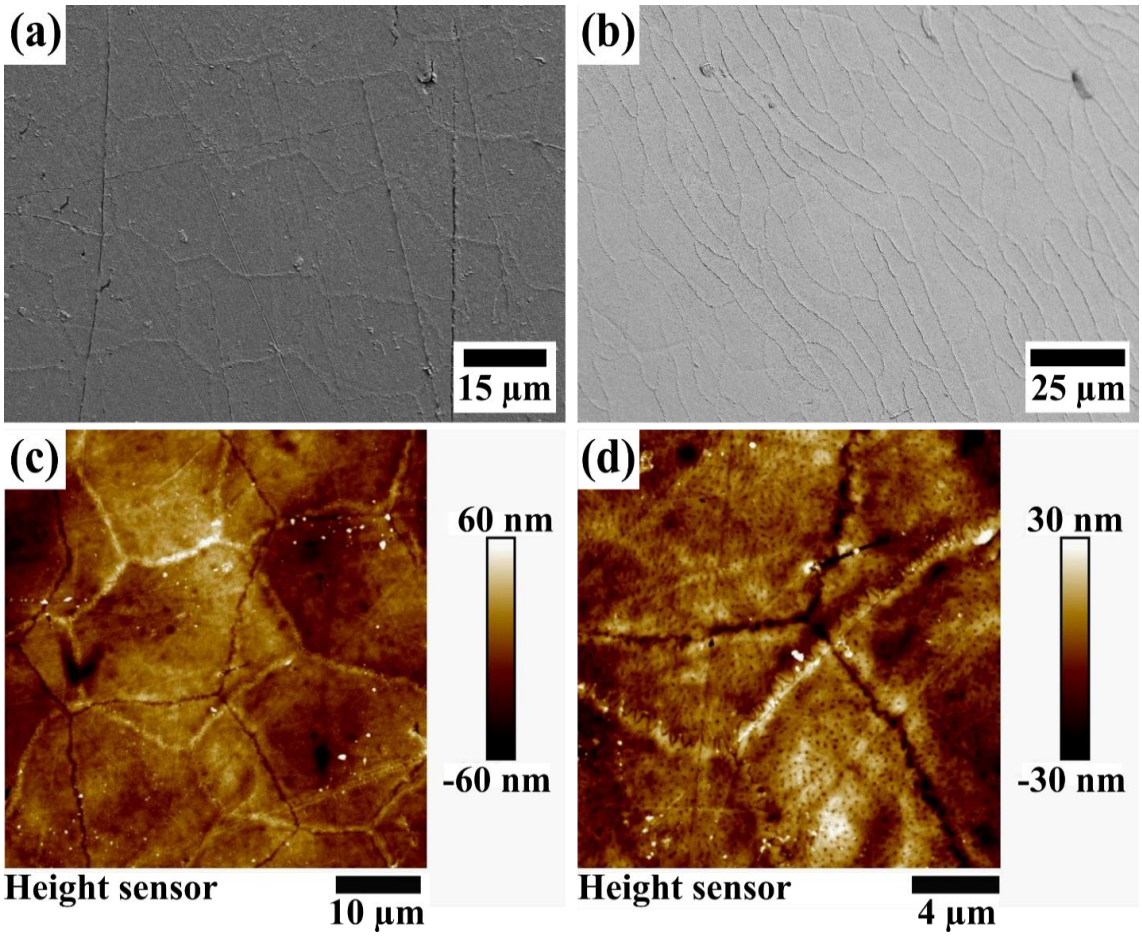

Figure 7.2: *Comparison of SEM and AFM images revealing the nanostructures on the spectacles of P. guttatus. SEM images (a) from the center and (b) from the edge region show pentagonal or hexagonal patterns formed by elevated borders. (c) An AFM image from the center reveals an additional border type. Narrow channels appear as dents and stitching boundaries emerge as ridges. (d) An enlargement in (c) reveals further details. All flat areas of the scale are covered with nanoscale pits. AFM scan are (c) 50 µm; (d) 20 µm* (The figure has been reproduced from the thesis of Weibin Wu [142]

20-30 µm diameter are found in the central regions. AFM images reveal different polygon borders and stitching boundaries on the same spectacle (Fig 7.2c). Polygon borders forming narrow channels (dark colors) and elevated stitching boundaries (light colors) are observed. These narrow channels resemble dents with a depth of 15 nm; whereas the elevated stitching boundaries are ridges with a height of 20 nm. The magnified image is provided in Fig 7.2 d). The analysis showed a microfibril-like pattern on the stitching boundaries similar to the ones observed on the ventral scales (details on the ventral scales are presented in Chapter 3). However, such structures are not found on the narrow channels. Numerous nano-pits are observed on the spectacles alongside stitching boundaries and narrow channels. These pits have a diameter of 100 nm and a depth of around 10 nm.

A similar topology is observed on the spectacles of *V. u. rakosiensis* and *N. atra.* The respective AFM images are presented in Fig 7.3. Narrow channels and stitching boundaries are also observed on the spectacles of *V. u. rakosiensis* (Fig 7.3a). These stitching boundaries and narrow channels show a height and depth of around 30 nm. Nano-pits observed in the magnified image have a diameter and depth of around 150 nm and 10 nm respectively (Fig 7.3b). Such nano-pits are also found on the spectacles of *N. atra* (Fig 7.3c). These pits are deeper than the ones found on *P. guttatus* and *V. u. rakosiensis*. These are about 150 nm and 30 nm in diameter and depth respectively. In both of these images, the nanopits are indicated by white arrows.

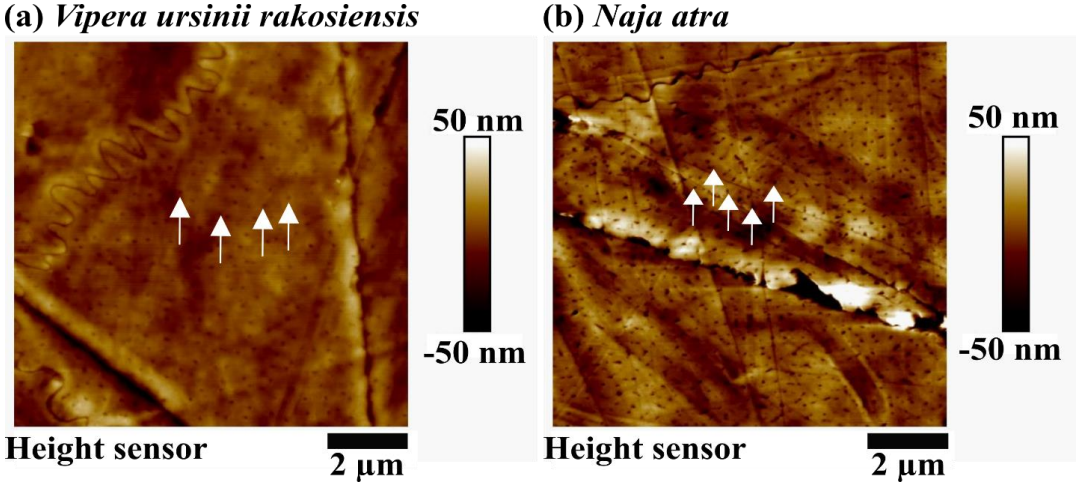

Figure 7.3: *AFM images of the spectacles of (a) V. u. rakosiensis and (b) N. atra. Similar to P. guttatus a flat surface with numerous nanopits is observed. White arrows indicate nanoscale pits in both images. AFM scan area 10 µm.*

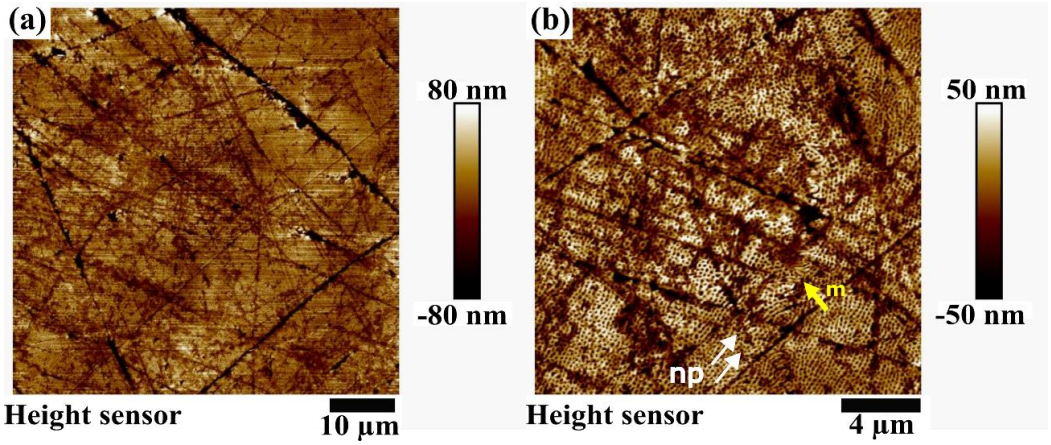

Figure 7.4: AFM images reveal nanopits on the spectacles of T. honsonensis. (a) In difference to the spectacles of P. guttatus, narrow channels, or stitching boundaries are not observed. However, several cracks and scratches (b) abundant nanopits (np marked with white arrows) can be spotted on the surface. These nanopits are much more pronounced. In comparison with the species reported in Figs. 7.2 and 7.3. Microfibrils (m, marked with a yellow arrow) are found on the surface. The scanning size of images (a) and (b) is 60 µm and 20 µm respectively.

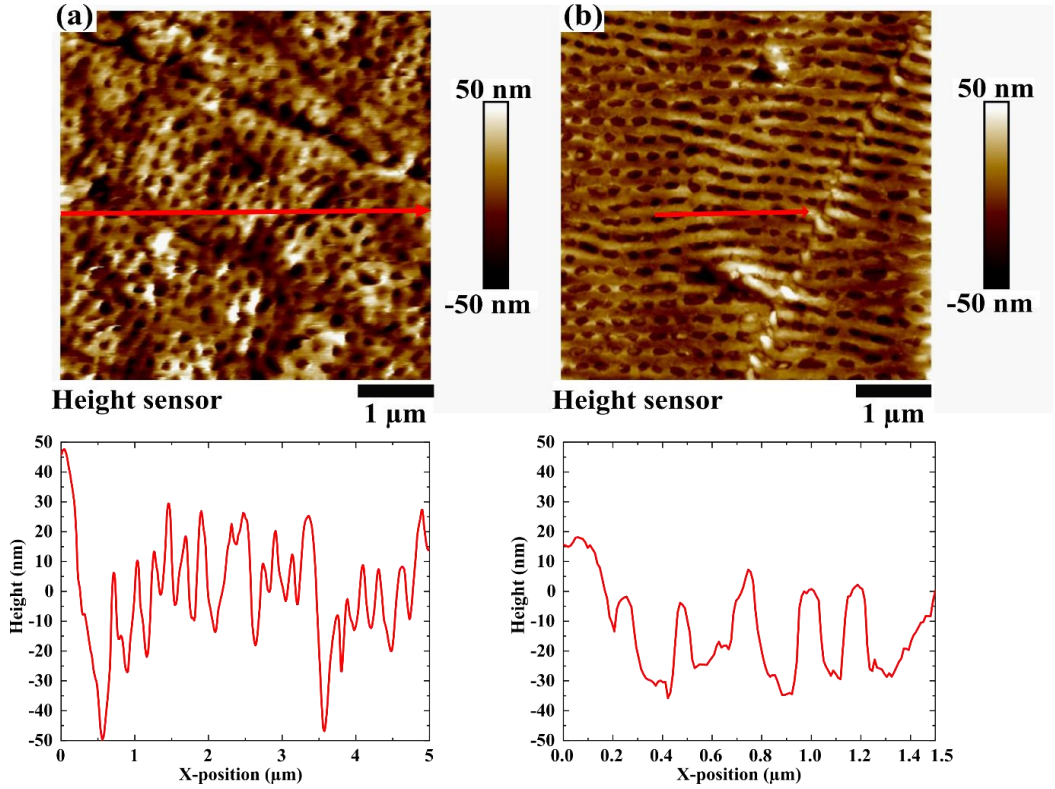

Figure 7.5: Enlarged AFM imaging of the spectacles of (a) T. honsonensis and (b) P. schultzei give an insight into the nanopits. In difference to other species, the nanopits found on the scales of P. schultzei are regularly arranged. For both of these species, the diameter and depth of these nanopits are roughly 300 nm and 50 nm, respectively. AFM scan area 5 µm

The surface topography of the spectacles of *T. honsonensis* is presented in Fig 7.4 a) and b). Narrow channels and stitching boundaries are not prominent on the scale surface of this species. However, similar to other species microfibril pattern (m, marked with yellow arrows) is found (Fig 7.4 b) on the spectacles. Similar to *P. guttatus, V. u. rakosiensis, and N. atra* numerous nanopits (np, marked with white arrows) are also observed. These nanopits' density is higher than those found on the spectacles of *P. guttatus, V. u. rakosiensis,* and *N. atra*. The diameter and depth of these nanopits are measured around 300 nm and 50 nm respectively which is larger and deeper than the nanopits observed in Fig 7.5a). A similar surface topology is also observed on the spectacles of *P. schultzei* (Fig 7.5b). The nanopits for this species, are arranged in a regular pattern. The diameter and depth of these pits are in the range of 300 nm and 50 nm, respectively.

7.2 Wettability of the Spectacles

Textured surfaces with nano- and micro-structures sometimes reduce surface energy which results in low adhesion of water droplets with the surface. Exploring these effects the famous lotus leaf theory was proposed where surface texturing resulted in a high contact angle and low roll of angle [11]. This mechanism keeps the surface clean as the water droplets collect possible debris while rolling off the surface. Inspired by this effect the water contact angles of the spectacles were

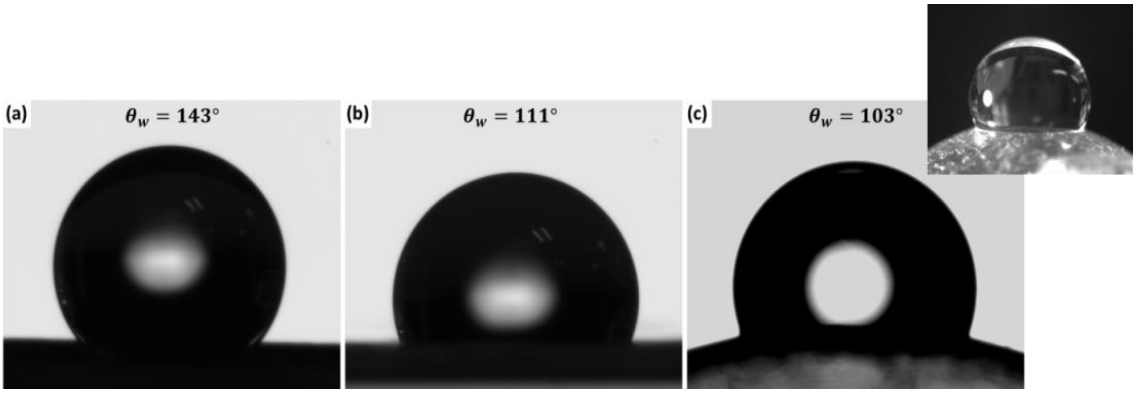

Figure 7.6: *Water contact angle measurement on (a) dorsal, (b) ventral, and (c) intact spectacle scales of S. m. barbouri with a 1 µL droplet of water. The inset in (c) shows the camera image of the water droplet on the same spectacle scale taken from the side indicating an isotropic wetting property* (The figure has been reproduced from the thesis of Weibin Wu [142]).

examined to address the question of how snakes clean their eyes. For comparison with the other body scales contact angles of the dorsal and ventral already discussed in Chapter 3 are also mentioned here.

Water droplets on the dorsal, ventral, and spectacle scale of *S. m. barbouri* revealing the CAs of 143°, 111°, and 103°, respectively are presented in Fig 7.6. The CA on the dorsal scale is the highest. Surprisingly, it is the smallest on the spectacles, where one might expect a high value if snakes clean their spectacles by exploring the wet self-cleaning property. The contact angle on the ventral scale lies in between. The water contact angles of the other snakes are summarized in Table 7.1.

This trend is observed for all the investigated snake species. The highest CAs were recorded on the dorsal scales. CAs over 140° were measured on the dorsal scales of *S. m. barbouri, V. aspis,* and *B. arietans*. CAs between 130° and 140° were observed on the scales of *P. guttatus*, and *M. spilota*. CAs between 120° and 130° were measured on the scales of *M. monspessulanus, V. u. rakosiensis, P. schultzei, N. atra, T. honsonensis,* and *S. diadema*. In difference to the dorsal scales, most snakes exhibit a CA of nearly 110° on their ventral scales except *M. monspessulanus* (118°) and *C. hortulana* (98°). Interestingly, some scales showed complete wetting, i.e., water droplets spread and wet the surface completely when dropped on some scales. The dorsal scales of *T. subannulatus*, for example, were wet completely, and the ventral scales are hydrophilic with a contact angle of 60°. A similar trend was also observed on the ventral scales of *B. arietans.* Nanopits on the scale surface might develop such hydrophilic surfaces.

Table 7.1: Contact angles of the spectacles in comparison with the subsequent ventral and dorsal scales of the same snake species.

Binomial name	**Common Name**	**Contact angle**		
		Dorsal Scales	**Ventral Scales**	**Spectacles**
Sisturus militaries barbouri	Dusky Pygmy Rattle Snake	143 ± 5°	111 ± 3°	103 ± 3°
Pantherophis guttatus	Eastern Corn Snake	133 ± 2°	108 ± 1°	98 ± 6°
Zamenis situla	European Ratsnake	*	108 ± 4°	97 ± 2°
Natrix helvetica	Barred Grass Snake	*	72 ± 16°	91 ± 1°

Natrix tessellata	Dice Snake	*	108 ± 5°	87 ± 4°
Malpolon monspessulanus	Montpellier Snake	130 ± 7°	118 ± 5°	101 ± 3°
Vipera ursinii rakosiensis	Hungarian Meadow Viper	123 ± 2°	106 ± 4°	109 ± 1°
Vipera aspis	Aspic Viper	141 ± 4°	111 ± 1°	103 ± 1°
Vipera seoanei	Seoane's viper	*	107 ± 3°	110 ± 2°
Vipera lotievi	Lotiev's Viper	*	112 ± 1°	109 ± 3°
Vipera renardi	Steppe Viper	*	108 ± 1°	101 ± 3°
Parias schultzei	Schultze's Pitviper	134 ± 2°	107 ± 3°	106 ± 3°
Tropidolaemus subannulatus	North Philippine Temple Pitviper	wetting	60 ± 7°	107 ± 2°
Naja atra	Chinese Cobra	122 ± 4°	111 ± 1°	102 ± 2°
Trimeresurus honsonensis	Hon Son pit viper	125 ± 3°	103 ± 2°	100 ± 2°
Morelia spilota	Carpet Python	134 ± 6°	108 ± 2°	92 ± 2°
Bitis arietans	Puff Adder	145 ± 3°	59 ± 3°	104 ± 2°
Spalerosophis diadema	Diadem Snake	126 ± 5°	109 ± 2°	96 ± 6°

* The samples were too small (<1mm) to conduct reliable measurement

On spectacles, the CAs are typically close to 100°. The smallest value of 92° is observed on *M. spilota*. Although the dimensions of the nano-pits observed on the spectacles of *P. schultzei* and *T. honsonensis* are comparable to the ones found on the ventral scales of *B. arietans*; the contact angle is still around 100°. The spherical geometry of the spectacles in comparison with the flat ventral scales of *B. arietans* might influence the observed CAs.

In general, low CAs revealing only slightly hydrophobic surfaces are observed on the spectacles. As low CA results in a high roll of angle, the current values do not satisfy the principle

of the “Lotus Effect”. Thus it is concluded that most snakes do not feature potential wet self-cleaning of their spectacles.

7.3 Optical properties of the spectacles

It was speculated that the spectacles are optimized for self-cleaning properties. Numerous nano-pits were observed on the spectacles of some species. However, such nano-pits did not reduce the surface energy of the spectacles. As high contact angles are not observed, self-cleaning properties are unlikely. As these structures are naturally grown on the spectacles, in this work it was assumed that these nano-patterns might optimize the optical properties of spectacles. As it is widely assumed that snakes can detect light in the UV range, the spectral response of these scales

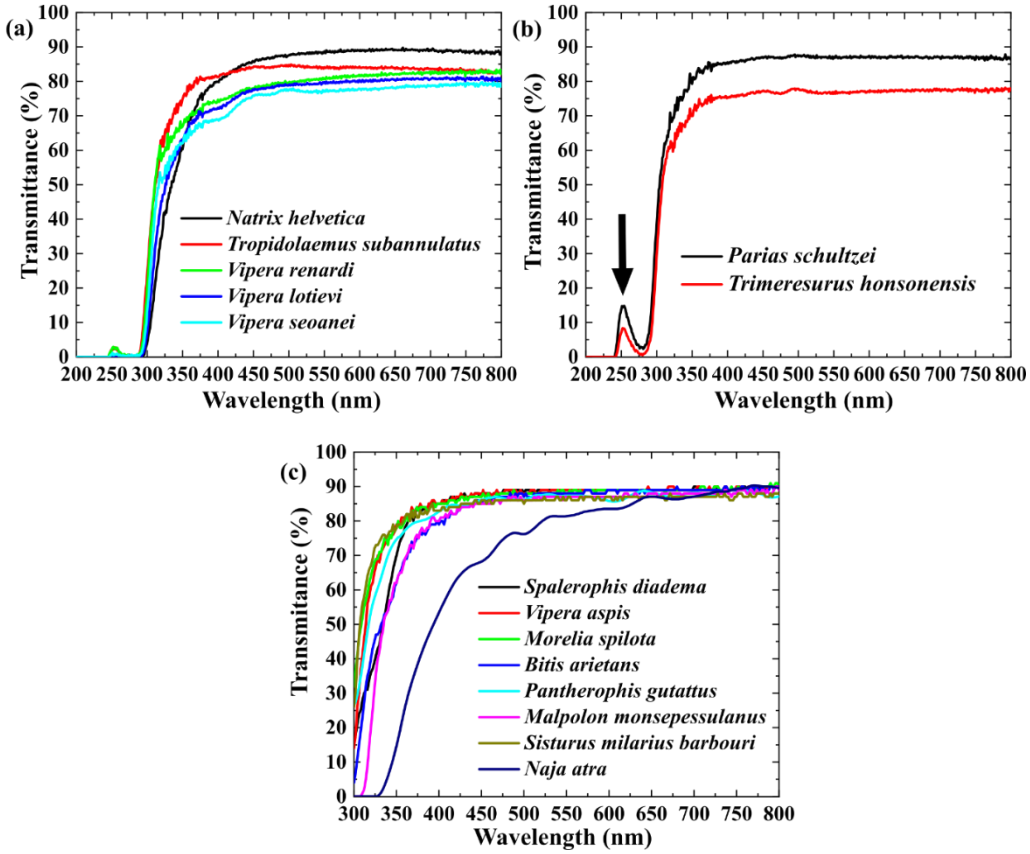

Figure 7.7: *(a) Optical transmittance of the spectacle of 7 snake species for wavelength between 200 and 800 nm. The transmittance is between 70% and 90% in the visible regime between 400 nm to 800 nm but reduces to nearly zero for wavelength below 300 nm. (b) The spectra P. schultzei and T. honsonensis are plotted in an additional graph to emphasize the peak around 250 nm. (c) The spectral transmittance for the rest of the snakes was measured in the range from 300 nm to 800 nm. The spectral resolution and beam spot size for all spectra are 1 nm and around 1 mm, respectively.* (The spectra of Fig 7.7 c) have been adapted from the thesis of Weibin Wu [142]).

was recorded in the wavelength range of 200-800 nm [85, 91-92, 140]. The results are presented in Fig 7.6.

In Fig 7 a), b) the transmittance is presented for the range of 200 nm to 800 nm while the spectra in c) were recorded in a slightly reduced range of 300 nm to 800 nm. The spectra in Fig 7 c) have been adapted from the thesis of Weibin Wu. The overall features of the spectra agree with previous studies [85, 91-92, 140]. In general, the spectacles are about 70-90% transparent in the visible regime. The transmittance reduces to 50% in the wavelength range of 300 nm - 350 nm. Interestingly, this reduction is observed at a higher wavelength for *N. atra* (394 nm). As it is widely assumed that snakes can detect light in that range, too, this transparency window ensures clear vision for snakes [85, 91-92, 140].

In the previous studies, it was already shown that the transmittance at snake's spectacles is very low for wavelengths below 300 nm [85, 140]. This high blockage of UV light by the spectacles might work as a UV filter. Nonetheless, a UV transmittance peak around the wavelength of 250 nm is observed on the spectacles of *P. schultzei* and *T. honsonensis*. Topological analyses on these spectacles indicate numerous nanopits on the surface (Fig 7.5). These nanopits are mostly circular and have a diameter around 250 nm. The analysis indicates that this UV transmittance peak around 250 nm appears when the nanopits have a diameter of around 250 nm. Similar nanopits with a diameter of around 250 nm are also found on the dorsal and ventral scales of numerous snake species. Interestingly, in reference to Fig 3.10 and 3.11 UV transmittance peaks are also found on the ventral and dorsal scales. In Chapter 3 a detailed analysis is presented on the scales which showed nanopits on the scale surface. Optical spectroscopy is conducted on the scales before and after infiltration with a refractive index matching oil which is comparable to the refractive index of snake scales. Results indicate that the intensity of the peak reduces after infiltration; however, it is not reduced to zero. In addition, peaks are even observed on the scales which did not show any nano-pores (*T. honsonensis* or *S. diadema*). Therefore, it is assumed that this UV peak is most likely a material property that might be enhanced by the nano-structures on the scale surface. As the nano-pits found on the spectacles of *P. schultzei* and *T. honsonensis* have a diameter of around 250 nm; it can be speculated that these nano-pits interact with the UV light to enhance UV transmittance peak around 250 nm.

In summary, in this work, it was speculated that snake spectacles might feature surface structures for self-cleaning. Results show that nano-structures on the spectacles are quite shallow and show very low contact angles which should not promote wet self-cleaning properties. It was further speculated that these structures on the spectacles might be optimized through evolution to enhance light capturing by the retina. However, the optical properties indicate that the nano-and

micro-features do not interact with visible light to enhance the vision. Results suggest that snakes' spectacles do not feature advantageous properties relating to wet self-cleaning or enhanced optical transmittance.

Results from the PhD thesis of Weibin Wu

From one completely shaded snake skin, only two spectacle scales are available for analysis. Therefore, Figures 7.1, 7.2, 7.6, and 7.7c) have been adapted from the PhD thesis of Weibin Wu [142]. In addition, the contact angle measurements of *Sisturus milarius barbouri, Pantherophis guttatus, Malpolon monspessulanus, Vipera aspis, Naja atra, Spalerosophis diadema* have also been adapted from his thesis.

A shortened version of this chapter was published as the conference proceeding "On the structural and optical properties of the Hungarian Meadow Viper (Vipera ursinii rakosiensis)" by KM S. Reza, W. Wu, M. M. Romel, R. Thelen, G. Gomard, H. Hölscher, Proc. SPIE 12481, Bioinspiration, Biomimetics, and Bioreplication XIII, 1248106 (2023)

A shortened version of this chapter will be published as the article, "On the Microornamentations and Spectral Transmittance of the Spectacle Scales of Snake" by W. Wu, KM S. Reza*, R. Thelen, G. Gomard, H. Hölscher (*both authors equally contributed)*

8 Nanopores Enhancing Reflection of Blue Hair of Female Carpenter Bee (*Xylocopa caerulea*)

The vibrant coloration of the blue hairs of the female carpenter bee had been a mystery to human understanding of color formation. Over the years it has been believed that the color is produced by pigments [94, 95]. Carpenter Bees of the genus *Xylocopa* often have bright-colored bodies and/or wings [94]. This vibrant color is important for their intraspecific recognition [94]. There is a wide variety of colors within the species. For example, male *X. caerulea* feature a blackish cuticle on their body; whereas, the female species have bright blue hairs on their head, thorax, and parts of the abdomen [94]. Historically it is assumed that the blue color originates from pigments [95]. In 2023, Stavenga analyzed the color of *X. caerulea* and other carpenter bees. He suggested that the pigment bilin produces the color [94]. However, no rigorous proof is found validating that the blue color is produced only by the pigments.

Due to this open research question, the morphological and optical properties of the blue hairs of *X. caerulea* are studied in detail in this study. As no textures are observed on the hairs, the inner structure of these hairs was analyzed. Indeed, imaging of the hair's cross-section revealed a porous core. Interestingly, no structure is observed underneath the external surfaces of the hairs. As it was suggested that the female blue coloration is important for interspecies communication [94], the hairs were optically analyzed by microphotometry between 300 nm to 800 nm. This is a wavelength range where the visibility of bees and other insects is expected [141]. High reflection is observed with a peak and a dent around 480 nm and 605 nm, respectively. As the topological analysis showed that the porous core results in such enhanced reflection the optical responses of the dry and index matching oil infiltrated hairs were recorded. Interestingly, the overall reflection reduced after the infiltration. However, no shift of the reflectance peak or dent is observed. Therefore, it is concluded that the nanoporous core acts as a white scatterer for back reflection. Consequently, the vibrant blue color is produced by pigments but retroreflection is greatly enhanced when light interacts with the nanopores found inside the hair's core.

8.1 Imaging of the blue hair

Blue hairs from the back of the female carpenter bee (*X. caerulea*) are analyzed in this study. Figure 8.1a) shows the photograph of the blue-haired female carpenter bee. Hairs found on the head, thorax, and parts of the abdomen are mostly blue. Optical microscopy imaging shows that

the hairs are branched (Fig 8.1b and c) and these sub-branches are attached to a primary branch which is defined here as the main branch. The main branch is thicker than the sub-branches. A closer look into the hair base, reveal transparent or translucent parts of the hair through which the underneath black surface can be seen. The specific region is marked with a red arrow in Fig 8.1c). This transparent region forms a narrow channel that originates from the base and expands towards the hair tip. To further investigate the color formation, the outer surface of the hairs was analyzed.

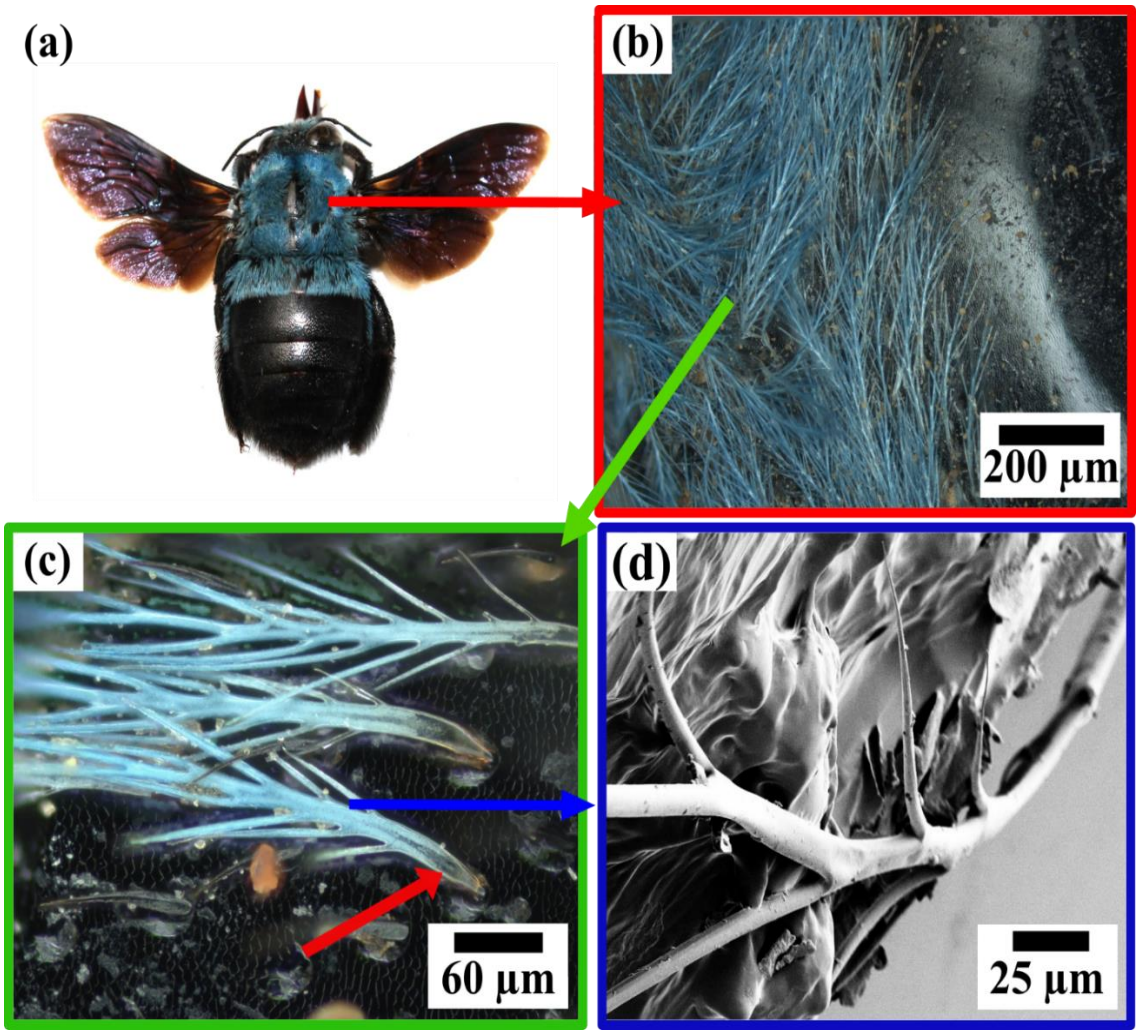

Figure 8.1: ***(a)*** *Photograph of the female blue-haired carpenter bee (X. caerulea).* ***(b)*** *Optical microscopy image of hairs on the back of the bee.* ***(c)*** *A zoom in the structure shows that small branches grow from the main hairs. The base of the hair is not blue but translucent (indicated by a red arrow); through which the underneath black surface is visible. A narrow channel extends from the base to the tip of the hair.* ***(d)*** *An SEM image shows that the thickness of the main branch is around 20 µm whereas the sub-branches are about 10 µm in thickness. No surface structure can be observed on the hair and its branches.*

The surface morphology of a single hair imaged with the SEM is shown in Fig 8.1d). The image does not show any specific nano- or micro-structures on the hair surface. It further indicates that the main branch is about 20 µm thick; whereas the sub-branches are about 10 µm in thickness. The results still do not explain the mechanism of color formation or transparency of the narrow channels within the hairs. Therefore, the hairs were cut with a razor blade and the cross-sections were analyzed.

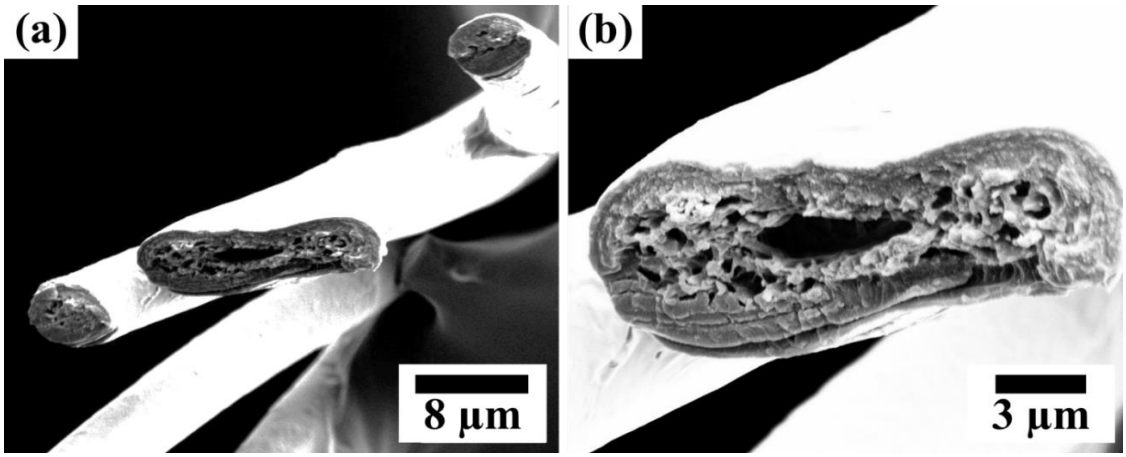

Figure 8.2: *(a) SEM image of cross-sections of the main and sub-branches of a female blue hair.* ***(b)*** *Further magnification of the main branch indicates numerous nanopores alongside a hollow microcavity inside the hair. The nanopores have diameters of some hundreds of nanometers and do not show any regular pattern. The microcavity in the main branch is about 3 µm in width and located in the core of the hair.*

Figures 8.2a) and b) present SEM images of the cross-section of a female's blue hair which shows a microcavity in the central region of the hair. The microcavity in the main branch is about 3 µm in width. This cavity might result in the transparency of the central region. Alongside this cavity, numerous nanopores are found in the main and sub-branches of the hair. Nanopores encircling the microcavity do not show any regular pattern. The nanopores are only spotted around the central cavity. Interestingly, no prominent structure is observed underneath the external surface of the hair. In the optical images, however, the blue coloration of the hairs is observed close to the hair boundary. Therefore, it is concluded that there is no significant geometry on the hair surface or in the cross-section that might cause this blue coloration through structural color. These nanopores embedded inside the hair interact with visible light to enhance the reflection. Nanopores are also found within the scales of white beetles. These nanopores scatter visible light to develop the white surface [139]. The size of the nanopores found within

the scales of white beetles and blue bee hairs is comparable. This further indicates that the whitish region in the central part of the hairs is caused due to the scattering of light by the nanopores.

8.2 Optical properties of the hairs

In 2023, Stavenga suggested that blue-colored hair is important for interspecies communication [95]. Therefore, the optical properties of the hairs were investigated in the wavelength range of 300 to 800 nm. This is a wavelength range where the visibility of bees and

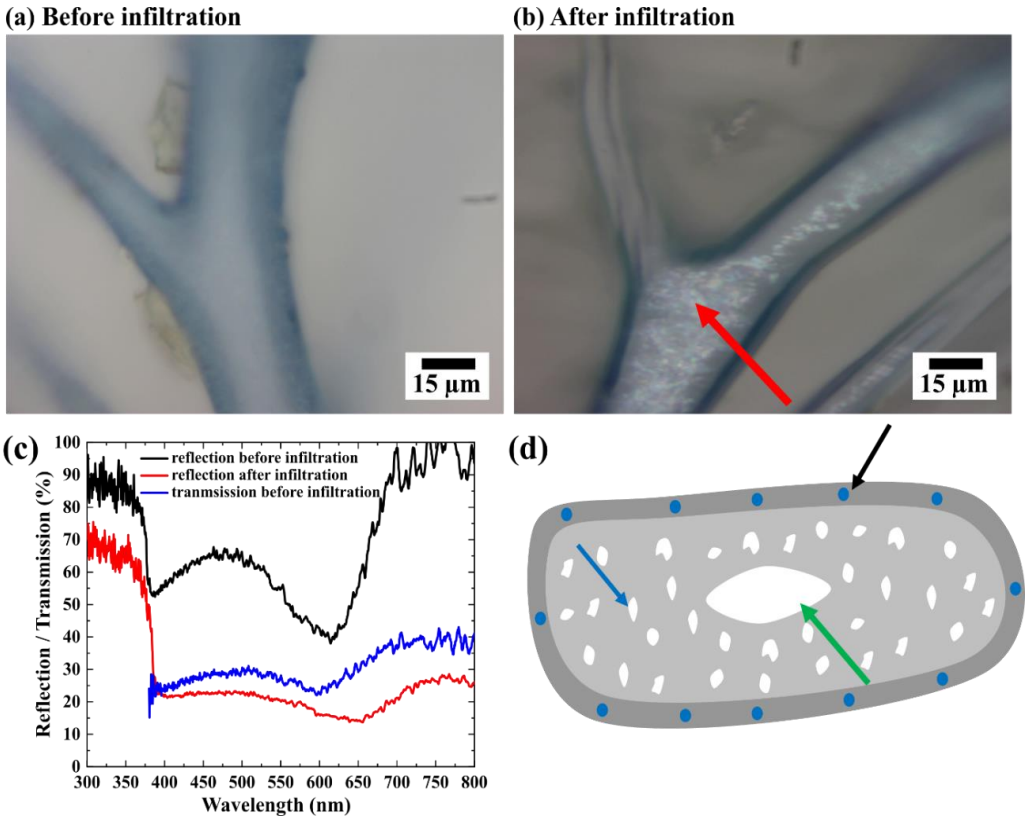

Figure 8.3: *Optical microscopy imaging of blue bee hair before* ***(a)*** *and after* ***(b)*** *infiltration with index matching oil (n = 1.545). The center of the hair is mostly white/translucent; however, the hair's boundary appears blue. The region where the oil infiltrated is marked with a red arrow.* ***(c)*** *The spectroscopic measurements of the dry and infiltrated hair show a dent around 600 nm. The reflection peak observed around 490 nm significantly reduces after the infiltration. High reflection is also observed for both dry and infiltrated hair in the UV light. A dent in both reflection and transmission spectra is found around 600 nm.* ***(d)*** *Schematic of the assumed model explaining the observed scattering effect of the hair's core. The black, blue, and green arrows indicate the possible location of the pigment, nanopores, and microcavity with the hairs.*

other insects is expected [141]. During the spectroscopic characterization, a beam spot size around 2.5 µm was selected and the respective regions were also imaged with the microscope.

Figure 8.3a) shows the region of dry hair where measurements were conducted. The central region of the hair mostly appears translucent or whitish. However, the edges of the hair are only blue in color. SEM presented in Fig 8.2 a) and b) shows no nanopores in the region just underneath the external surface. It indicates that the pigments producing this blue color might be present in this specific region.

It is assumed that the reflection of the hairs is strongly enhanced due to the interaction of light with the nanopores embedded within the hairs. To verify the assumptions, hairs were cut and infiltrated with refractive index matching oil (n = 1.545). Microscopic images and spectroscopic data of the dry and infiltrated hairs were recorded with Microphotometry equipped with a microscope. This specific index-matching oil was used as Stavenga stated that the hairs are composed of materials with similar refractive index [94]. The hairs were cut with a sharp razor blade near the base and were placed on PTFE, Teflon foil which was wrapped around a glass slide. One droplet of the index-matching oil was dropped near the hair. The spreading of oil on the PTFE, Teflon foil was observed under the microscope. After about 5 minutes, oil flowed towards the hair and the capillary forces of the hair pulled the oil from the base towards the tip. Figure 8.3b) shows a microscopic image of the infiltrated hair. Similar to the dry hair, the blue color was observed only around the edges of the hair. The red mark indicates the region where the oil infiltrated.

Spectroscopic measurements of dry and infiltrated hairs were conducted in the UV and visible regimes. The results presented in Fig 8.3c) indicate that the overall reflection reduces after infiltration. This effect can be explained with the model presented in Fig 8.3d). The black, blue, and green arrows indicate the possible location of the pigment, nanopores, and microcavity with the hairs. Due to the filling of nanopores with oil, the retro-reflection effect is significantly reduced, and the blue color reflection is only generated by the back reflection of the regions with blue pigments. This further indicates that light interacts with the nanopores to enhance reflection. A reflectance peak is observed around 490 nm. Interestingly, the intensity of this peak reduces after the infiltration. A dent in the reflection spectra is observed for both dry and infiltrated hairs around 600 nm. Such a reduction is also found in the transmittance spectrum. The absorption, $A\ (1 - R - T)$ at this specific wavelength might be caused by the presence of any pigment. The bile pigment, bilin has a reflection in the blue regime and a high absorption around 605 nm [94]. Thus, Stavenga [94], assumed that this blue color is produced by these pigments; however, the

reflection is strongly enhanced when light interacts with the nanopores found inside the hairs. Interestingly, high reflection in the range of 300 nm – 400 nm is observed for both non-infiltrated and infiltrated hairs. Similar to the entire spectrum of consideration, reflection of the infiltrated hair reduces when measured in the UV regime. Results in Chapter 4 confirm that numerous nanopores are found within the reflecting white ventral scales of some snake species. These nanopores work as scattering units to reflect UV, visible, and near-infrared light. Interestingly, the spectroscopic analysis of the porous blue hairs indicates that the nanopores found within the hairs also reflect the UV light. The nanopores found in both reflecting white ventral scales and blue hairs have a length of around 0.5 µm. These investigations give strong evidence that nanopores inside the blue bee hairs and or snake scales interact with the UV light to generate high reflection which might protect the bees and snakes from harmful radiation.

In summary, results are partly similar to previous results where it was assumed that blue-colored hairs found on the head, thorax, and parts of the abdomen of female carpenter bees are produced by pigments [94, 95]. This investigation further predicts that the pigments responsible for the blue color are found mostly in the region just underneath the external surface. The central region of the hair is porous and light interacts with these nanopores to enhance the reflection. Similar nanopores are also found within the reflecting white ventral scales of some snake species. Results from Chapter 4 and Chapter 8 confirm that nanopores play a significant role in producing vibrant coloration and thermoregulation in nature.

A shortened version of this chapter will be published as the article, "Porous Core Enhances the Reflection of the Blue-Colored Hairs of the Female Carpenter Bee (Xylocopa caerulea)" KM S. Reza, L. Borgmann, G. Gomard, U. Lemmer, and H.Hölscher.

9 Conclusion and Outlook

Over the millions of years of evolution, different organisms in nature have optimized themselves to survive in their respective habitats. They have adopted different strategies to achieve a wide variety of optical and mechanical properties by varying material composition or by developing nano- and microstructures. Structural growth has assisted these organisms to perform different multifunctional activities such as communication [18-19], mating [20], camouflage [21-22], locomotion [44-57], and thermoregulation [58-59], light optimization [35, 64-65], water harvesting [66], developing anti-contaminated surfaces [11, 62, 67-68] and even sound production in danger [69-70]. Over the years, snakes and bees have optimized their optical and mechanical properties through evolution. In this thesis, some of these characteristics are discussed, and some mechanisms through which snakes and bees achieve such properties are explained.

Multifunctionalities of the dorsal and ventral Scales of Snakes

In nature, snakes are the most common reptiles. They locomote in direct contact with the substratum through their ventral scales [29-33]. Numerous studies were conducted on the ventral scales to understand the optimizations adopted by snakes to ease their locomotion [44-57]. Snakes mostly follow four different locomotion traits. Thus, in this thesis, a study is made on the surface textures of their ventral scales in correlation with their locomotion.

Molted ventral scales of snake species from different geographical locations and habitats were investigated with the SEM and AFM. Mostly spike-shaped microfibril patterns are found on the scale surfaces of most species. In addition to microfibrils, nanopits and even smooth surfaces with no prominent textures are also observed. The results confirm that snakes develop these varieties of structures to optimize their locomotion. The wetting properties of the scales were further analyzed with a contact angle goniometer. In general, a contact angle of around 110^{o} is observed on the ventral scales of most snake species. The scales are mostly transparent or translucent in the visible regime. When measured with a UV-Vis-NIR spectrometer, transmittance around 70-90% was recorded.

Surface structures are also observed on the dorsal scales of snakes. In comparison with the ventral scales, a wide variety of textures are found on the dorsal scales. In reference to previous studies in this thesis, these patterns are defined as verrucate patterns [35], canaliculate ridges [36], cristate apical patterns [41], crosshatched patterns [37, 40], papillate patterns [42], and reticulate or porous structure [43]. The functionality of these structures is yet to be understood completely.

Higher water contact angles are observed on the dorsal scales in comparison with the ventral scales. However, these contact angle values are not high enough to conclude that these structures promote wet self-cleaning properties. In general, snakes develop dark colors on their dorsal side. Thus reduced transmittance is observed on the dorsal scales of most snake species which might have resulted due to the absorption by melanin or by the scattering of light by the nano- and micro-structures often found on the scale surface.

Nanopores create broadband reflection in snake scales

In addition to locomotion, some snake species living in warm habitats develop reflecting white bellies. These venters help them to avoid overheating [58-59]. Comparative analysis of the reflecting white and transparent scales of the genus *Bitis* shows that nanopores embedded within the reflecting white scales scatter light to develop such surfaces.

Five snake species of the genus *Bitis* living in different geographical locations and habitats were analyzed in this study. Microscopic imaging of the scale surface showed microfibrils, nanoridges, and nanopits on the surface. This thesis already confirms that such nano- and micro-structures on the surface are optimized to ease snake locomotion and they have little to no effect in enhancing whiteness or reflection, but they potentially can contribute to the haze and scattering (transmitted light). Therefore, the internal structures of these scales were imaged with the SEM. The cross-section images revealed numerous nanopores within the reflecting white scales; however, no nanopores are found within the transparent scales. The results indicate that nanopores interact with the visible light to develop such surfaces. As snakes develop such reflecting white scales to avoid overheating, the scales were optically characterized in the wavelength range of 300-2000 nm. The transparent or translucent scales showed low reflection (comparable to the reflectance of glass) in the UV, visible, and near-infrared light. However, higher reflection is observed for the reflecting white scales in the entire regime of consideration. As high reflection is observed in the near-infrared wavelength range, the results confirm that the scales are optimized to achieve thermoregulatory properties. These nanopores work like scatterers to reflect the UV, visible, and near-infrared light to develop a reflecting white surface through the retro-reflection mechanism.

Micro-cavities developing anisotropically reflecting scales in snakes

Some snakes such as the Chinese Cobra (*Naja atra*) develop anisotropically reflecting ventral scales. The results presented in Chapter 5 show that visible light interacts with the tilted micro-cavities found inside the scales to develop such an optical appearance.

A comparative study made on the anisotropically reflecting and transparent or translucent scales of two different snake species explains the mechanism adopted by the Chinese Cobra. Interestingly, the reflection of these anisotropically reflecting scales increases when the scales are tilted from the head to the tail direction whereas it reduces when tilted from the tail to the head direction. Cross-section imaging of the scales revealed alternate layers of tilted microcavities within the anisotropically reflecting scales. However, micro-cavities are not found within the transparent or translucent scales. These tilted microcavities interact with the visible light to develop anisotropically reflecting surfaces. The scales were further characterized in the wavelength range of 400-800 nm by varying the incidence angle from 0^{o} to 45^{o}. The reflection was measured in both head to tail direction and the tail-to-head direction of the snake body. Low reflectance is recorded for the transparent or translucent scales. The reflection decreased with the increase in incidence angle when measured both along and against the microfibrils. Thus no reflection anisotropy is observed for the transparent scales. However, a difference in optical response was recorded for the anisotropically reflecting scales. Reflection of the scales increases with the increase in angle of incidence when measured from head to tail direction; whereas it reduces with the increase in angle of incidence when measured from tail to head direction. This difference in reflectance pattern is caused due to the interaction of light with the internal structure of these scales. The results confirm that snakes develop tilted micro-cavities within their scales to develop anisotropically reflecting surfaces.

Differences in surface topography with the variation in optical appearance

Cold-blooded animals tend to develop dark-colored appearance. However, this dark coloration increases their detection, resulting in vulnerability to predators [75-78]. Interestingly, most Vipers exhibit a patterned dorsal side with dark-colored scales within a zigzag pattern [83]. Such patterns might favor snakes to camouflage and also maintain their melanistic properties [84]. Previous study assumed that the nano- and micro-structures found on the dark-colored scales are optimized for effective thermoregulation within the snake body [65]. However, further analyses are required to further verify this theory.

In this thesis, a comparative study is presented on the high and low-pigmented scales of snake species from different geographic locations and habitats. The zigzag pattern is found on the dorsal scales of these snake species. Scales within the zigzag pattern are presumably rich in melanin in comparison with the neighboring scales outside the pattern. Interestingly, structural difference is also observed between high and low-pigmented scales. To verify if the structures on the high-pigmented scales are optimized for efficient thermoregulation, the scales were optically characterized in visible and near-infrared light. Low reflection is observed for the high-pigmented scale in comparison with the low-pigmented scales in the wavelength range of 400-1050 nm. However, higher reflection is observed for the highly pigmented scales in comparison with the low-pigmented scales in the higher wavelength (1050-2000 nm). One would expect reduced reflection for the high-pigmented scales in the near-infrared light as the structures are assumed to be optimized for efficient thermoregulation. Therefore, nano- and micro-structures found on the scales were replicated in PMMA material following the nanoimprint lithography technique to understand the optical response of the structures. Interestingly, higher reflection is observed for the replicas prepared from the high-pigmented scales in comparison with the ones developed from the low-pigmented scales for the entire spectrum of consideration. In 2013, Spinner et al assumed that the structures found on the dark-colored scales are optimized for effective thermoregulation as their coloration helps them to absorb more heat [65]. Considering this functionality of snake scales and their developed structures one would expect lower reflection in the near-infrared regime. However, our results show higher reflection for the high-pigmented scales in comparison with the low-pigmented scales in the near-infrared light. Thus, it can be assumed that these high-pigmented scales are not optimized for thermoregulation, as they primarily increase reflection in the region of the electromagnetic spectrum associated with heat generation. The results also confirm that a difference in nano- and micro-structures is observed with the difference in pigment concentration of these scales.

Micro-ornamentation and spectral transmittance of the spectacle scales

Snakes, fossorial lizards, and most geckos develop a transparent integument, brille, or spectacle on their eyes [85]. The wet self-cleaning property of the spectacles is explored in this thesis to understand how snakes clean their spectacles as they do not have any extremities to clean them.

Nature sometimes optimizes its surface texture to achieve self-cleaning properties. Inspired by the theory of the “Lotus effect’’ [11], spectacles of snakes belonging to different habitats and geographical locations were studied in comparison with the nano- and micro-structures found on the scale surface. In general narrow channels and stitching boundaries are

observed on the spectacles. In addition, numerous nano pits are also found on the scale surface. Water contact angles of around 100º were observed on the spectacles of most species which are low enough to exclude self-cleaning properties of the spectacles. The results further show that spectacles are transparent for the visible light but the structures found on the scale surface are not optimized to enhance the vision of snakes. The observations and analyses indicate that the spectacles have tiny to no surface structures on the surface. These structures found on the spectacles do not promote specific functionality or optical properties. Therefore, the benefits to snakes for the development of these nano-structures are still an open question.

Nanopores enhancing the reflection of the blue hair of female carpenter bee (*Xylocopa caerulea*)

The female carpenter bee (*Xylocopa caerulea*) develops vibrant blue hairs. Over the years it has been believed that the color is produced by the virtue of pigments [94-95]. As the current results do not explain the origin of color production explicitly, the hairs are analyzed in detail in this study. Results show that the bright blue color is produced as a combination of pigments and light reflection.

The microscopic bright blue hairs are mostly found on the head, thorax, and parts of the abdomen of female carpenter bees. These blue hairs are mostly found in the female species. To investigate further into the color formation, the hairs were initially examined with the SEM. The surface textures and internal structures of the hairs were examined with a SEM. No prominent textures are observed on the hair surface which could explain the process of color formation. Therefore, the internal structure of the hairs was investigated. Numerous nanopores encircling a microcavity are found in the hair cross-section. These nanopores scatter visible light to develop a reflecting white central region. The blue pigments might be present around the hair boundary where no nanopores are observed. The results confirm that the blue color is produced by a pigment; however, the hair reflection is strongly increased due to the interaction of light with these nanopores, which enhances the coloration by the pigment.

Outlook

In this thesis, different mechanical and optical strategies adopted by snakes and blue carpenter bees have been explained. They achieve these multi-functionalities by virtue of nano- and microstructures. These structures can be artificially fabricated to develop technical surfaces with specific optical and mechanical properties.

The overall efficiency of solar panels, LEDs, OLEDs, and similar optoelectronic devices is heavily compromised due to soiling. Several water-based solutions are in practice to clean such devices. However, current processes require water, which is scarce in several regions of the world. Snakes often develop specific nano-patterns on their ventral scales. These features assist snakes in locomotion by generating frictional anisotropy. These tactics opted by snakes to ease their locomotion can be further explored to develop a dry self-cleaning coating for solar panels. As snakes develop these nano-patterns to ease their locomotion, these structures can be further optimized to modify the locomotion of crawling robots.

Recent studies have speculated that some snakes living in equatorial regions and other hot, humid climates develop reflecting white venters to avoid overheating. This thesis shows that nanopores found inside the scales interact with the incident light to develop such reflecting white surfaces. Similar air voids can be created in technical polymer to enhance their reflection properties. The modified foils will be an alternative to the current white paints, which contain harmful TiO_2 (titanium dioxide) particles. As the snakes develop such scales to avoid overheating, this light reflection mechanism can be further explored to develop energy-efficient walls for next-generation smart houses.

Some snakes develop anisotropically reflecting ventral scales. Tilted microcavities found inside these scales interact with visible light to develop such surfaces. The reflection of these scales varies when viewed from a different angle. Following the underlying physics of this optical phenomenon smart windows can be developed that block UV, visible, and even near-infrared light depending on the tilting angle of these windows.

Female carpenter bees develop vibrant blue-colored hairs on their head, thorax, and parts of the abdomen. The pigmentary color of these hairs is strongly enhanced due to the interaction of light with the hollow core found in these hairs. This optical strategy can be adopted to increase the color contrast of technical surfaces, paintings, etc. Such technical surfaces and paintings might even promote heat retention.

The prime objective of this thesis remained in understanding the underlying physics of these nano- and micro-features which enhance the mechanical, optical, and thermoregulatory properties in the snakes and bees. These structures can be further explored to develop next-generation devices with enhanced optical, mechanical, and thermoregulatory properties.

Bibliography

[1] Endler, J. A., Westcott, D. A., Madden, J. R. & Robson, T. Animal Visual Systems And The Evolution Of Color Patterns: Sensory Processing Illuminates Signal Evolution. *Evolution* **59**, 1795–1818 (2005).

[2] McNamara, M. E., Briggs, D. E. G., Orr, P. J., Noh, H. & Cao, H. The original colours of fossil beetles. *Proceedings of the Royal Society B* **279**, 1114–1121 (2012).

[3] Vinther, J., Briggs, D. E. G., Clarke, J., Mayr, G. & Prum, R. O. Structural coloration in a fossil feather. *Biology Letters* **6**, 128–131 (2010).

[4] Parker, A. R. 500 million years of structural colour. *Journal of Optics A: Pure and Applied Optics* **2**, R15–R28 (2000).

[5] Bhushan, B. Biomimetics: lessons from nature - an overview. *Philosophical Transactions of the Royal Society A* **367**, 1445-1486 (2009).

[6] Choi, J. *et al*. Biomimetics: forecasting the future of science, engineering, and medicine. *International Journal of Nanomedicine* **5701** (2015).

[7] Dai, Z., Tong, J. & Ren, L. Researches and developments of biomimetics in tribology. *Chinese Science Bulletin* **51**, 2681–2689 (2006).

[8] Ivanović, L., Vencl, A., Stojanović, B. & Marković, B. Biomimetics Design for Tribological Applications. *Tribology in Industry* **40**, 448–456 (2018).

[9] Singh, R. A. & Yoon, E.-S. Biomimetics in Tribology - Recent Developments. *Journal of the Korean Physical Society* **52**, 656–668 (2008).

[10] Ruibal, R. & Ernst, V. The structure of the digital setae of lizards. *Journal of Morphology* **117**, 271–293 (1965).

[11] Barthlott, W. & Neinhuis, C. Purity of the sacred lotus, or escape from contamination in biological surfaces. *Planta* **202**, 1–8 (1997).

[12] Wen, L., Weaver, J. C. & Lauder, G. V. Biomimetic shark skin: design, fabrication and hydrodynamic function. *The Journal of Experimental Biology* **217**, 1656–1666 (2014).

[13] Motta, P., Habegger, M. L., Lang, A., Hueter, R. & Davis, J. Scale morphology and flexibility in the shortfin mako *Isurus oxyrinchus* and the blacktip shark *Carcharhinus limbatus*. *Journal of Morphology* **273**, 1096–1110 (2012).

[14] Chen, H., Zhang, L., Zhang, D., Zhang, P., Han, Z., Bioinspired surface for surgical graspers based on the strong wet friction of tree frog toe pads, *ACS Applied Materials & Interfaces* **7**, 13987-13995 (2015).

[15] Federle, W., Barnes, W. J. P., Baumgartner, W., Drechsler, P. & Smith, J. M. Wet but not slippery: boundary friction in tree frog adhesive toe pads. *Journal of the Royal Society Interface* **3**, 689–697 (2006).

[16] Iturri, J. *et al.* Torrent Frog-Inspired Adhesives: Attachment to Flooded Surfaces. *Advanced Functional Materials* **25**, 1499–1505 (2015).

[17] Kemp, D. J., Herberstein, M. E. & Grether, G. F. Unraveling the true complexity of costly color signaling. *Behavioral Ecology* **23**, 233–236 (2012).

[18] Vukusic, P., Sambles, J. R., Lawrence, C. R. & Wootton, R. J. Quantified interference and diffraction in single Morpho butterfly scales. *Proceedings of the Royal Society London B* **266**, 1403–1411 (1999).

[19] Loyau, A. *et al.* Iridescent structurally based coloration of eyespots correlates with mating success in the peacock. *Behavioral Ecology* **18**, 1123–1131 (2007).

[20] Mäthger, L. M., Denton, E. J., Marshall, N. J. & Hanlon, R. T. Mechanisms and behavioural functions of structural coloration in cephalopods. *Journal of the Royal Society Interface* **6**, (2009).

[21] Wilts, B. D., Michielsen, K., Kuipers, J., De Raedt, H. & Stavenga, D. G. Brilliant camouflage : photonic crystals in the diamond weevil, *Entimus imperialis*. *Proceedings of the Royal Society B* **279**, 2524–2530 (2012).

[22] Schultz, T. D. & Hadley, N. F. Structural Colors of Tiger Beetles and Their Role in Heat Transfer through the Integument. *Physiological Zoology* **60**, 737–745 (1987).

[23] Pouya, C., Stavenga, D. G. & Vukusic, P. Discovery of ordered and quasi-ordered photonic crystal structures in the scales of the beetle Eupholus magnificus. *Optics Express* **19**, 11355 (2011).

[24] Yin, H. *et al.* Amorphous diamond-structured photonic crystal in the feather barbs of the scarlet macaw. *Proceedings of the National Academy of Sciences U.S.A.* **109**, 10798–10801 (2012).

[25] Chen, Y. *et al.* Influence of disorders on the optical properties of butterfly wing: Analysis with a finite-difference time-domain method. *The European Physical Journal B* **86**, 472 (2013).

[26] Wiens, J. J., Brandley, M. C. & Reeder, T. W. Why Does A Trait Evolve Multiple Times Within A Clade? Repeated Evolution of Snakeline Body form in Squamate Reptiles. *Evolution* **60**, 123–141 (2006).

[27] Astley, H. C. Long Limbless Locomotors Over Land: The Mechanics and Biology of Elongate, Limbless Vertebrate Locomotion. *Integrative and Comparative Biology* **60**, 134–139 (2020).

[28] Bergmann, P. J., Mann, S. D. W., Morinaga, G., Freitas, E. S. & Siler, C. D. Convergent Evolution of Elongate Forms in Craniates and of Locomotion in Elongate Squamate Reptiles. *Integrative and Comparative Biology* **60**, 190–201 (2020).

[29] Gray, J. & Lissmann, H. W. The Kinetics of Locomotion of the Grass-Snake. *The Journal of Experimental Biology* **26**, 354–367 (1950).

[30] Gray, J. The Mechanism of Locomotion in Snakes. *The Journal of Experimental Biology* **23**, 101–120 (1946).

[31] Marvi, H. & Hu, D. L. Friction enhancement in concertina locomotion of snakes. *Journal of the Royal Society Interface* **9**, 3067–3080 (2012).

[32] Hu, D. L., Nirody, J., Scott, T. & Shelley, M. J. The mechanics of slithering locomotion. *Proceedings of the National Academy of Sciences U.S.A.* **106**, 10081–10085 (2009).

[33] Goldman, D. I. & Hu, D. L. Wiggling Through the World: The mechanics of slithering locomotion depend on the surroundings. *American Scientist* **98**, 314–323 (2010).

[34] Leydig, F., Ueber die äusseren Bedeckungen der Reptilien und Amphibien. *Archiv für mikroskopische Anatomie* **9**, 753-794 (1873).

[35] Beyerlein, P., Studies on the significance of microdermatoglyphics in viperid systematics. I. The microdermatoglyphics of desert vipers (Squamata: Serpentes: Viperidae). *Herpetozoa* **11**, 79-86 (1998).

[36] Chiasson, R. B., Bentley, D. L., Lowe, C. H., Scale Morphology in Agkistrodon and Closely Related Crotaline Genera. *Herpetlogica* **45**, 430-438 (1989).

[37] Chiasson, R. B. & Lowe, C. H. Ultrastructural Scale Patterns in Nerodia and Thamnophis. *Journal of Herpetology* **23**, 109 (1989).

[38] Fontarnau, R. & Bea, A. A Quick, Simple Method of Replicating for Scanning Electron Microscopy Applied to the Oberhautchen Micro-Ornamentation Study. *Journal of Herpetology* **21**, 366 (1987).

[39] Hoge, A. R. & Santos, P. S. Submicroscopic Structure of 'Stratum Corneum' of Snakes. *Science* **118**, 410–411 (1953).

[40] Price, R. Microdermatoglyphics: The Liodytes-Regina Problem. *Journal of Herpetology* **17**, 292 (1983).

[41] Price, R. & Kelly, P. Microdermatoglyphics: Basal Patterns and Transition Zones. *Journal of Herpetology* **23**, 244 (1989).

[42] Price, R. M. Dorsal Snake Scale Microdermatoglyphics: Ecological Indicator or Taxonomic Tool? *Journal of Herpetology* **16**, 294 (1982).

[43] Stille, B. Dorsal Scale Microdermatoglyphics and Rattlesnake (Crotalus and sistrurus) Phylogeny (Reptilia: Viperidae: Crotalinae). *Herpetologica*, **43**, 98-104 (1987).

[44] Abdel-Aal, H. A. On the surface structure and friction regulation in reptilian limbless locomotion. *Journal of the Mechanical Behavior of Biomedical Materials* **22**, 115–135 (2013).

[45] Abdel-Aal, H. A. & El Mansori, M. Tribological analysis of the ventral scale structure in a *Python regius* in relation to laser textured surfaces. *Surface Topography: Metrology and Properties* **1**, 015001 (2013).

[46] Abdel-Aal, H. A., Vargiolu, R., Zahouani, H. & El Mansori, M. Preliminary investigation of the frictional response of reptilian shed skin. *Wear* **290–291**, 51–60 (2012).

[47] Baum, M. J., Heepe, L. & Gorb, S. N. Friction behavior of a microstructured polymer surface inspired by snake skin. *Beilstein Journal of Nanotechnogy* **5**, 83–97 (2014).

[48] Baum, M. J., Kovalev, A. E., Michels, J. & Gorb, S. N. Anisotropic Friction of the Ventral Scales in the Snake *Lampropeltis getula californiae*. *Tribology Letters* **54**, 139–150 (2014).

[49] Benz, M. J., Kovalev, A. E. & Gorb, S. N. *Anisotropic frictional properties in snakes. Proceedings SPIE 8339, Bioinspiration,* Biomimetics, and Bioreplication 83390X (2012).

[50] Filippov, A. E. & Gorb, S. N. Modelling of the frictional behaviour of the snake skin covered by anisotropic surface nanostructures. *Scientific Reports* **6**, 23539 (2016).

[51] Hazel, J., Stone, M., Grace, M. S. & Tsukruk, V. V. Nanoscale design of snake skin for reptation locomotions via friction anisotropy. *Journal of Biomechanics* **32**, 477–484 (1999).

[52] Berthé, R. A., Westhoff, G., Bleckmann, H. & Gorb, S. N. Surface structure and frictional properties of the skin of the Amazon tree boa *Corallus hortulanus* (Squamata, Boidae). *Journal of Comparative Physiology A* **195**, 311–318 (2009).

[53] Greiner, C. & Schäfer, M. Bio-inspired scale-like surface textures and their tribological properties. *Bioinspiration and Biomimetics* **10**, 044001 (2015).

[54] Wu, W. *et al.* Characterization of the microscopic tribological properties of sandfish (*Scincus scincus*) scales by atomic force microscopy. *Beilstein Journal of Nanotechnology* **9**, 2618–2627 (2018).

[55] Wu, W. *et al.* Snake-Inspired, Nano-Stepped Surface with Tunable Frictional Anisotropy Made from a Shape-Memory Polymer for Unidirectional Transport of Microparticles. *Advanced Functional Materials* **31**, 2009611 (2021).

[56] Wu, W. *et al.* Variation of the frictional anisotropy on ventral scales of snakes caused by nanoscale steps. *Bioinspiration and Biomimetics* **15**, 056014 (2020).

[57] Rieser, J. M., Li, T.-D., Tingle, J. L., Goldman, D. I. & Mendelson, J. R. Functional consequences of convergently evolved microscopic skin features on snake locomotion. *Proceedings of the National Academy of Sciences U.S.A.* **118** (2021).

[58] Moreno Azócar, D. L. *et al.* Variation in body size and degree of melanism within a lizards clade: is it driven by latitudinal and climatic gradients? *Journal of Zoology* **295**, 243–253 (2015).

[59] Goldenberg, J., D'Alba, L., Bisschop, K., Vanthournout, B. & Shawkey, M. D. Substrate thermal properties influence ventral brightness evolution in ectotherms. *Communications Biology* **4**, 26 (2021).

[60] Chinese Cobra. wikipedia.org/wiki/Chinese_cobra Accessed: 2021-04-15

[61] Lin, H.-C., Li, S.-H., Fong, J. & Lin, S.-M. Ventral coloration differentiation and mitochondrial sequences of the Chinese Cobra (*Naja atra*) in Taiwan. *Conservation Genetics* **9**, 1089–1097 (2008).

[62] Gower, D. J. Scale microornamentation of uropeltid snakes. *Journal of Morphology* **258**, 249–268 (2003).

[63] Tsai, T.-S. *et al.* Species Identification of Shed Snake Skins by Scanning Electron Microscopy, with Verification of Intraspecific Variations and Phylogenetic Comparative Analyses of Microdermatoglyphics. *Herpetological Monographs* **34**, (2020).

[64] Porter, W. P. Solar Radiation through the Living Body Walls of Vertebrates with Emphasis on Desert Reptiles. *Ecological Monographs* **37**, 273–296 (1967).

[65] Spinner, M., Kovalev, A., Gorb, S. N. & Westhoff, G. Snake velvet black: Hierarchical micro- and nanostructure enhances dark colouration in *Bitis rhinoceros*. *Scientific Reports* **3**, 1846 (2013).

[66] Comanns, P. *et al.* Moisture harvesting and water transport through specialized micro-structures on the integument of lizards. *Beilstein Journal of Nanotechnology* **2**, 204–214 (2011).

[67] Gans, C. & Baic, D. Regional Specialization of Reptilian Scale Surfaces: Relation of Texture and Biologic Role. *Science* **195**, 1348–1350 (1977).

[68] Spinner, M., Gorb, S. N., Balmert, A., Bleckmann, H. & Westhoff, G. Non-Contaminating Camouflage: Multifunctional Skin Microornamentation in the West African Gaboon Viper (*Bitis rhinoceros*). *PLOS ONE* **9**, e91087 (2014).

[69] Kimmich, P. J. and Blaney, R. M. Scanning electron micrographs of dorsal scales of the saw-scaled viper *Echis carinatus*. *HISS (Herpetological Information Search Systems) News-Journal* 1, **85**, (1973).

[70] Young, B. A. & Brown, I. P. The Physical Basis of the Rattling Sound in the Rattlesnake Crotalus viridis oreganus. *Journal of Herpetology* **29**, 80 (1995).

[71] Clusella Trullas, S., Van Wyk, J. H. & Spotila, J. R. Thermal melanism in ectotherms. *Journal of Thermal Biology* **32**, 235–245 (2007).

[72] Clusella-Trullas, S., Terblanche, J. S., Blackburn, T. M. & Chown, S. L. Testing the thermal melanism hypothesis: a macrophysiological approach. *Functional Ecology* **22**, 232–238 (2008).

[73] Clusella-Trullas, S., Wyk, J. H. & Spotila, J. R. Thermal benefits of melanism in cordylid lizards: a theoretical and field test. *Ecology* **90**, 2297–2312 (2009).

[74] Reguera, S., Zamora-Camacho, F. J. & Moreno-Rueda, G. The lizard *Psammodromus algirus* (Squamata: Lacertidae) is darker at high altitudes: Colour variation in *Psammodromus algirus*. *Biological Journal of the Linnean Society* **112**, 132–141 (2014).

[75] Luiselli, L. Reproductive Success in Melanistic Adders: A New Hypothesis and Some Considerations on Andrén and Nilson's (1981) Suggestions. *Oikos* **64**, 601 (1992).

[76] Forsman, A. Heating rates and body temperature variation in melanistic and zigzag Vipera berus: does colour. *Annales Zoologici Fennici* **32**, 365-374 (1995)

[77] Martínez-Freiría, F., Pérez I De Lanuza, G., Pimenta, A. A., Pinto, T. & Santos, X. Aposematism and crypsis are not enough to explain dorsal polymorphism in the Iberian adder. *Acta Oecologica* **85**, 165–173 (2017).

[78] Valkonen, J., Niskanen, M., Björklund, M. & Mappes, J. Disruption or aposematism? Significance of dorsal zigzag pattern of European vipers. *Evolutionary Ecology* **25**, 1047–1063 (2011).

[79] King, R. B. Polymorphic populations of the garter snake Thamnophis sirtalis near Lake Erie. *Herpetologica* **44**, 451–458 (1988).

[80] Andrén, C. & Nilson, G. Reproductive success and risk of predation in normal and melanistic colour morphs of the adder, Vipera berus. *Biological Journal of the Linnean Society* **15**, 235–246 (1981).

[81] Capula, M. & Luiselli, L. Reproductive strategies in alpine adders, Vipera berus. The black females bear more often. *Acta Oecologica*. **15**, 207–214 (1994).

[82] Castella, B. *et al.* Melanism, body condition and elevational distribution in the asp viper. *Journal of Zoology* **290**, 273–280 (2013).

[83] Pizzigalli, C. *et al.* Eco-geographical determinants of the evolution of ornamentation in vipers. *Biological Journal of the Linnean Society* **130**, 345–358 (2020).

[84] Ruxton, G. D., Sherratt, T. N. & Speed, M. P. *Avoiding Attack* Oxford University Press, Oxford (2004).

[85] Van Doorn, K. & Sivak, J. G. Spectral transmittance of the spectacle scale of snakes and geckos. *Contributions to Zoology* **84**, 1–12 (2014).

[86] Da Silva, M. O. *et al.* Comparative morphology of the snake spectacle using light and transmission electron microscopy. *Veterinary Ophthalmology* **19**, 285–290 (2016).

[87] Bourdelle, E. Les yeux et la vision des Vertébrés, par M. Rochon-Duvigneaud. *Bulletin de l'Académie Vétérinaire de France*, 97, 130-131 (1944)

[88] Walls, G. L. The Significance of the Reptilian "Spectacle". *American Journal of Ophthalmology* **17**, 1045–1047 (1934).

[89] Arnold, EN, Relationships of the palaearctic lizards assigned to the genera Lacerta, Algyroides, and Psammodromus (Reptilia: Lacertidae). *Bulletin of the British Museum (Natural History)Historical Series* **25**, 289-366 (1973).

[90] Campbell, A. L., Bunning, T. J., Stone, M. O., Church, D. & Grace, M. S. Surface Ultrastructure of Pit Organ, Spectacle, and Non Pit Organ Epidermis of Infrared Imaging Boid Snakes: A Scanning Probe and Scanning Electron Microscopy Study. *Journal of Structural Biology* **126**, 105–120 (1999).

[91] Hart, N. S., Coimbra, J. P., Collin, S. P. & Westhoff, G. Photoreceptor types, visual pigments, and topographic specializations in the retinas of hydrophiid sea snakes. *Journal of Comparative Neurology* **520**, 1246–1261 (2012).

[92] Simões, B. F. *et al.* Visual Pigments, Ocular Filters and the Evolution of Snake Vision. *Society of Molecular Biology and Evolution* **33**, 2483–2495 (2016).

[93] Gerling, D., Velthuis, H. H. W. & Hefetz, A. Bionomics of the Large Carpenter Bees of the Genus Xylocopa. *Annual Review of Entomology* **34** 163-190 (1989)

[94] Stavenga, D. G. Pigmentary colouration of hairy carpenter bees, genus Xylocopa. *The Science of Nature* **110**, 22 (2023).

[95] Mason, C. W. Structural Colors in Insects. I. *The Journal of Physical Chemistry* **30**, 383–395 (1926).

[96] PRADA, E. Elektromagnetický akčný člen pre pohon lokomočnej štruktúry umelého hada. Diploma thesis. TUKE, SjF, Košice (2011)

[97] Good, R. J. On the Definition of Adhesion. *The Journal of Adhesion* **8**, 1–9 (1976).

[98] Davim, P. Book Review: Tribology on the small scale by C. Mathew Mate. *International Journal of Surface Science and Engineering* **2**, 550 (2008).

[99] Amontons G., De la résistance causée dans les machines, *Mémoires de l'Académie Royale A*, 257-282 (1699).

[100] Gao, J., Luedtke W. D., Gourdon D., Ruths M., Israelachvili J. N., Landman U., Frictional forces and amontons' law: from the molecular to the macroscopic scale, *The Journal of Physical Chemistry B* **108**, 3410-3425 (2004).

[101] Phadnis, A., Manning, K. C., Schuett, G. W. & Rykaczewski, K. Role of Scale Wettability on Rain-Harvesting Behavior in a Desert-Dwelling Rattlesnake. *ACS Omega* **4**, 21141–21147 (2019).

[102] Young, T. An essay on the cohesion of fluids. *Philosophical Transactions Royal Society* **95**, 65–87 (1805).

[103] Roach, P., Shirtcliffe, N. J. & Newton, M. I. Progess in superhydrophobic surface development. *Soft Matter* **4**, 224–240 (2008).

[104] Nishino, T., Meguro, M., Nakamae, K., Matsushita, M. & Ueda, Y. The Lowest Surface Free Energy Based on $-CF_3$ Alignment. *Langmuir* **15**, 4321–4323 (1999).

[105] Quéré, D. Rough ideas on wetting. *Physica A: Statistical Mechanics and its Applications* **313**, 32–46 (2002).

[106] Quéré, D. Wetting and Roughness. *Annual Review of Materials Research* **38**, 71–99 (2008).

[107] Moulinet, S. & Bartolo, D. Life and death of a fakir droplet: Impalement transitions on superhydrophobic surfaces. *The European Physical Journal E* **24**, 251–260 (2007).

[108] Gorb, S. *Functional Surfaces in Biology*. Springer Netherlands, Dordrecht (2009).

[109] Mayser, M. J. & Barthlott, W. Layers of Air in the Water beneath the Floating Fern Salvinia are Exposed to Fluctuations in Pressure. *Integrative and Comparative Biology* **54**, 1001–1007 (2014).

[110] Wenzel, R. N. Resistance of solid surfaces to wetting by water, *Industrial and Engineering Chemistry Research* **28**, 988–994 (1936).

[111] Cassie, A. B. D. & Baxter, S. Wettability of porous surfaces. *Transactions of the Faraday Society* **40**, 546 (1944).

[112] Marmur, A. Wetting on Hydrophobic Rough Surfaces: To Be Heterogeneous or Not To Be?, *Langmuir* **19**, 8343–8348 (2003).

[113] Jacobsen, K. W. & Schiøtz, J. Surface Chemistry of Fakir droplets. *Nature Materials* **1**, 15–16 (2002).

[114] Callies, M. & Quéré, D. On water repellency. *Soft Matter* **1**, 55 (2005).

[115] Ghasemlou, M., Daver, F., Ivanova, E. P., Adhikari, B., Bio-inspired sustainable and durable superhydrophobic materials: from nature to market. *Journal of Materials Chemistry A* **7**, 16643-16670 (2019).

[116] Hecht, E. *Optics*. Addison-Wesley (2002).

[117] Macleod, H. A. *Thin-Film Optical Filters*. Institute of Physics Pub, Bristol ; Philadelphia (2001).

[118] Shawkey, M. D., Morehouse, N. I. & Vukusic, P. A protean palette: colour materials and mixing in birds and butterflies. *Journal of the Royal Society Interface* **6**, (2009).

[119] Xia, Y., Whitesides, G. M., Soft lithography, *Angewandte Chemie International Edition* **37**, 550-575 (1998)

[120] Qin, D., Xia, Y. & Whitesides, G. M. Soft lithography for micro- and nanoscale patterning. *Nature Protocols* **5**, 491–502 (2010).

[121] Hünig, R. *et al.* Flower Power: Exploiting Plants' Epidermal Structures for Enhanced Light Harvesting in Thin-Film Solar Cells. *Advanced Optical Materials* **4**, 1487–1493 (2016).

[122] Erdman, N., Bell, D. C., Reichelt, R. *Springer Handbook of Microscopy*. Springer International Publishing (2019).

[123] Meyer, E. *et al.* Atomic force microscopy for the study of tribology and adhesion. *Thin Solid Films* **181** 527–544 (1989).

[124] Eaton P., West P. *Atomic Force Microscopy*. Oxford University Press. (2010).

[125] Guo, D., Xie, G. & Luo, J. Mechanical properties of nanoparticles: basics and applications. *Journal of Physics D: Applied Physics* **47**, 013001 (2014).

[126] Mate, C. M., McClelland, G. M., Erlandsson, R. & Chiang, S. Atomic scale friction of a tungsten tip on a graphite surface. *Physical Review Letters* **59**, (1987).

[127] Liu, E., Blanpain, B. & Celis, J. P. Calibration procedures for frictional measurements with a lateral force microscope. *Wear* **192**, 141–150 (1996).

[128] Chung, K. H., Pratt, J. R., Reitsma, M. G., Lateral force calibration: accurate procedures for colloidal probe friction measurements in atomic force microscopy. *Langmuir*, **26**, 1386-1394 (2010).

[129] Reitsma M. G., Gates R. S., Cook R. F., Lateral force cantilever for precise atomic force microscope friction measurements. *Proceedings of the XIth International Congress and Exposition, Society for Experimental Mechanics Inc.* (2008).

[130] Bogdanovic, G., Meurk, A. & Rutland, M. W. Tip friction — torsional spring constant determination. *Colloids and Surfaces B: Biointerfaces* **19**, 397–405 (2000).

[131] Schwarz, U. D., Köster, P. & Wiesendanger, R. Quantitative analysis of lateral force microscopy experiments. *Review of Scientific Instruments* **67**, 2560–2567 (1996).

[132] Leite, F. L., Bueno, C. C., Da Róz, A. L., Ziemath, E. C. & Oliveira, O. N. Theoretical Models for Surface Forces and Adhesion and Their Measurement Using Atomic Force Microscopy. *International Journal of Molecular Sciences* **13**, 12773–12856 (2012).

[133] Feldman, A. & Meiri, S. Length-mass allometry in snakes: Snake Length-Mass Allometry. *Biological Journal of the Linnean Society* **108**, 161–172 (2013).

[134] Maderson, P. F. A., Rabinowitz, T., Tandler, B. and Alibardi, L. Ultrastructural contributions to an understanding of the cellular mechanisms involved in lizard skin shedding with comments on the function and evolution of a unique Lepidosaurian phenomenon. *Journal of Morphology* **236**, 1-24 (1998).

[135] Sivak, J. G. The role of the spectacle in the visual optics of the snake eye. *Vision Research* **17**, 293–298 (1977).

[136] Xiao, M., Shawkey, M. D. & Dhinojwala, A. Bioinspired Melanin-Based Optically Active Materials. *Advanced Optical Materials* **8**, 2000932 (2020).

[137] Sahraei, N., Forberich, K., Venkataraj, S., Aberle, A. G. & Peters, M. Analytical solution for haze values of aluminium-induced texture (AIT) glass superstrates for a-Si:H solar cells. *Optics Express* **22**, A53 (2014).

[138] Simonsen, I., Larsen, Å., Andreassen, E., Ommundsen, E. & Nord-Varhaug, K. Haze of surface random systems: An approximate analytic approach. *Physical Review A* **79**, 063813 (2009).

[139] Burresi, M. *et al.* Bright-White Beetle Scales Optimise Multiple Scattering of Light. *Scientific Reports* **4**, 6075 (2014).

[140] Van Doorn, K. Investigations on the Reptilian Spectacle. Ph.D. Thesis, University of Waterloo, Canada, 2012.

[141] Briscoe, A. D. & Chittka, L. The Evolution of Color Vision in Insects. *Annual Review of Entomology* **46**, 471–510 (2001).

[142] Wu, W. Tribological characterization of reptile scales and its inspired, tunable friction anisotropy surfaces. Ph.D. Thesis, Karlsruhe Institute of Technology, Germany, 2020.

[143] BudgetSensors. www.budgetsensors.com/all-in-one-afm-probes Accessed: 2021-06-1

[144] Springsteen, A. & Ricker, T. M. The Use of Center Mount Sample Holders in Reflectance Spectroscopy.

[145] Blue Bee. www.exobeetles.de/ Accessed: 2023-08-15

[146] Tingle, J. L. Facultatively Sidewinding Snakes and the Origins of Locomotor Specialization. *Integrative and Comparative Biology* **60**, 202–214 (2020).

List of Publications

Peer-reviewed Articles

[1] KM Samaun Reza, Weibin Wu, Mahiuddin Mahmud Romel, Richard Thelen, Guillaume Gomard, Hendrik Hölscher, On the structural and optical properties of the Hungarian Meadow Viper (*Vipera ursinii rakosiensis*), *Proc. SPIE 12481, Bioinspiration, Biomimetics, and Bioreplication XIII, 1248106, 2023*.

[2] Weibin Wu*, KM Samaun Reza*, Felix Buck, Shudong Yu, Richard Thelen, Hendrik Hölscher, Guillaume Gomard, On the multi-functionality of snake scales: structural properties, wettability, and spectral transmittance of dorsal and ventral scales by the example of twenty-five snake species, *In preparation*. (* Equal Contribution)

[3] KM Samaun Reza, Junchi Chen, Luisa Maren Borgmann, Guillaume Gomard, Uli Lemmer, Hendrik Hölscher, Nanopores in ventral snake scales cause white venters in the genus *Bitis*, *In submission.*

[4] KM Samaun Reza, Guillaume Gomard, Uli Lemmer, Hendrik Hölscher, Micro-cavities Developing Anisotropically Reflecting Scales in Snakes, *In preparation*

[5] Weibin Wu*, KM Samaun Reza*, Richard Thelen, Guillaume Gomard, Hendrik Hölscher, On the Microornamentations and Spectral Transmittance of the Spectacle Scales of Snake, *In preparation*. (* Equal Contribution)

[6] KM Samaun Reza, Luisa Maren Borgmann, Guillaume Gomard, Uli Lemmer, Hendrik Hölscher, Porous Core Enhances the Reflection of the Blue-Colored Hairs of the Female Carpenter Bee (*Xylocopa caerulea*), *In preparation*.

Conference contribution (Oral)

[1] KM Samaun Reza, Weibin Wu, Mahiuddin Mahmud Romel, Richard Thelen, Guillaume Gomard, Hendrik Hölscher, On the structural and optical properties of the Hungarian Meadow Viper (*Vipera ursinii rakosiensis*), SPIE Smart Structures + NDE 2025, Long Beach, California, USA, March 12-16, 2023.

[2] KM Samaun Reza, Luisa Maren Borgmann, Junchi Chen, Richard Thelen, Guillaume Gomard, Uli Lemmer, Hendrik Hölscher, How Nanopores Generate White Ventral Snake Scales for Thermoregulation, Symposium Nano-BW 2023, Bad Herrenalb, Germany, December 5-6 2023.

[3] KM Samaun Reza, Luisa Maren Borgmann, Junchi Chen, Richard Thelen, Guillaume Gomard, Ulrich Lemmer, and Hendrik Hölscher Nanopores generate broadband reflecting structures in snakes and bees, SPIE Smart Structures + NDE 2025, Long Beach, California, USA March 24-28 2024.

Conference contribution (Poster)

[1] KM Samaun Reza, Luisa Maren Borgmann, Junchi Chen, Richard Thelen, Guillaume Gomard, Uli Lemmer, Hendrik Hölscher, How Nanopores Enhance Reflection in the Blue Colored Hairs of Carpenter Bee (*Xylocopa caerulea*), Symposium Nano-BW 2023, Bad Herrenalb, Germany, December 5-6 2023.

[2] KM Samaun Reza, Luisa Maren Borgmann, Junchi Chen, Hans Gunstheimer, Richard Thelen, Guillaume Gomard, Uli Lemmer, Hendrik Hölscher, How Nanopores and Microcavities Control the Light Reflectance Properties of Snake Ventral Scales, The 1st International Online Conference on Biomimetics, May 15-17 2024.

[3] KM Samaun Reza, Luisa Maren Borgmann, Junchi Chen, Hans Gunstheimer, Richard Thelen, Guillaume Gomard, Uli Lemmer, Hendrik Hölscher, Optically Functional Nano- and Micro-structures found in Nature, KSOP Summer School, Bad Herrenalb, Germany, September 26-27 2024.

Acknowledgment

Since its evolution, nature has been optimizing itself for billions of years. Inspired by its numerous modifications I started looking into snakes and bees to understand if these creatures optimize themselves to survive in their respective habitats. The results presented in this thesis show that nano- and microstructures optimize specific mechanical, optical, and thermoregulatory properties in them. The work performed in the last four years to write this thesis would not have been possible without many people's valuable support and suggestions. Here, I would like to take the opportunity to thank my dear colleagues, friends, and family who have always supported me in this journey.

First of all, I would like to thank Prof. Dr. Ulrich Lemmer for allowing me to write this thesis. I am grateful to him for his continuous scientific and personal support during this time. I am truly indebted to him for his advice in the work and the extensions he provided me to write this thesis properly. Thanks a lot, Uli; things would have been very difficult without your help.

I express my deepest gratitude to my supervisor Prof. Dr. Hendrik Hölscher who has been a constant source of inspiration and an excellent mentor in these years. I admire him for his support, encouragement, and advice whenever necessary. I appreciate his enthusiasm to help and support his students and colleagues to learn. He helped me a lot in writing my articles, this thesis, and presentation slides and even helped me to present my works in the preliminary days of the PhD work. I came to learn many things from him in both professional and interpersonal regard. Thank you, Hendrik, it was a pleasure to work with you and I hope to continue.

I would like to thank Dr. Guillaume Gomard from the Zeiss Innovation Hub @ KIT who has introduced me to the field of Bio-inspired photonics. He has always supported me throughout my Master's study and my PhD study at the KIT. He has appreciated all my ideas and has supported me in all possible ways in this PhD work. The snake scales I worked with were brought to us from almost all over the world through the strong network of Guillaume. I appreciate the amount of time he has spent on all my projects. Thanks a lot, Guillaume, you have helped me a lot in shaping this thesis and my projects.

Next, I would like to thank my colleagues in the group of Biomimetic Surfaces and Scanning Probe Technologies and the Institute of Microstructure Technology (IMT), KIT. Specially Dr. Luisa Borgmann and Mr. Richard Thelen. Luisa helped me a lot in the lab and in interpreting the results of all of my projects. Thank you Luisa I hope to finish our joint projects

soon and continue this collaboration in the future. Richard had a very big impact on my work here at the IMT. With his experience and deep knowledge of metrological analysis, he has provided valuable insights into my projects. He never said no to any of my requests. Thanks a lot, Richard. My work in the lab was much easier as you were always there to help us.

Now I would like to take the opportunity to thank my colleagues at the Light Technology Institute (LTI), KIT especially the members of the MNOS group. I would like to mention Dr. Junchi Chen, Dr. Qiaho Jin, and Dr. Mohamed Hussein Ahmed. I am truly indebted to the help I have received from Junchi, Qihao, and Mohamed. I would also like to mention Mr. Biruk Alemu and Mr. Raghuraman Anantharaman. The long discussions we had about science and life in general inspired me to work on my project.

At this point, I would like to acknowledge all my collaborators who have provided me with the snake scales. I am particularly grateful to Mr. Alexandre Bauer, Mr. Christoph Rothenbühler, Mr. Franz Gries, Ms. Nina Giraud, Mr. Philippe Wolf, Mr. René Woning, and Mr. Alfred Wallner for providing the samples analyzed in this study and providing valuable information and photographs of numerous snake species. In this regard, I would also like to thank Dr. Guillaume Gomard for establishing this collaboration with the snake keepers and collecting all the samples.

I would also like to thank my friends here in Karlsruhe. Life is much easier here thousands of miles away from home for you people. I want to mention Salek Bhai, Rimi Bhabi, Romel Bhai, Rabia Bhabi, Shovon Bhai, and Ashif Bhai. The memories we made together are precious and I will remember them for the rest of my life. I will miss the movie nights in Romel Bhai's place, and our every tour where Salek Bhai remained as the constant pilot and the 'chill mood' discussions with Ashif Bhai. I would also like to thank Sakib Bhai and Adib Bhai for their valuable suggestions in writing this thesis and conducting the PhD work in general. I will always remember Sakib Bhai pushing me before submission and deadline for the betterment of my work. I must agree it would have been difficult to complete this work in time without your support. Thank you Sakib Bhai.

This thesis would not have been complete without the constant support of my parents, my wife, and my sister. I especially appreciate my parents for encouraging me to pursue science. I remember my Baba (father) calling me every time after my conference presentations asking me about the work in detail and taking the next moment to post it on his Facebook page with lots of pride and joy. I always refrained from posting on social media; well, this never worked out and I believe I would do the same for my child regardless of his/her refrains. Thank you Baba you are

a true inspiration and my hero. My Ammu (mother) has always been by my side throughout my academic life. She has sacrificed her career in Economics for the well-being of my sister and myself. You deserve all my degrees as much as I deserve them. I appreciate her curiosity about my work. Ammu I have reached this point in life only because of you. From the bottom of my heart, I thank my sister for her encouragement in this journey. I am extremely happy to write that you are already taking your first steps toward higher studies with your Master's program in the USA. I have no doubt you will succeed there with flying colors. I would also like to thank my father and mother-in-law for their support in this journey.

Lastly, I would like to thank my dear wife Mehreen Mansur who has been by my side on this journey. It was not only my dream to do a PhD rather it was our dream and she helped me in every possible way to reach here. I guess it's very normal in PhD life to work over the weekends but it is not easily acceptable for others who are not going through the process. But Mehreen never complained and has always encouraged me. She has always put my work as the top priority. Life will not get any easier but I strongly believe all challenges can be dealt with when you are by my side. I don’t want to judge your support by thanking you.

In the past four years, I have learned a lot and have lost which is beyond any repair. I deeply remember with all my respect my Nanumoni (grandmother), my Boro Chacchu (paternal uncle), and my Arefeen Bhaiya (brother-in-law); may the Almighty bless them with the highest place in Paradise. Life is not the same without you all.

In the loving memory of my Nanumoni, my Boro Chacchu, and my Arefeen Bhaiya.

KM Samaun Reza
December, 2024
Karlsruhe, Germany